5102-117
Solar Thermal Power Systems
Advanced Solar Thermal Technology Project

DOE/JPL-1060-20
Distribution Category UC-62b

Advanced Subsystems Development

Third Semiannual Progress Report

October 1, 1978 to April 1, 1979

August 15, 1979

Prepared for
U.S. Department of Energy
Through an agreement with
National Aeronautics and Space Administration
by
Jet Propulsion Laboratory
California Institute of Technology
Pasadena, California
and
NASA Lewis Research Center
Cleveland, Ohio

(JPL PUBLICATION 79-107)

5102-117
Solar Thermal Power Systems
Advanced Solar Thermal Technology Project

DOE/JPL-1060-20
Distribution Category UC-62b

Advanced Subsystems Development

Third Semiannual Progress Report

October 1, 1978 to April 1, 1979

August 15, 1979

Prepared for
U.S. Department of Energy
Through an agreement with
National Aeronautics and Space Administration
by
Jet Propulsion Laboratory
California Institute of Technology
Pasadena, California
and
NASA Lewis Research Center
Cleveland, Ohio

(JPL PUBLICATION 79-107)

Prepared by the Jet Propulsion Laboratory, California Institute of Technology, for the U.S. Department of Energy through an agreement with the National Aeronautics and Space Administration.

The JPL Solar Thermal Power Systems Project is sponsored by the U.S. Department of Energy and forms a part of the Solar Thermal Program to develop low-cost solar thermal electric generating plants.

FOREWORD

The advanced solar thermal technology subprogram is a part of the Thermal Power Systems activity of the Department of Energy Division of Solar Technology. The primary objective of the subprogram is to support the development of advanced, high-performance, low-cost, long-life and reliable solar thermal power components and subsystems.

The Jet Propulsion Laboratory (JPL) and the NASA Lewis Research Center (LeRC) were selected in 1977 to assist in managing and coordinating this subprogram. These two organizations, working with universities, government agencies, industry and the scientific community in general, are to lead in developing new concepts and establishing a broad general, technology base in advanced small power systems which can be used to accelerate the development of cost-effective power systems.

This Semiannual Progress Report is the third to be issued (the first was released in June 1978; the second in November 1978). It covers six months (October 1978 to April 1979) of work on the JPL/LeRC advanced subsystems development task. It is used as a means of publishing the results of the work on advanced concepts and widely disseminating the technology. It is hoped that the open approach of NASA in providing easy access to the results, procedures, and the data base developed in this task will stimulate early adaptation of the most promising concepts. Considerable detail is provided in some sections and in appendices so that the report may be used by a wide variety of organizations. If the reader needs additional information or if he wishes to discuss any items, please contact Floyd Livingston, the Advanced Subsystems Development Task Manager, at the Jet Propulsion Laboratory, FTS 792-9416, Commercial (213) 577-9416 or write to him at the Jet Propulsion Laboratory, Mail Stop 506-328, 4800 Oak Grove Drive, Pasadena, California 91103.

ABSTRACT

This document summarizes the results of the work performed by the Advanced Subsystems Development Task of the Advanced Solar Thermal Technology Project. The activities described were managed by the Jet Propulsion Laboratory, California Institute of Technology and the Lewis Research Center for the U.S. Department of Energy during the period beginning in October 1978 and ending in April 1979.

During this reporting period, preliminary design for a prototype small (20 kWe) solar thermal electric generating unit was completed, consisting of several subsystems. The concentrator and the receiver collect solar energy and a thermal buffer storage with a transport system is used to provide a partially smoothed heat input to the Stirling engine. A fossil-fuel combustor is included in the receiver designs to permit operation with partial or no solar insolation (hybrid). The engine converts the heat input into mechanical action that powers a generator. To obtain electric power on a large scale, multiple solar modules will be required to operate in parallel. The small solar electric power plant used as a baseline design will provide electricity at remote sites and small communities.

During this period the Advanced Subsystems Development Task "moved out" with contractors to implement development of a directly coupled solar receiver, a heat pipe solar receiver with thermal energy storage, kinematic Stirling engines, and advanced solar concentrator components. Organizations involved in the task now include the General Electric Co., Mechanical Technology, Inc., Fairchild/Stratos Div., Acurex Corp., United Stirling (Sweden), academic consultants at the University of Pennsylvania and at Oklahoma State University, the NASA Lewis Research Center, and the Jet Propulsion Laboratory.

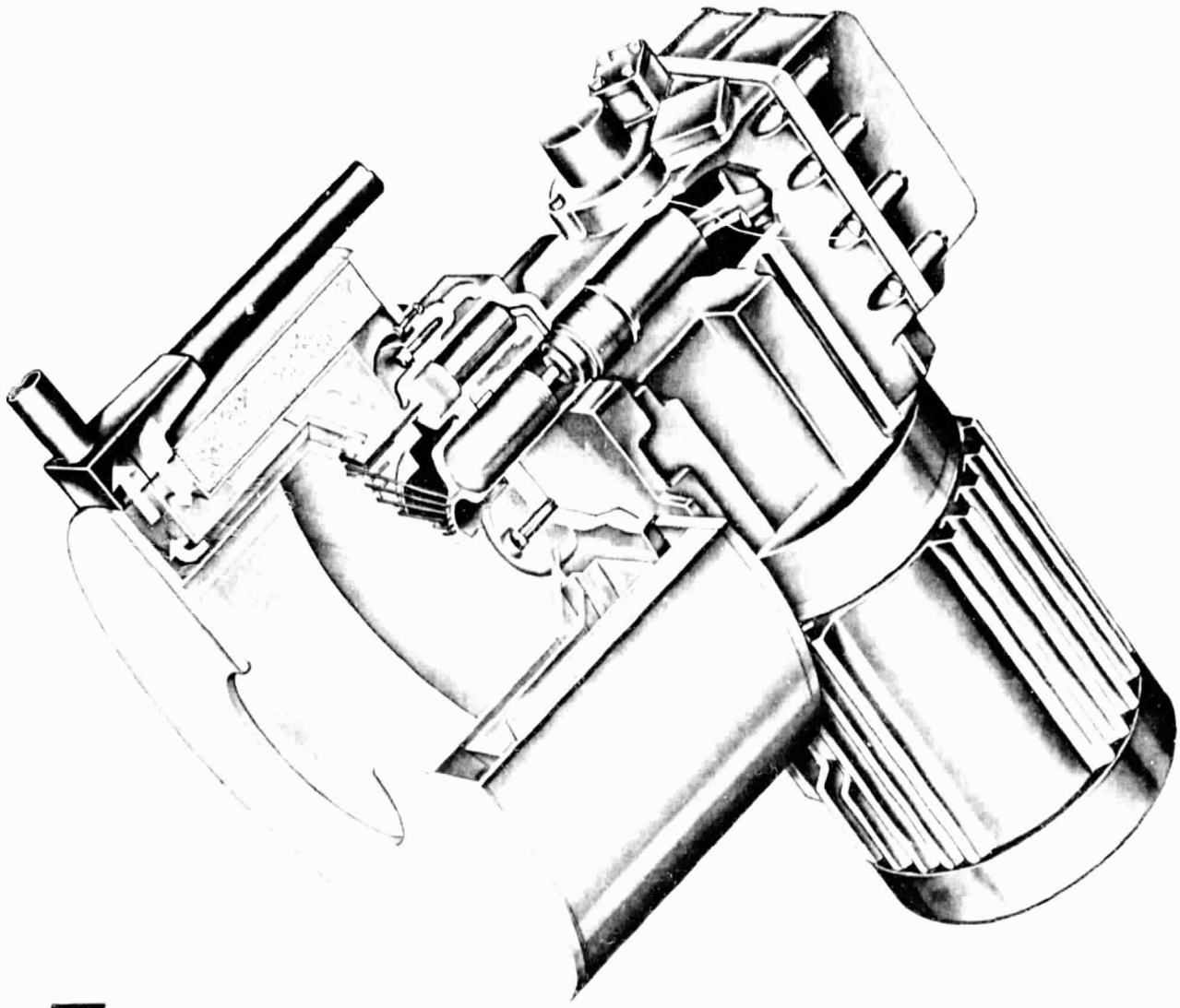

FAIRCHILD
STRATOS DIVISION

EXECUTIVE SUMMARY

INTRODUCTION

The challenge in solar energy development is to bring performance and cost of systems into a competitive position with other potential sources of electric power generation. The approach taken in the advanced subsystem development task is to bring together a team of industrial contractors to adapt the high technology of aerospace programs and the low-cost quantity production capabilities of industry in order to apply these methods to solar power generation.

The dish-Stirling solar thermal-electric power system experiment will demonstrate high performance technology for application to solar generation. The designs selected will be amenable to low cost producibility in the late 1980's. Stirling cycle power conversion at 1500°F (816°C) was selected for the following reasons:

- Exceptional power conversion efficiency at temperatures which can be achieved with existing, well known materials
- Reasonable materials cost
- Availability of existing small Stirling engine designs
- High overall solar collection efficiency (electricity output/solar insolation).

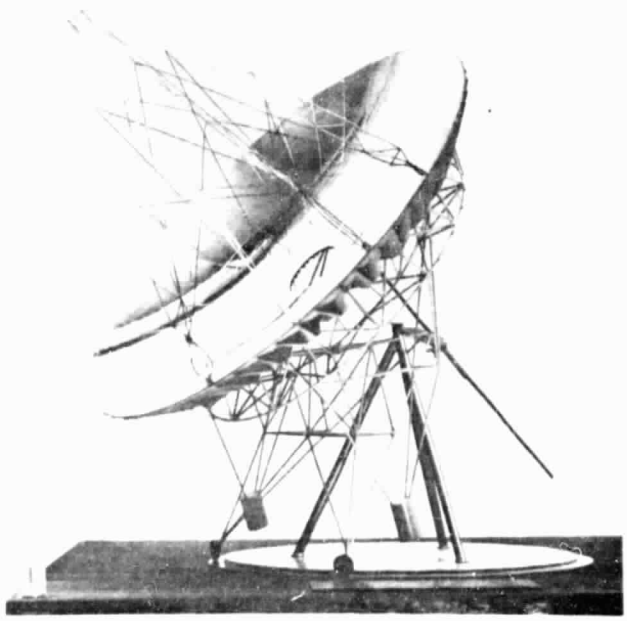

Figure 1. Preliminary Configuration, Dish-Stirling System No. 1 (ADS-1), 1981 Demonstration

The Stirling engine, coupled with a point-focusing concentrator (dish) is scheduled for first system demonstration in early CY'81. Designated Advanced Development System No. 1 (ADS-1) (Figure 1) this experiment includes:

- A 20-kWe Stirling-cycle engine driven alternator having an electricity-out to heat-in efficiency of 35-40% and a production cost potential under $200/kWe at about 10,000 units/year
- An advanced receiver operating at temperatures of 800-900°C (1500-1650°F) and having a cost potential under $25/kWe
- A fossil fuel combustion hybrid augmentation for system operation at constant power output and high capacity rating, and potentially costing under $12/kWe
- A test bed concentrator from the JPL PFDRT Project

The object of the experiment is to provide a subsystem-level module feasibility test of dish-Stirling technology, to identify performance parameters affecting system optimization, and to evaluate system potential for meeting cost goals.

Subsystems will be designated with a view toward annual production quantities on the order of 100,000 to 1,000,000. Factory prefabrication will be emphasized to minimize field assembly and site preparation. In order to minimize cost, components are designed for low mass, minimum materials cost, low complexity, and long life. By use of the hybrid combustor, the system is designed for continuous, constant-power, maximum efficiency operation with either variable or no solar insolation.

To support the module feasibility experiment, two quite different receiver alternatives are being developed at the same time. A heat pipe solar receiver with thermal energy storage (TES) will be demonstrated; and a minimum-cost, direct-coupled receiver, without TES, is being developed. Both receivers include a fossil fuel combustion capability to smooth the variations of solar flux. Kinematic Stirling engine-alternator contracts are in process for units rated at approximately 37% efficiency. It is expected that future modification will provide efficiency increases to 43% without significantly increasing operating temperatures.

As indicated above, the early feasibility test of the engine/receiver modules will be with an 11 meter diameter test bed concentrator. However, in parallel to the development of the engine/receiver module, work is in progress to design an advanced low cost concentrator capable of mass production costs below 100 $/m^2. The concept selected for development utilizes structural cellular glass with back silvered mirrors. As part of this project's work, structural cellular glass panels will be developed.

STIRLING ENGINE-ALTERNATOR

The Stirling engine is at the heart of the dish-Stirling system. The high efficiency of the Stirling cycle is important to the solar thermal-electric system. Although the technology has been brought to a reasonable level of maturity by companies in the Netherlands and Sweden during the 1960s and 1970s, there were very few Stirling engine applications until recently. Risk capital is always limited and there has been no urgent demand for Stirling technology. Today, however, the picture is changing. With energy and environmental constraints so critical, the Stirling cycle is no longer to be ignored. Several companies are actively moving towards Stirling applications in the automobile and recreational vehicle markets.

The two kinematic Stirling engines currently available (USS[1] P-40 and NAP[2] 1-98) will be used in the dish-Stirling system. Only minor modifications of the heat exchanger, oil passages, and water passages are required for operation with a solar receiver at 20 kWe and a temperature of 816°C (1500°F).[3] Engines can be modified and delivered within 10-15 months of ordering, with engine-generator efficiencies of 37% anticipated. Improvement of efficiency to 43% is expected with additional development. This higher efficiency is accomplished by reducing mechanical drive losses and by optimizing engine thermodynamic and mechanical operation. Such "solarizing" modification is relatively low cost and can be accomplished on the schedule shown in Figure 2.

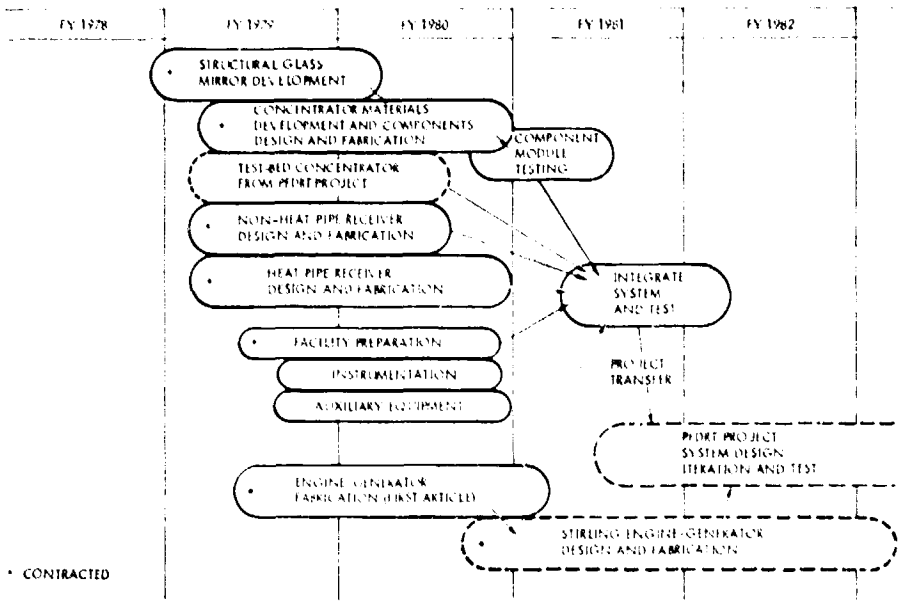

Figure 2. Schedule Dish-Stirling Engine-Alternator Development

[1]United Stirling Sweden

[2]North American Phillips

[3]First tests will be at a lower temperature

ADVANCED CONCENTRATOR

Besides the Stirling engine, successful implementation of the dish-Stirling system is dependent on developing a high-performance, low-cost, parabolic concentrator. There are three factors that contribute to the low cost in this approach. First, low-cost materials are utilized, particularly in the structural cellular glass construction of the parabolic mirror substrate. Second, this subsystem is to be designed for minimum mass, which in automated production, is equated to minimum cost. Third, the subsystem is to be minimumly complex, both structurally and mechanically. The extent to which these elements are provided will ultimately define how well cost goals can be achieved.

The early monolithic, cellular glass, gore concentrator concept studied by JPL will be reconfigured, designed, and critical components will be fabricated and tested by an industrial contractor (Acurex). The mirrored, cellular glass substrate concept is the primary developmental requirement, and it is expected to yield minimum cost. A substantial design effort is needed in the area of wind loading limitations and environmental constraints. It is the responsibility of the concentrator developer to produce a design and develop the critical components which will lead to low-cost, automated production.

ADVANCED RECEIVERS

Two completely different receiver technologies are to be demonstrated in the dish-Stirling system. The Dish-Stirling Solar Receiver (DSSR), is a minimum-cost receiver directly coupled to the Stirling engine. As shown in Figure 3, concentrated insolation is directed through the aperture of a quartz plate and impinges on the surface of a conical receiver body.

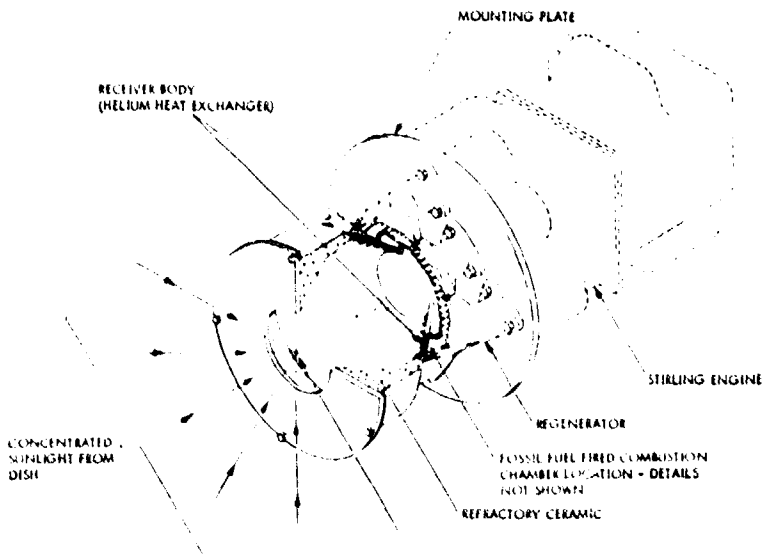

Figure 3. Direct-Coupled Dish-Stirling Solar Receiver, Showing P-40 Stirling Engine

Seventy-two helium heat exchanger tubes are formed or contained within this receiver body, and will operate at an average tube wall temperature of 816°C (1500°F). The heat exchanger tubes are carried back to the Stirling engine and brazed to manifolds at the engine regenerators and cylinder heads. Every effort is made to minimize complexity and cost of the receiver. Other than thermal inertia of the receiver structure, no thermal storage is provided. System optimization with buffer storage will be the subject of later development. Fossil-fuel burners behind the solar receiver plate provide for operation at an essentially constant power level with either a reduced or full solar input.

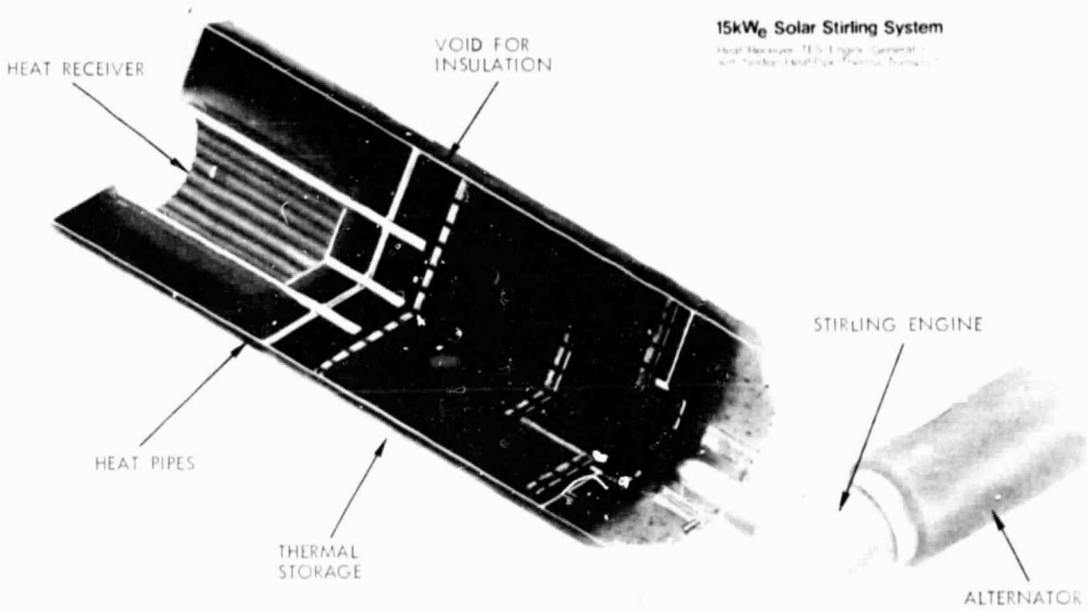

Figure 4. Heat Pipe Solar Receiver with TES, Showing 1-98 Stirling Engine

The second dish-Stirling receiver technology to be demonstrated is the Heat Pipe Solar Receiver with Thermal Energy Storage (HPSR/TES) (Figure 4). This concept evolved from liquid metal heat transport applications studies of FY'78. The HPSR/TES employs a primary and secondary heat-pipe arrangement to perform this heat transport. In the design above, approximately two hours of TES are provided with the receiver. Concentrated insolation impinges on the surface of 27 primary heat pipes forming the cylindrical receiver cavity. These heat pipes

transport the heat through a header into a large-diameter secondary heat pipe containing a large number of externally "wicked," cylindrical TES capsules. The TES capsules operate at slightly lower temperature than the primary heat pipes, assuring needed heat transport to charge the capsules. At the opposite end of the secondary heat pipe, the Stirling engine heat exchanger tubes intrude into the vapor space and receive heat from the TES. The entire unit is enclosed in an insulated jacket to prevent excessive loss of stored heat. The Stirling engine is also designed for minimum heat conduction loss. The primary heat pipes are unwicked at the condenser end to prevent heat flow-back from the TES into the receiver cavity.

The HPSR/TES also includes hybrid operation with a fossil-fuel combustor. As in the DSSR, a combustion unit is to be placed around the outside of the primary heat transfer surface. For the HPSR, the combustion heating is around the outside of the primary heat pipes. Heat losses through the receiver aperture by radiation and convection will be larger than desired, but acceptable for an early demonstration unit. An aperture cover for the DSSR is under consideration. For the HPSR, because of the decoupling from the Stirling engine by the TES, alternate ways of introducing combustion heating are to receive future study.

SYSTEM DEVELOPMENT

Two iterations (or phases) of advanced technology development are planned as shown in Figure 5.

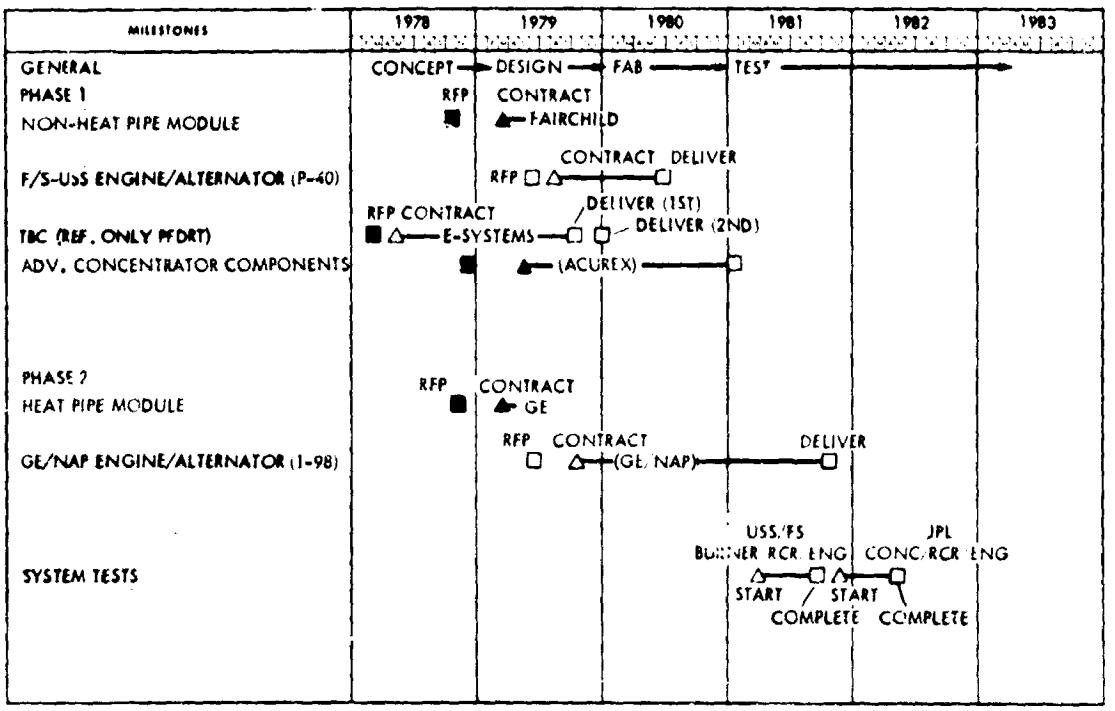

Figure 5. Dish-Stirling System Development Schedule

The first is a technology feasibility phase, which establishes the readiness of technology for application. The second phase is technology optimization, which includes all improvements of technology necessary to show potential for meeting the performance, life, and cost goals. These latter improvements will include:

- An advanced kinematic Stirling engine-alternator having an efficiency up to 43%
- A high performance hybrid receiver or an advanced TES subsystem developed specifically for low cost

Optimization for the dish-Stirling system will be heavily involved with matching of system operation to the load requirements. Exceptional versatility has been introduced into the optimization process by two options:

- Thermal energy storage (TES)
- Fossil fuel hybrid operation

These elements allow individual units to operate either at constant power output, or to supply a variable power load and to do so reliably.

Constant Power Operation

Ability to operate individual Stirling engine-alternators at fixed rated power has been shown to be an important system concept. This type of operation shows potential for yielding high efficiency at low cost. Unit size is minimum because peak-to-average power ratio is unity. The controls will operate on speed, temperature, burner operation, tracking, etc. Output power is delivered at constant frequency (60 Hz) and can be directly tied into an electric utility load without costly or inefficient processing.

Constant power operation is achieved in one of two ways. First, hybrid operation is provided by the fossil fuel combustor on the receiver. Variable solar heat is thus augmented by combustion heating to produce a fixed power level. The second method of achieving constant power operation is with TES. It is being evaluated in the heat pipe receiver design. The latent heat TES provides a constant power input into the Stirling engine without itself needing a constant power input. This allows a further simplification of controls. Furthermore, the need to operate the fossil-fuel combustor at a low power level, with its resultant low-energy effectiveness, is eliminated. The TES cycle efficiency has been shown to be potentially high (97%).

LOAD MATCHING

Operation of a dish-Stirling system with an electric utility load is considered the primary application. For such an application, there is a strong correlation noted between the daily insolation profile and the

daily load demand profile of a utility (Figure 6). This correlation will be a major contributor in defining a high capacity rating for solar power systems at minimum system cost.

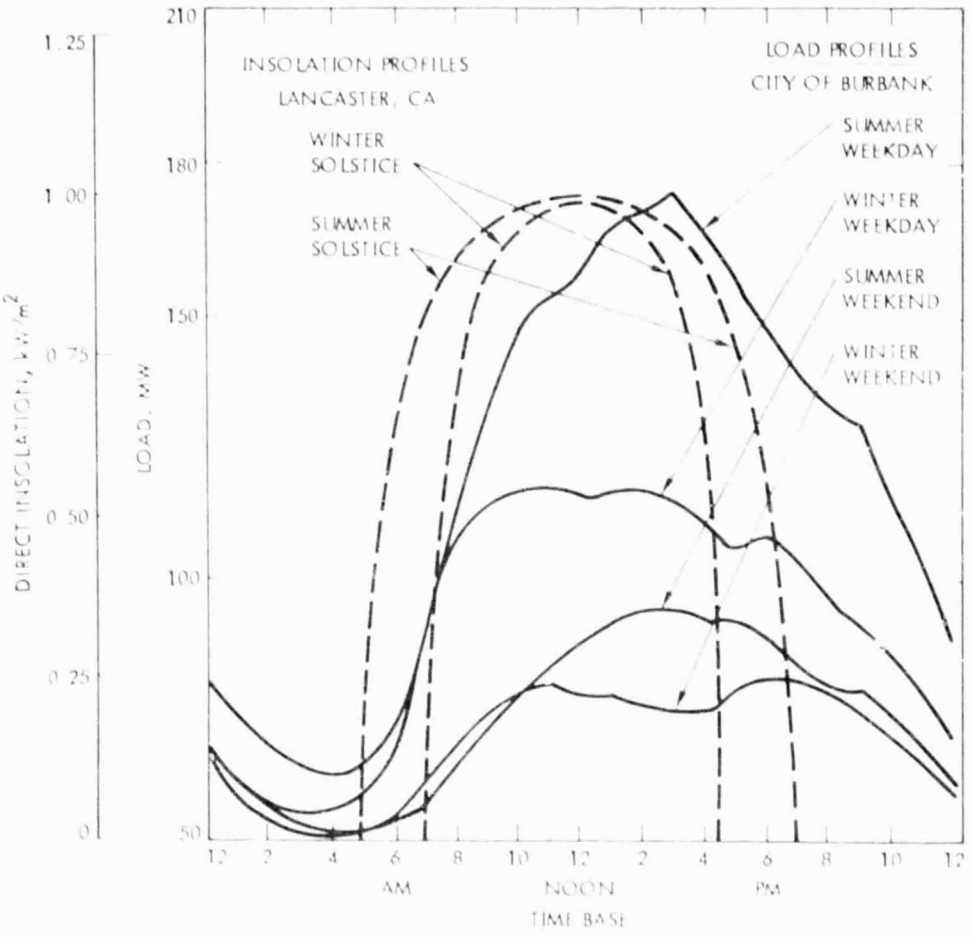

Figure 6. Load and Insolation Profiles

The characteristic 1976 load profile of the city of Burbank, CA, is compared against the insolation profile of Lancaster, CA. The shapes of the load curves are fairly typical for any city, with the large variation between weekday and weekend power levels being indicative of a heavy "industrial" load (44%). The early start time and noon lunch break for industry are clearly shown. The characteristic secondary peaking of residential load in the 6:00-9:00 p.m. region is also evident. Approximately half the generator capacity of Burbank is used only between the hours of 6:00 a.m. and midnight. The summer peaking at 3:00 p.m. is characteristic of maximum air conditioning demand.

Cloud-free insolation profiles are shown for extremes of summer and winter solstice. Peak insolation in both cases is approximately 1 kW/m^2, a condition typical of desert regions. Excluding approximately

the first and last half hour of the day (to accommodate startup and shutdown), average insolation flux level is about 0.85kW/m^2.

Cloud cover is characteristically random and has a significant effect for approximately 20% of the days. Approximately 20% of the annual solar energy is obscured by cloud cover and other atmospheric effects. The number of cloud passage incidents is almost exactly the inverse of the time for cloud passage.

Thermal energy storage is to be used to shift (timewise) and to shape the insolation profile to match the load profile. By use of microprocessor logic and switching, the matching is accomplished automatically in increments of 20-25 kWe. If thermal storage is not available, augmentation by fossil fuel combustion can accomplish a similar function, although with a different optimization. As noted previously, the combustor is designed to operate in a fossil-fuel fluid mode for constant power operation and cloud cover makeup so only additional fuel is required to meet any load demands.

Progress in the technology demonstration experiment has thus far been rapid. Performance expectations are staying high, while production costs in some areas of technology are indicating lower values than originally estimated. Unique system optimization concepts appear to be paying off.

The dish-Stirling near term and far term objectives are summarized in Table 1. The system development plan is presented in Table 2. The preliminary design and development step in the plan are now underway. Contractors have been selected who are defining design concepts through performance analysis and are planning verification experiments.

Table 1. Dish-Stirling Generation System Objectives

PERFORMANCE	EXPERIMENT (1981)	PRODUCTION (1990)
Efficiency (Electric to solar)	24%	35%
(Combustor to electric)	30%	40%
Power Output (constant)		
*No Thermal Energy Storage	22 kWe	10 MWe
*2 hour Thermal Energy Storage	17 kWe	10 MWe
Voltage	208V, 3ϕ	13.8kV, 3ϕ
Peak Engine Temperature	820°C (1510°F)	820°C (1510°F)
Average Coolant Temperature	50°C (122°F)	50°C (122°F)
COST		
Initial ($1979)	N/A	$6 million
Life Cycle (5,000 hours/year)	N/A	40 mills/kWeh
Scheduled Maintenance	N/A	10 mills/kWeh
OPERATION AND MAINTENANCE		
(Modular Redundancy Included)		
Life	25,000 hours	150,000 hours
Ambient Temperature Range	-18 to 50°C (0-122°F)	-30 to 50°C (-22 to 122°F)
Maximum Wind Condition (Stowed with combustor operation)	125 km/h (70 mph)	145 km/h (90 mph)
Automatic Cleaning (During peak operation)	N/A	Twice weekly
Scheduled Service Period (Excluding night-time replacement of failed modules)	N/A	10,000-15,000 hours
SAFETY AND ENVIRONMENTAL IMPACT		
Fencing and Lighting	Meets all Standards	Meets all Standards
Controls and Interlocks		
Toxicity and Corrosives		
Emissions and Effluents		
Noise and Aesthetics		
Erosion and Debris		

*Two alternate receiver concepts are being developed.

Table 2. Dish-Stirling System Development Plan

Study Phase	Mission Analysis	• Select Mission Type for Early Production Potential
	Performance Objectives	• Assess State-of-the-Art, Utility Requirements
	Trade-off Studies	• Size Components, Assure Interface Compatibility
		• Maximum Reliability, Safety
		• Minimize Cost, Fuel Consumption
Present Position	Preliminary Design and Development	• Select Contractors
		• Define System Design Concept
		• Perform Design Analysis, Verification Experiments
Feasibility Demonstration Phase	Detailed Design and Fabrication	• Prepared Detailed Drawings and Specifications Emphasizing Low Cost Practices
		• Fabricate and Assemble Test Unit
	Test and Evaluation	• Verify Performance and Perform Sensitivity Analysis
		• Identify System Optimization Criteria
Technology Development Phase	Component Improvement	• Cost Reduction and Scaling Studies Analysis
		• Interface Enhancement
		• Performance, Life and Materials Improvement
		• Control Optimization
	Design Optimization	• Define Load Requirements and Perform Cost Minimization
		• Minimize Installation Requirements
Technology Optimization Phase	Final Design	• Prepare Detailed Specifications and Drawings for a Design Amenable to Mass Production

CONTENTS

Figures

Tables

SECTION I

INTRODUCTION

A. GENERAL

The general goal of the Advanced Solar Thermal Technology subprogram is to accelerate the availability of cost-effective solar thermal power systems for a variety of applications by reducing the cost of components and improving system performance. These cost and performance improvements will be achieved through the application of advanced technology to the design, construction, and operation of solar thermal power systems.

The specific goals of the subprogram are to:

(1) Demonstrate by the mid-1980s the technical viability of advanced large and small solar thermal systems having the potential for energy costs 25% to 50% lower than systems based on current or near-term technology

(2) Identify new, economically viable applications of solar thermal power to help reduce the nation's dependence on critical fossil fuels

In line with the above goals, a task was initiated to complete a dish-Stirling subsystem feasibility experiment by FY 1981, with subsequent transfer of the technology to the development and engineering applications projects.

Energy costs of solar thermal power systems may be reduced through the use of lower-cost, longer-life surfaces and components, by increasing system operating efficiencies, and by reducing the requirements for maintenance. At this time, emphasis is being placed on improving conversion efficiencies and reducing costs of the key components. Figure 1-1 shows the effect on energy costs of improved system efficiency and decreased collector costs.

B. OBJECTIVE AND BACKGROUND

The task undertaken by JPL/LeRC for the Advanced Thermal Technology subprogram is to develop advanced technology to improve life cycle costs of solar thermal electric power plants.

As a result of the systems and advanced studies activities, a point-focusing concentrator, Stirling engine/alternator solar thermal electric power plant concept was identified in FY'77 as the most likely, cost-effective, candidate system to be developed for future small solar power applications.* The dish-Stirling Advanced

*T. Fujita, et al, "Projection of Distributed-Collector Solar-Thermal Electric Power Plant Economics to Years 1980-2000," DOE/JPL 1060-77/1, Dec. 1976

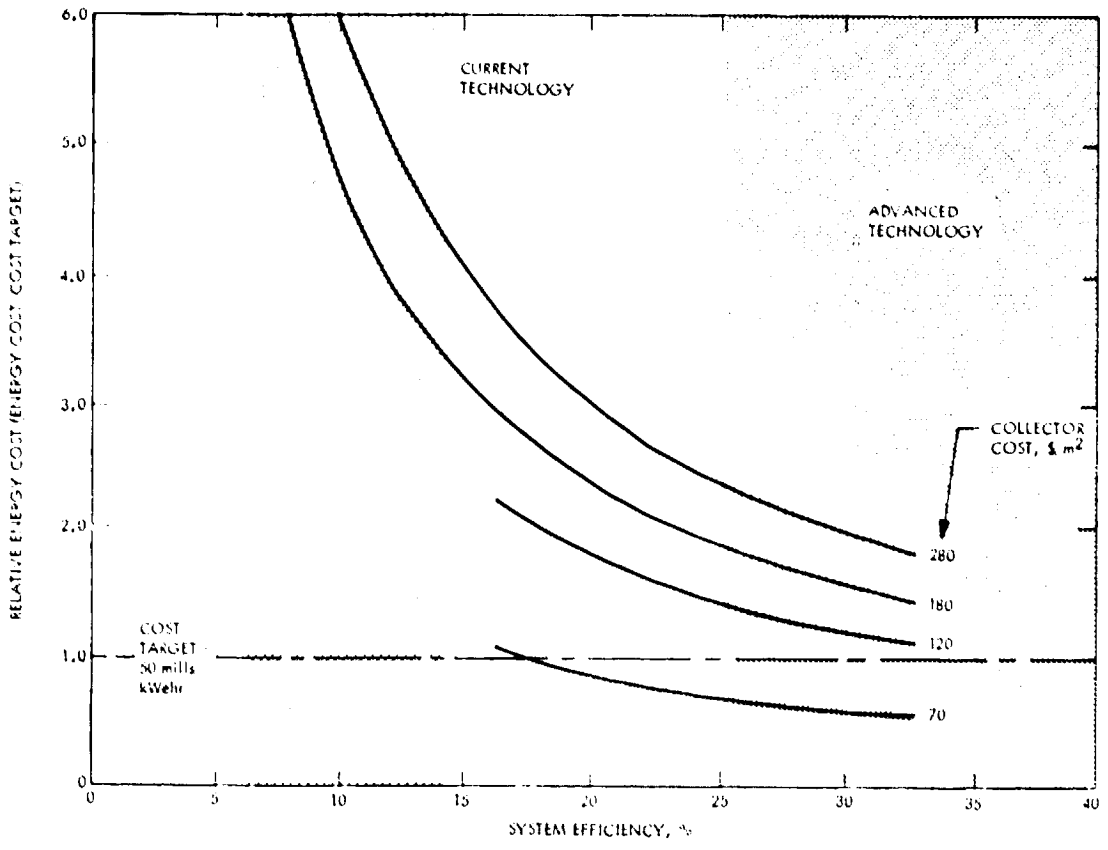

Figure 1-1. Effect of Improvements in System Efficiency on Energy Cost Reductions

Technology Development Task was initiated in October 1977 with the goal of demonstrating the feasibility of the concept through a single prototype module test program within six years. The 1984 objective is greater than 25% system efficiency in generating electricity with a module direct cost of less than $700 (1978) dollars per peak kilowatt of electricity (kWe) at the generator. A somewhat longer-term goal is to reduce the module cost to less than $600 per peak kilowatt of electricity at the generator.

C. THIS REPORT

This report covers work completed during the last six months on the task of design, fabrication, assembly and test of a paraboloidal dish Stirling engine/alternator module. Since the beginning of the task in October 1977, a selected conceptual design has emerged from many alternatives. During fiscal year 1979, the preliminary design of all subsystems will be completed. After detail design, fabrication, assembly and test, selected key components and subsystems will be assembled for system test and proof-of-concept demonstration in fiscal year 1981.

Throughout the course of this task, progress will be reported at monthly task meetings, quarterly Advanced Solar Thermal Technology Project meetings held at the Jet Propulsion Laboratory, Pasadena, California, and at semiannual reviews of the Advanced Solar Thermal Power System subprogram held in conjunction with the Solar Energy Research Institute in Denver, Colorado. The purpose of this report is not only to meet programmatic objectives, but also to disseminate information about key technical innovations which may be of value or interest to technological corporations engaged in research and development of solar thermal electricity generating plants. In addition to several hundred copies distributed directly by JPL, the report will also be published and distributed to a wide range of organizations by the DOE Technical Information Center.

Task members at the Jet Propulsion Laboratory and the Lewis Research Center have defined the basic conceptual design, and will specify the major system requirements and direct system test and operations. Industry will be utilized in the performance of technical work to the maximum extent feasible to develop detailed designs, fabricate and test components, and eventually to produce the subsystems and systems for applications.

A small (less than 10 MWe) solar-thermal electric generating plant design concept was completed as a baseline system design using projected 1985 technology. This concept, when in mass production, should meet the solar thermal electric plant capital cost target of $600 per kWe (1978 dollars). Operations and maintenance costs should be sufficiently low so that the cost of electricity from the plant would be about 50-60 mills per kilowatt-hour (1978 dollars). An engineering prototype model of one 20 kWe module of the small solar thermal electric generating plant was completed (Figure 1-2).

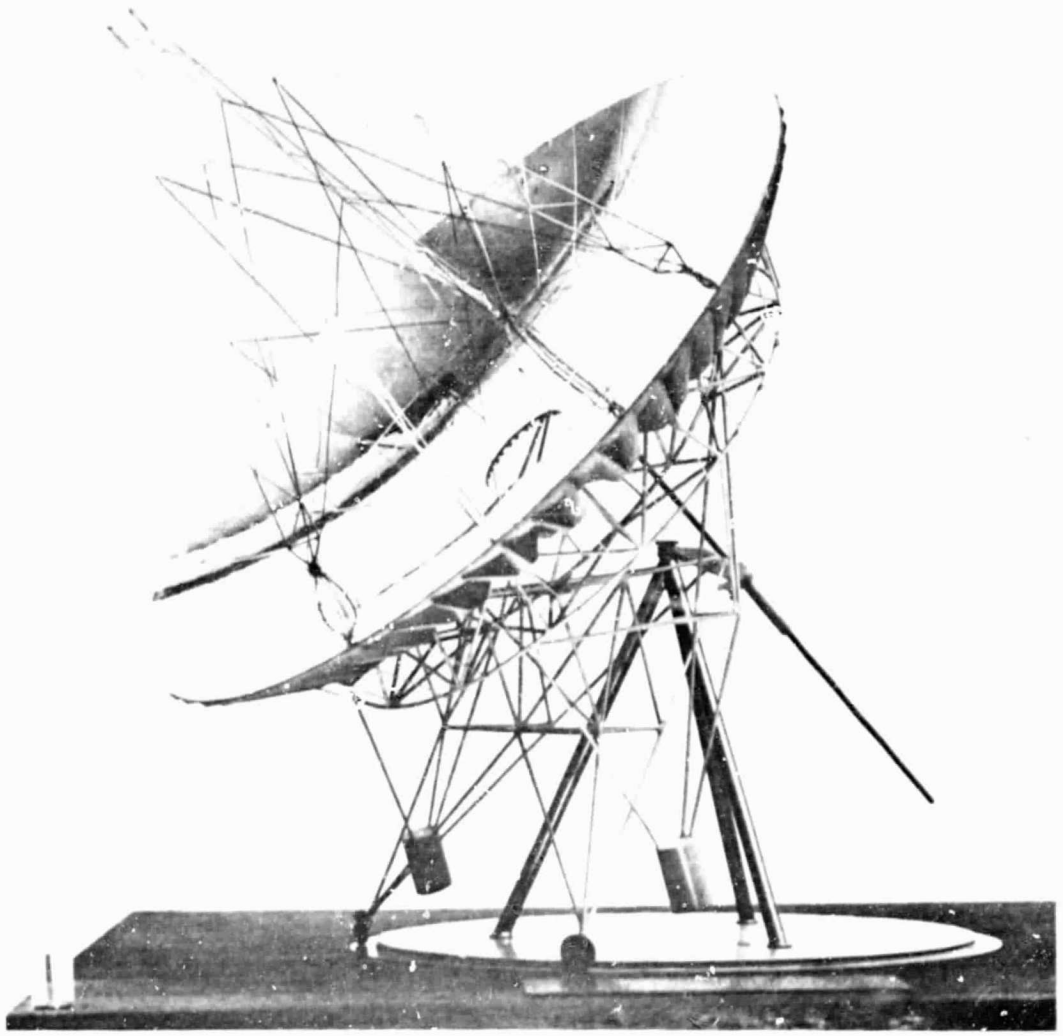

Figure 1-2. Model of the Point-Focusing Concentrator, Stirling Cycle Engine Powered Generating Module

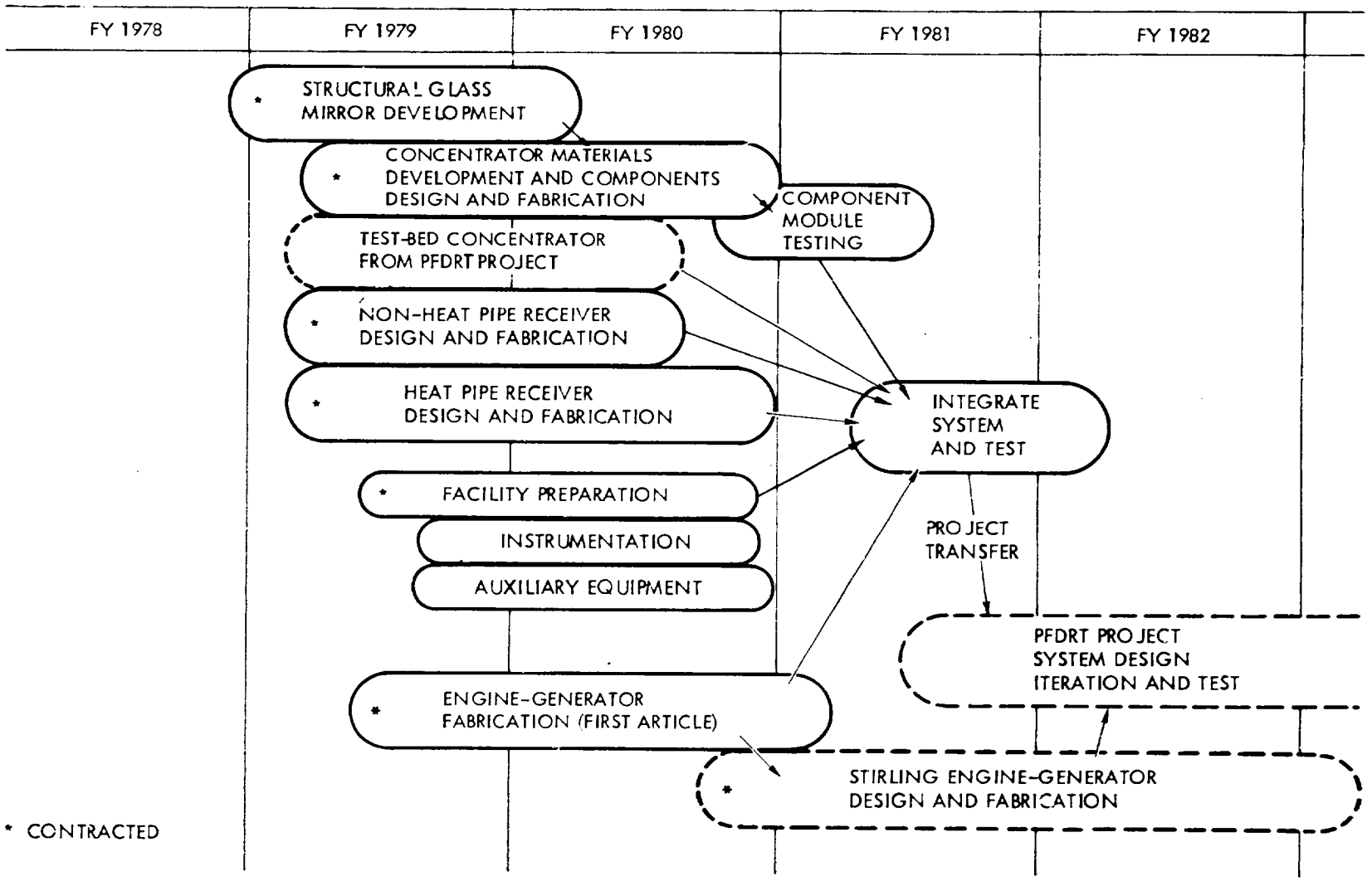

Figure 1-3. Schedule Dish-Stirling Development

Implementing the conceptual design through preliminary design, detail design, fabrication, assembly, and component test by industry has been the thrust of the FY'79 effort on this task. These current and forthcoming procurement actions, as well as some of the results of ongoing contractual conceptual design efforts, are described in the present report.

For convenience, this report is divided into sections relating to systems integration, component design, and analytical methodology employed. These sections are:

I. Introduction

II. System Description

III. Technical Approach

- A. System Design
- B. Solar Receivers
- C. Stirling Engine
- D. Solar Concentrator
- E. Liquid Metal Transport
- F. Power Processing/Management

D. SUMMARY

In this task, emphasis is placed on utilizing a team of industrial contractors to develop and demonstrate advanced solar thermal electric technology at the system level. Efforts include; component conceptual design, evaluation of alternatives, detailed design of the best cost-effective and high performance concepts, fabrication and assembly of components, and integration and test of a complete subsystem module of the smallest size that will demonstrate potential system performance. Components and/or subsystems may be transferred at any appropriate time into engineering development programs. The Advanced Subsystems Development task will then proceed to the next technology improvement. Figure 1-3 shows the present plan for development of the dish-Stirling concept as the first advanced development system.

During FY'79, the principal effort has been directed toward initiating contracts for all major dish-Stirling system components, detailed specification of the prototype demonstration hardware, detailed specification of the prototype system interfaces and test requirements, and detailed design of prototype demonstration hardware. The early system technology demonstration will include a 37%-38% efficient (electric out/thermal in) kinematic Stirling engine with heater wall temperature of approximately 816°C (1500°F). Two receiver alternatives will be built and tested. One receiver will

have thermal energy storage and the other will be direct-coupled to the Stirling engine. Both concepts will include hybrid system operation with a fossil-fuel combustor. The solar receiver, thermal storage, and engine will be affixed to the concentrator dish, TBC, (approximately 11 meters in diameter) at its focal point. The engine-generator will operate at a constant power level (approximately 60 kWt input) and provide a precise three-phase electric output to a load. System testing is scheduled for FY'81.

Fossil-fuel hybrid operation and thermal storage requirements are being optimized for low cost. Since, for public utility power applications, it may be desirable to make use of the significant correlation between the available, direct, solar insolation and the load demand profiles, system optimization is defined parametrically. Thermal storage and liquid metal heat transport studies are being performed under subcontract to the General Electric Company. These studies are augmented by limited in-house investigations. Contractors for the early system technology demonstration are identified in Table 1-1.

Power processing and distribution for both primary and parasitic loads is based on a large field of small power units having constant power and fixed frequency output from their power conversion units. Cost optimization and cost reduction concepts are being detailed as part of the Advanced System Development Studies.

Table 1-1. Dish-Stirling Technology Prototype Contractors

Component	Contractor	Estimated Prototype Delivery
Non-Heat Pipe Solar Receiver	Fairchild Stratos Div.	6/80
Non-Heat Pipe Solar Receiver	General Electric Co.	6/81
Stirling Engine/Generator	United Stirling (Sweden)	6/80
Stirling Engine/Generator	GE/No. Amer. Phillips	6/81
Heat Pipe Solar Receiver/TES	General Electric Company	10/80
Advanced Concentrator Components Development and Conceptual Design	Acurex Corporation and Pittsburgh Corning Corp.	1/81
Advanced Cellular Glass Concentrator Conceptual Design	Solaramics	6/80

SECTION II

SYSTEM DESCRIPTION

A dish-Stirling solar thermal electric generating concept is being developed for small power systems applications. The Stirling engine coupled with a two-axis tracking, point-focusing concentrator (dish) has potential for high efficiency at low cost. A first system for demonstration, designated Advanced Development System No. 1 (ADS-1) and depicted in Figure 1-2, is to be completed in FY'81. Significant features of the system include:

(1) a point-focusing solar concentrator, (test-bed concentrator from PFDRT Project)

(2) a 20 kWe Stirling cycle engine driven alternator

(3) 800-900°C (1500-1650°F) advanced receiver

(4) fossil-fuel combustion hybrid operation

(5) a thermal energy storage option

A high technology approach is thus defined and a team of industrial contractors has been selected for development of the subsystems. The dish-Stirling system will be assembled and tested by JPL at DOE's Point-Focus Solar Test Site (PFSTS) near Lancaster, CA.

Early system development and test is scheduled (Figure 2-1) for the ADS-1. Two quite different receiver alternatives are being developed in parallel. A heat pipe solar receiver with thermal energy storage (TES) will be demonstrated as well as a minimum-cost, direct-coupled receiver which includes a fossil fuel combustion capability to smooth the variations of solar flux (insolation). Kinematic Stirling engine-generator contracts are in process for a 37% efficient unit. Figure 2-2 shows the dish-Stirling system block diagram.

A. STIRLING ENGINE-GENERATOR

The Stirling engine is at the heart of the dish-Stirling system. Although the technology has been brought to a reasonable level of maturity by companies in the Netherlands and Sweden during the 1960s and 1970s, there has been very little Stirling engine application until now. Risk capital is always limited, and there has been no urgent demand for Stirling technology. Today, small, efficient, quiet and non-polluting Stirling engines are without peer. The Stirling cycle can no longer be ignored now that energy and environmental constraints are so critical. Several companies are moving towards large scale production of small Stirling engines for automotive and/or recreational vehicle applications.

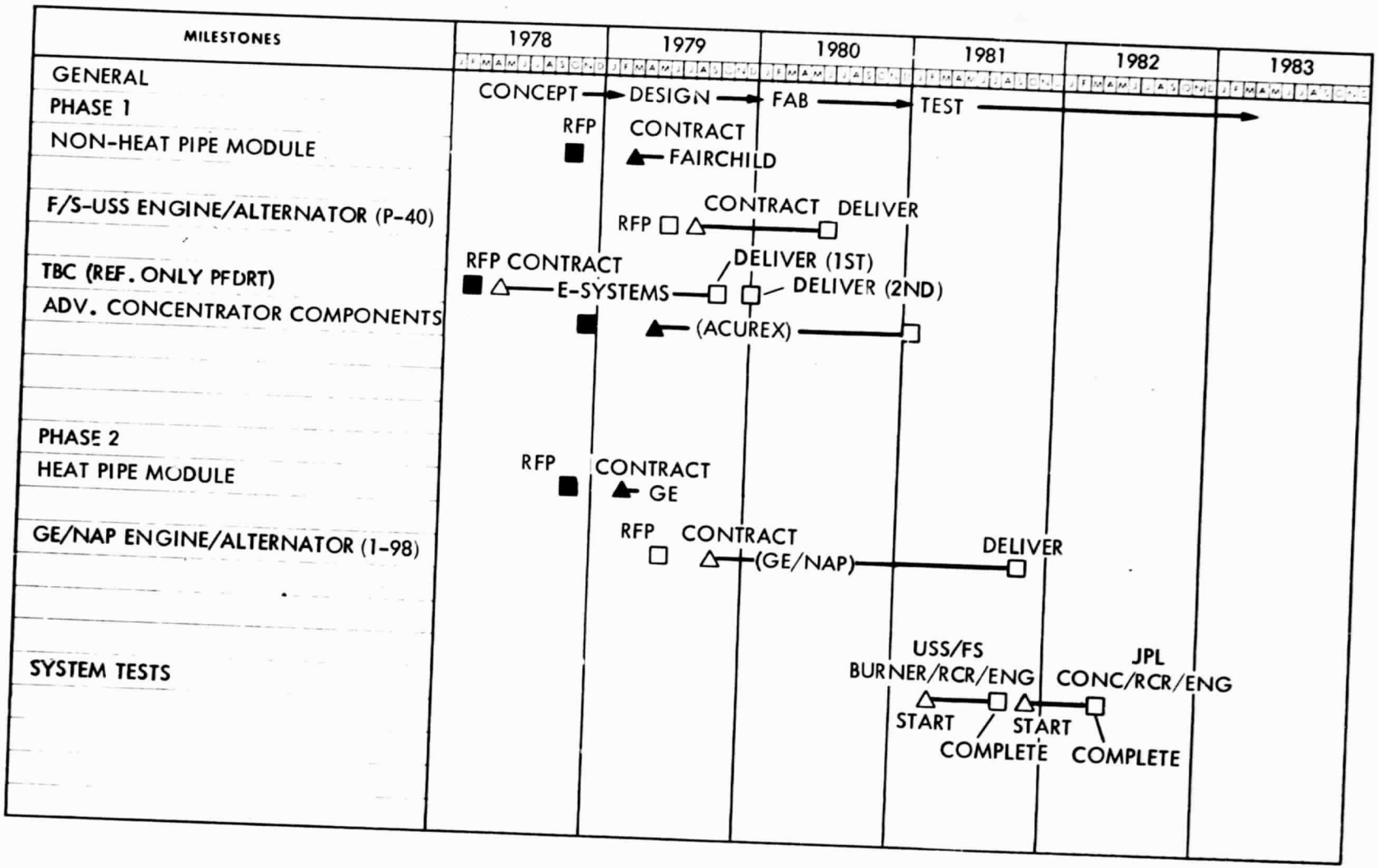

Figure 2-1. Dish-Stirling System Test Schedule

The unique high efficiency of the Stirling cycle is a result of its isothermal heat addition and removal during expansion and compression, and through isothermal regenerative heat addition and removal at a constant volume. Present efficiency capability for the Stirling cycle engine is approaching 60% of Carnot. Future expectations are 70% Carnot efficiency. High efficiency is important to the solar thermal electric system. Because of the unavoidably larger concentrator, it is cost effective to develop a high-efficiency energy collection and conversion system.

The kinematic Stirling engines currently available will be used in the early dish-Stirling system. The direct-coupled, Fairchild/Stratos design is shown in Figure 2-3. Only minor modifications of heat exchanger and lubrication are required for operation of the USS P-40 engine with a solar receiver at 20 kWe and 816°C (1500°F). Engines can be modified and delivered within 10-15 months. Initial versions are expected to attain 37% engine-generator efficiencies. Further improvement of efficiency to 43% is expected later by reducing mechanical drive losses and by optimizing engine thermodynamic and mechanical operation. Such modification is a relatively low-cost operation and can be accomplished on the schedule shown in Figure 2-1.

B. ADVANCED CONCENTRATOR

Besides the Stirling engine, the dish-Stirling system is dependent on the development of a high-performance, low-cost parabolic concentrator. Three factors contribute to low cost in the current approach. First, low-cost materials are utilized, particularly in the cellular glass construction of the parabolic mirror substrate. Second, this subsystem is to be designed for minimum mass. In automated production it is equated to minimum cost. Third, the subsystem is to have minimum complexity, both structurally and mechanically. Factory prefabrication is to be emphasized, with absolutely minimum field assembly and site preparation required. The extent to which these elements are provided will ultimately define how well cost goals can be achieved. The cost goals are dependent on the success and provision of these elements.

The early dish-Stirling concept studied by JPL (Figure 1-2) will be reconfigured and designed, and critical materials and subsystems will be fabricated and tested by an industrial contractor. The mirrored, cellular glass substrate concept is shown in Figure 3-11. It is the responsibility of the concentrator developer to produce a design that will lead to low-cost automated production.

C. ADVANCED RECEIVERS

Two completely different receiver technologies are to be demonstrated in the dish-Stirling system. The first of these, the dish-Stirling solar receiver (DSSR), is a minimum-cost receiver directly coupled to the Stirling engine (Figure 2-3). Concentrated insolation is directed through the receiver aperture and impinges on the surface of a conical receiver body. Seventy-two helium heat-exchanger tubes are formed or contained within this receiver body and

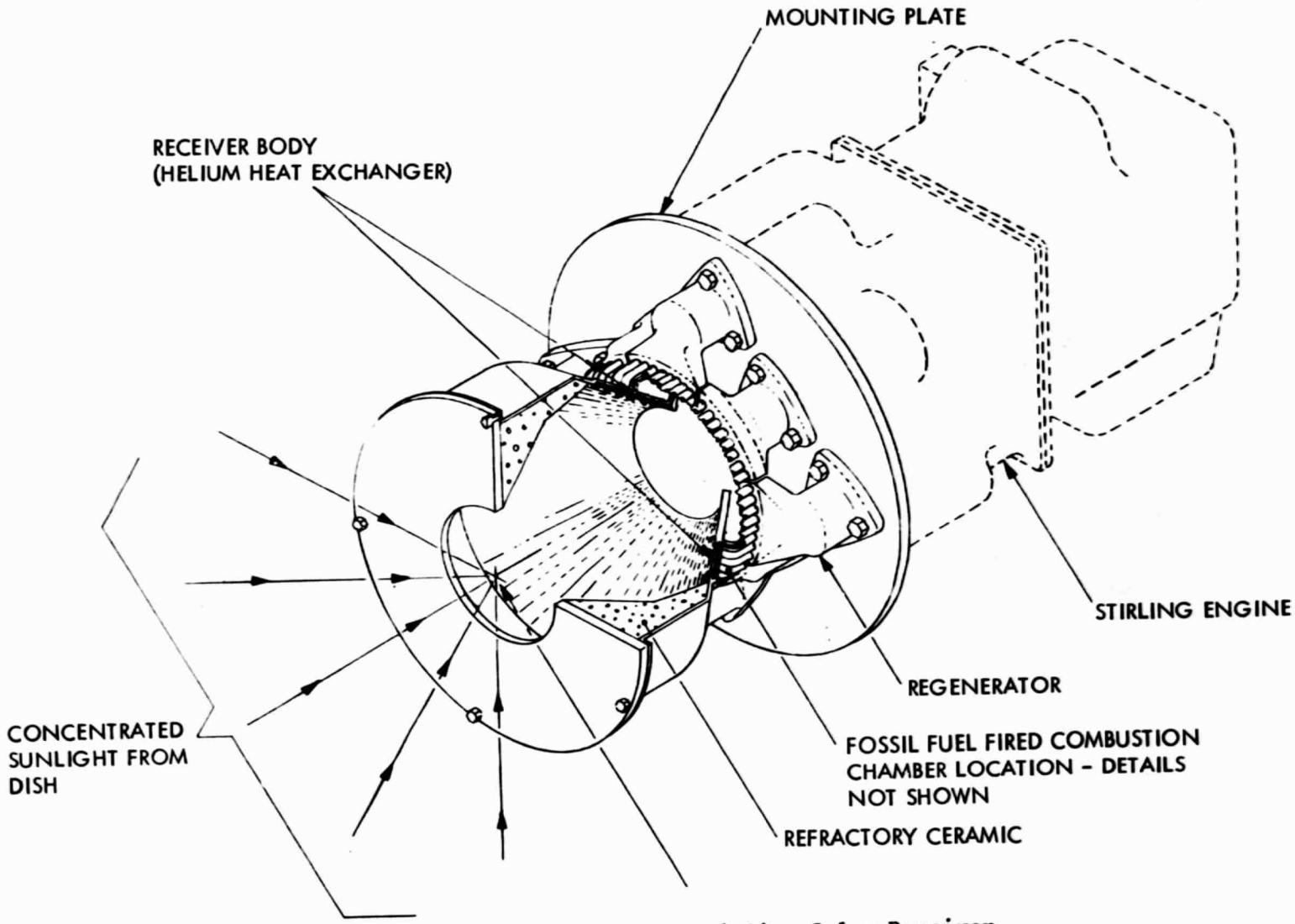

Figure 2-3. Direct-Coupled Dish-Stirling Solar Receiver Showing P-40 Stirling Engine

will operate at an average tube wall temperature of 816°C (1500°F). The heat-exchanger tubes are carried back to the Stirling engine and brazed to manifolds at the engine regenerators and cylinder heads. Every effort is made to minimize complexity and cost of the receiver. No thermal storage is provided, other than thermal inertia of the receiver structure.

The second dish-Stirling receiver technology to be demonstrated is the Heat Pipe Solar Receiver with Thermal Energy Storage (HPSR/TES). This concept (Figure 2-4) evolved from liquid metal heat transport applications studies of FY'78. The data showed that any significant thermal storage in a solar receiver leads to high receiver temperatures unless auxiliary heat transport is provided. The HPSR/TES employs a primary and secondary heat pipe arrangement to perform this heat transport. The receiver provides approximately one to two hours of TES. Concentrated insolation impinges on the surface of 27 primary heat pipes forming the cylindrical receiver cavity. These heat pipes transport the heat through a header into a large-diameter secondary heat pipe containing a large number of externally "wicked," cylindrical TES capsules. The TES capsules operate at slightly lower temperature than the primary heat pipes, assuring needed heat transport to charge the capsules. At the opposite end of the secondary heat pipe, the Stirling engine heat exchanger tubes intrude into the vapor space and receive heat from the TES. The entire unit is enclosed in an insulated jacket to prevent excessive loss of stored heat. The Stirling engine is also designed for minimum heat conduction loss. The primary heat pipes are unwicked at the condenser end to prevent heat flowback from the TES into the receiver cavity.

Both the HPSR/TES and DSSR are to include hybrid operation with a fossil-fuel combustor. In each receiver, a combustion unit is to be placed around the outside of the primary heat transfer surface. For the DSSR, the combustion heating is from the back side of the conical heater body into the heat exchanger tubes. For the HPSR, the combustion heating is around the outside of the primary heat pipes. Heat losses through the receiver aperture by radiation and convection will be larger than desired, but acceptable. An aperture cover for the DSSR has been suggested. Alternate ways of introducing combustion heating for the HPSR are to receive future study because of the decoupling from the Stirling engine by the TES.

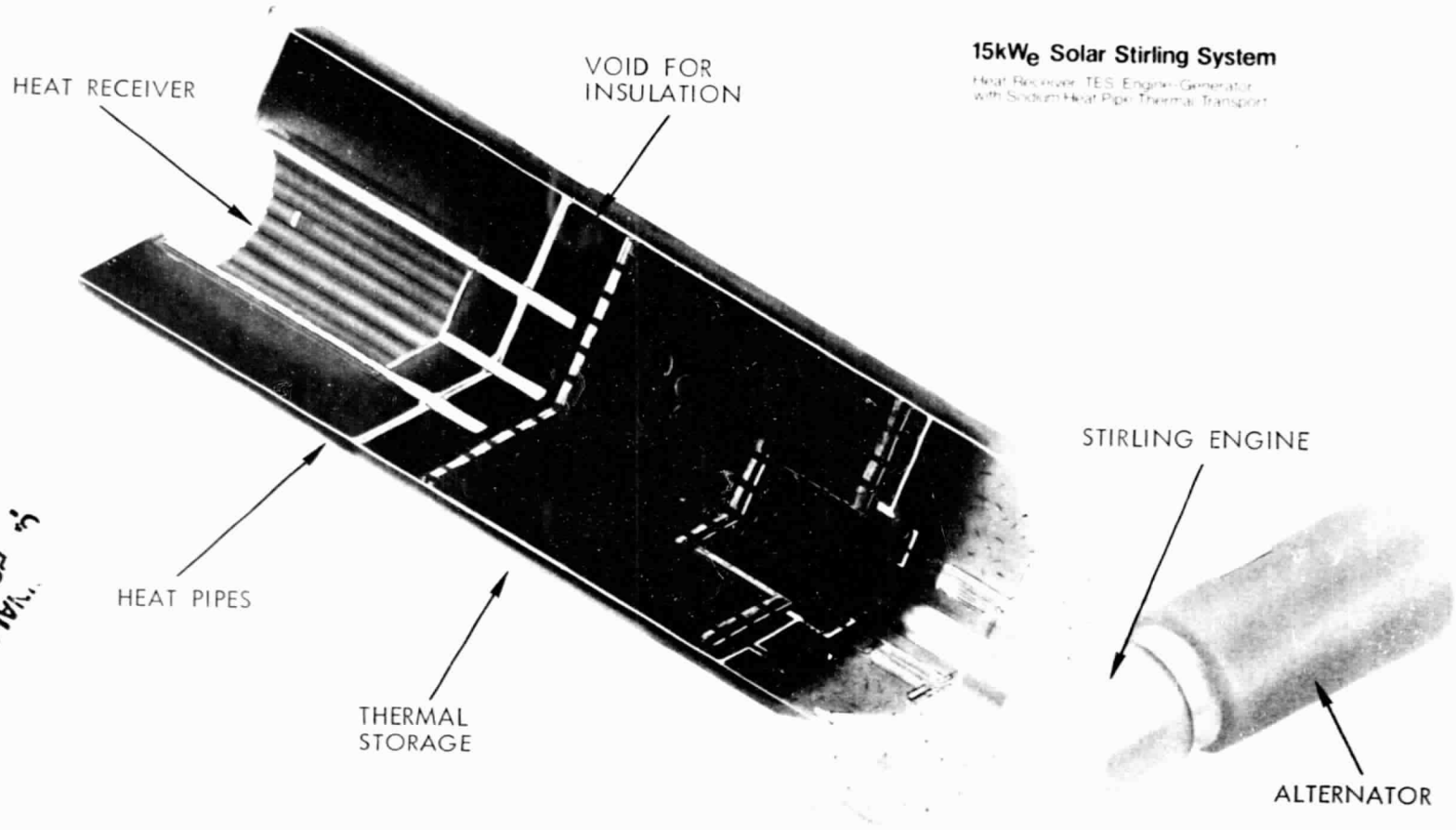

Figure 2-4. 15 kW_e Solar Stirling System Heat Receiver/TES/Engine-Generator with Sodium Heat Pipe Thermal Transport

SECTION III

TECHNICAL APPROACH

A. SYSTEM DESIGN

A high technology approach to system design has been defined. The objectives of the dish-Stirling experiment are: (1) to demonstrate availability of the needed technology at the system level, (2) to identify the performance parameters that affect system optimization, and (3) to evaluate the potential of the system for meeting cost goals. System efficiency is exceptionally important. Every effort is made to design for high efficiency, to operate at peak efficiency, to eliminate complex components and controls, and to provide features (such as TES and hybrid operation) to increase the worth of the energy produced. Temperature constraints of presently available, low cost materials establish the maximum power conversion operating temperature at approximately 816°C (1500°F).

Two iterations of advanced technology are therefore planned. The first system demonstration provides early evaluation of technology. Several technology improvements to be made depend somewhat on better definition of the parameters from the initial demonstration. A more advanced system demonstration, will follow with at least the following improvements:

(1) An advanced Stirling engine-generator having an efficiency above 45%

(2) An advanced thermal energy storage (TES) subsystem, developed specifically for low cost

(3) An advanced combustor design with improved efficiency

1. Constant Power Operation

The early system will demonstrate a constant-power, constant-frequency, 20 kWe unit output. Operation at constant power allows maximum efficiency and minimum control and interface complexity of the engine-generator. Furthermore, output can be tied directly into a utility distribution grid without costly or inefficient processing.

Constant power operation is achieved in one of two ways. First, hybrid operation is provided by the fossil-fuel combustor on the receiver. Variable solar heat is thus augmented by combustion heating to produce a fixed power level. The second method of achieving constant power operation is with TES, and this is being evaluated in the heat pipe receiver design. The latent-heat TES provides a constant power output to the Stirling engine without itself needing a constant power input. This permits a further simplification of controls. Furthermore, the need to operate the fossil fuel combustor

at low power level, with resultant low energy effectiveness, is eliminated. The TES cyclic efficiency is high (97%).

2. Operating Load

There appears to be a strong correlation between the daily solar input (insolation) profile and the daily load demand profiles of a utility (Figure 3-1). Further study is now in progress concerning the implications of this correlation in establishing a capacity rating for solar power systems. In Figure 3-1, the typical load profile of the city of Burbank is compared with the insolation profile of Lancaster (near the PFSTS). This correlation indicates that a minimum of diurnal storage will be needed, either TES or fossil fuel, in order to accommodate all except base load requirements.

Cloud cover is characteristically random and has a significant effect for approximately 20% of the days. At Lancaster, approximately 20% of the annual solar energy is obscured by cloud cover. Such conditions call for augmentation by fossil fuel energy in order to assure a maximum capacity rating for the solar energy system. For reliability, the large, modular array of units, all with hybrid and TES operation, will have minimum requirements for redundancy. Reliability analysis is needed to define this need.

With TES, individual units may be turned on and off as load varies. Thermal storage continues to accept the full insolation independently of load. Operational usage of the individual units may be automatically sequenced as the available thermal storage is saturated or depleted. Programming includes a coarse integration of measured insolation for best utilization of energy.

3. Economic Trade-offs

A hybrid solar power plant has both an energy rating and a capacity rating. Energy cost is typically associated with fossil fuel operation and with energy storage. Production cost of a dish-Stirling system, should be under $500-600/kWe. Although this cost may be more favorable when compared to a base load plant, it must also compete with a gas turbine peaking unit costing approximately $150/kWe installed. The gas turbine has its associated high cost of critical fuels, operation, and maintenance. Minimizing the fuel, storage and O&M costs of the solar plant is therefore necessary.

Use of the present configuration of the dish-Stirling solar power system as a baseload plant should be limited. Hybrid fossil fuel operation is not highly efficient if the combustor is incorporated in the receiver volume. Presently available thermal storage, if used in large amounts, will require a major increase in collector field size. It is for swingload applications that the solar power system has the strongest potential.

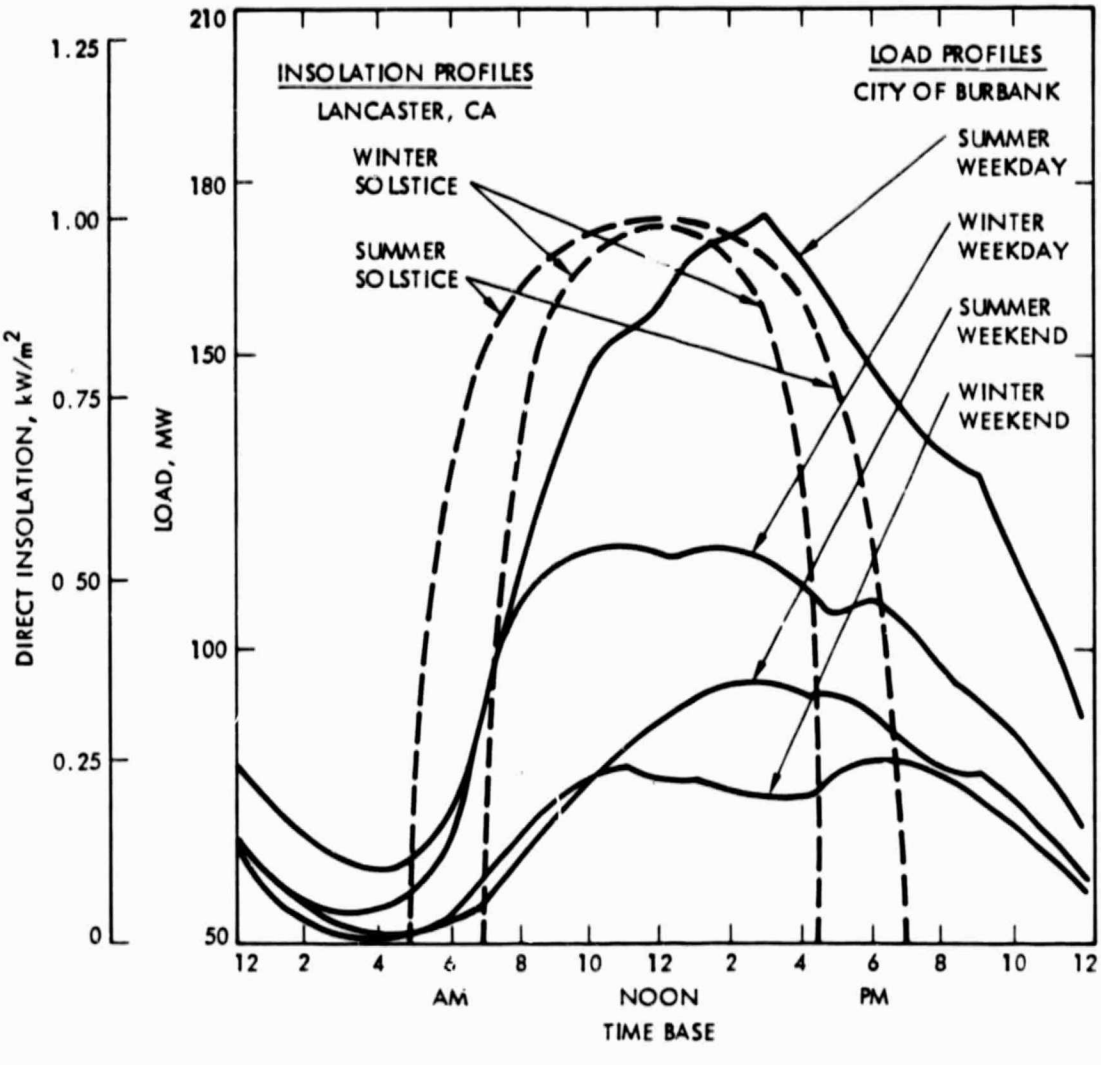

Figure 3-1. Comparison of Typical Load and Insolation Profiles

Cost optimization for a small solar power system with receiver-mounted TES is shown by Figure 3-2. For a given set of assumptions, cost of subsystems and fossil energy may be plotted as a function of installed TES. At a constant unit power output, engine-generator cost is fixed. Receiver and TES costs are estimated to increase linearly with the amount of installed TES. Concentrator costs, however, will increase very rapidly with increasing TES based on presently available materials. Not only must the concentrator size increase, but also the structure to support a larger TES must increase.

Fossil fuel energy cost is indicated in Figure 3-2 as if it were a capacity cost. Such approximation is inaccurate and requires additional study. For large values of TES, the fossil fuel requirement is low. It is used only for cloud cover makeup. The principal cost element should be the capital cost of the fossil fuel combustor. But when TES is reduced and more of the diurnal storage requirement replaced by fossil fuel, the fossil fuel energy cost will become significant. It is expected that the detailed studies now being planned will show a distinct minimum cost condition with some amount of TES.

Changing capacity rating of the system will also change the optimum value of TES. A full treatment of these parameters will be provided in future reports.

B. SOLAR RECEIVERS

1. Dish-Stirling Solar Receiver (DSSR)

A cross section of the DSSR is shown in Figure 3-3. The unit is 68.5 cm diameter and 46 cm long. Aperture diameter has been initially specified as 22 cm, based on a concentrator slope error of 2 mr.

The conical receiver body is sloped at 60° to the axis (half angle), at a maximum distance of approximately 34 cm behind the focal plane. At this position, incident solar flux shown in Figure 3-4 is analyzed to be a maximum of 353 kW/m^2. A removable ceramic plug at the center of the receiver cone, allows access to mounting bolts for the P-40 engine. The pebble bed gas combustion unit at the back of the receiver body operates at a temperature below 1650°C (3000°F) and provides a low NO_x emission characteristic. The cylindrical/conical inlet and exit air passages and the air preheater heat exchanger are still in early stages of design. Minimum pressure is achieved by the pebble bed configuration of the combustion and requires only about 0.1 kW of fan power. An alternate combustor design without a pebble bed appears very promising and will be evaluated during the next period.

Design studies have been done for two alternative concepts for the conical receiver body. The first, shown in Figure 3-5, utilizes two plates of Inconel 617 with grooved helium passages in their

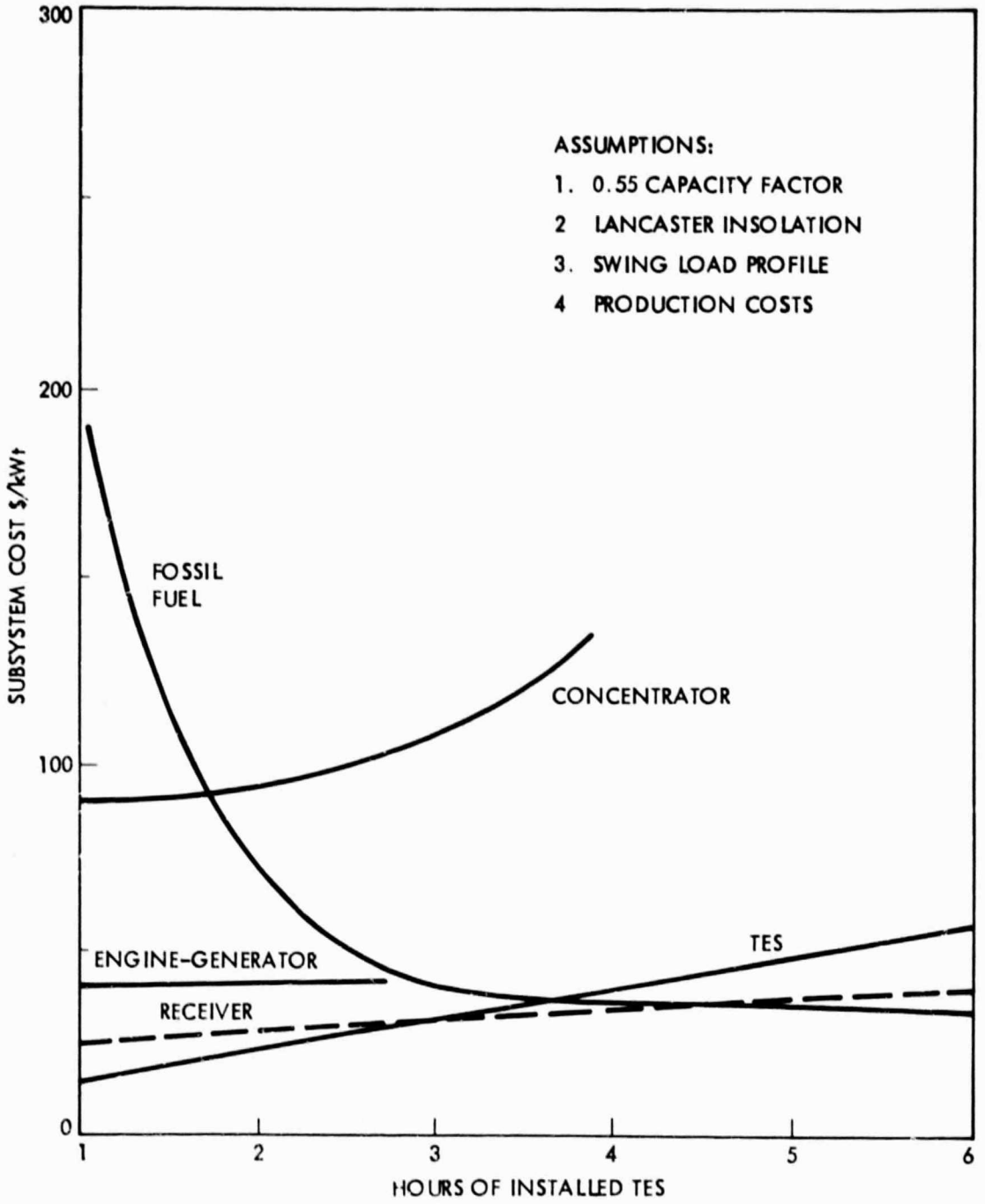

Figure 3-2. Cost Trade-offs for Received-Mounted TES

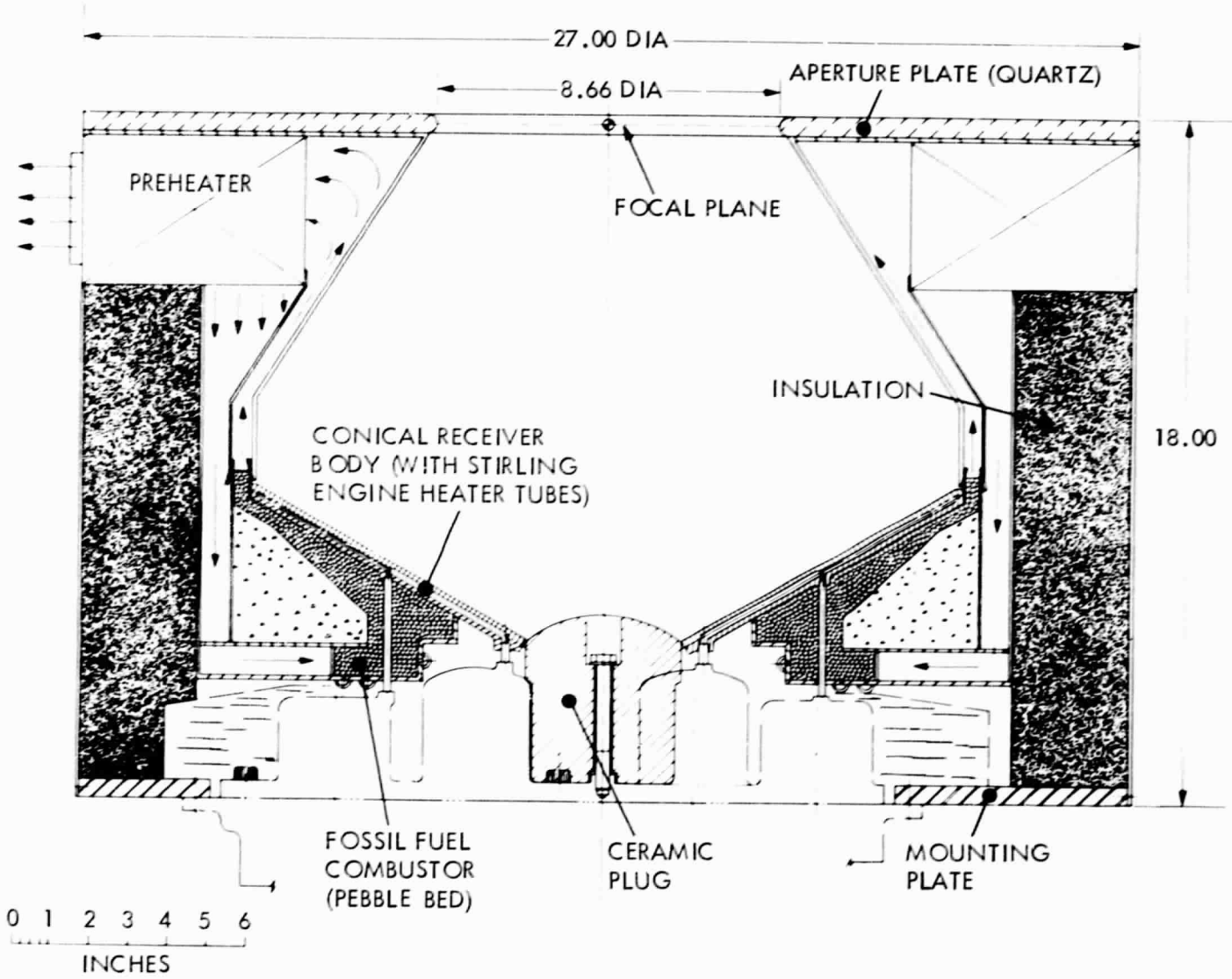

Figure 3-3. Dish-Stirling Solar Receiver Cross Section

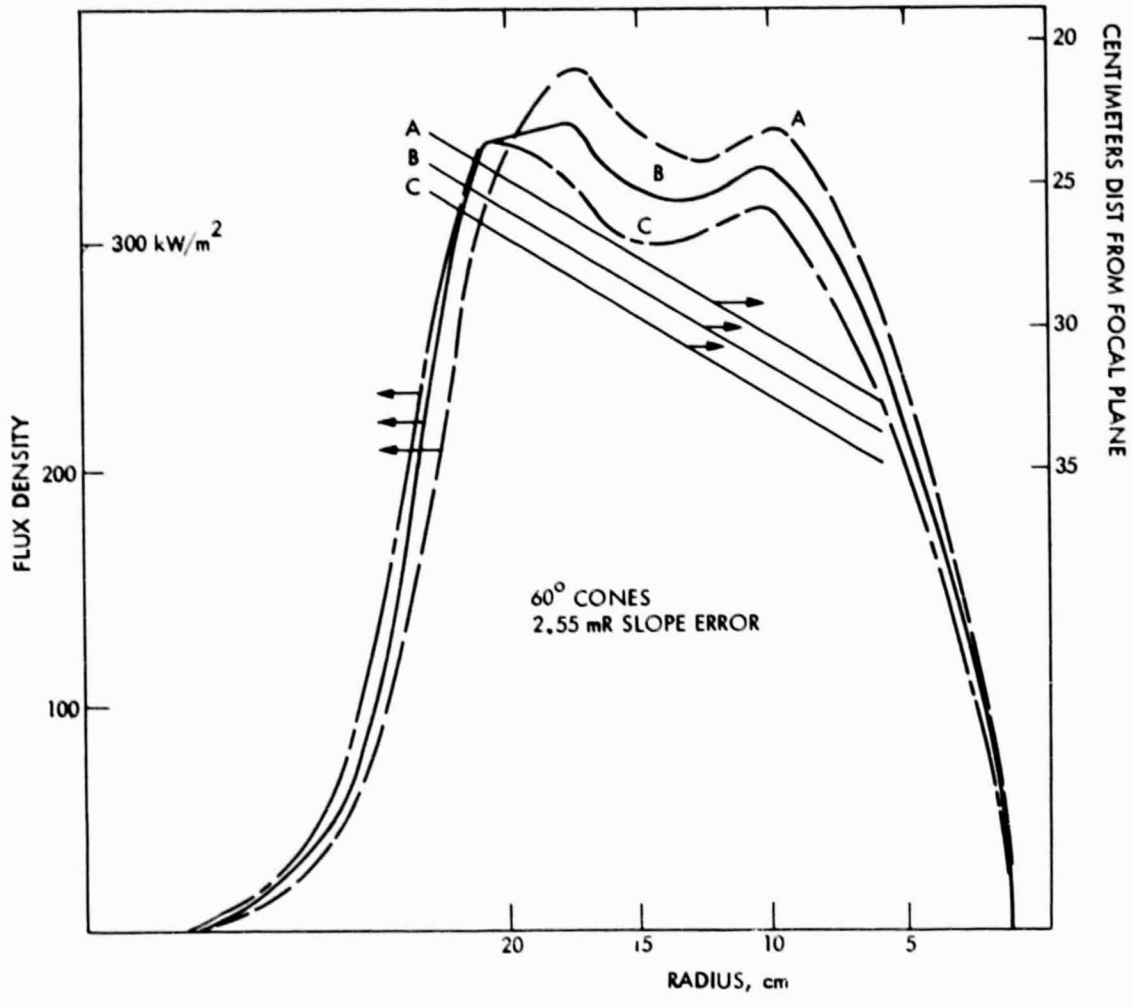

Figure 3-4. Flux Density Sensitivity with Distance from Focal Plane (60° Cone)

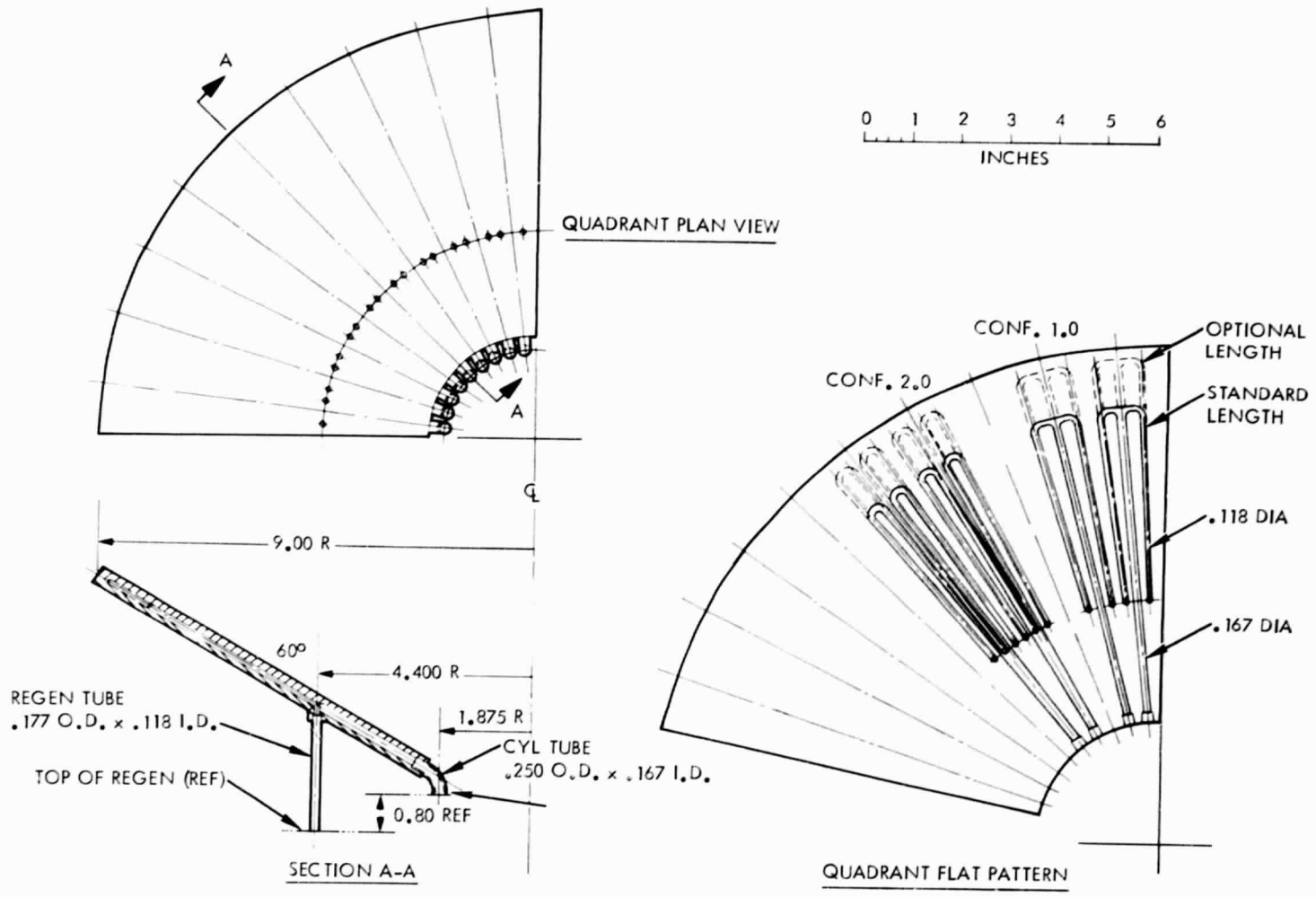

Figure 3-5. Conical Receiver Body

matching faces. The plates are then brazed together with the interface tubing from the Stirling engine in a single assembly braze operation. The design alternative, which may be less expensive utilizes 72 multimet (N=155) tubes with the inter-tube volume filled with a plasma sprayed material such as copper or nickel alloys at 95% or greater material density.

At the Stirling engine interface, the solar receiver proper is cantilevered from the Stirling engine. The mass of the basic receiver is approximately 25 kg. The fossil fuel combustor and outer ring of insulating material have a mass of 25-50 kg. The aft mounting ring is attached to the engine structure independently of the receiver body. The receiver aperture is precisely mounted with respect to the Stirling engine and the engine is then aligned to the concentrator. The curves of Figure 3-4 show that receiver positioning within approximately 1 cm is vital.

C. STIRLING ENGINE

1. General

A key task of the Advanced Solar Thermal Technology Project is the design and development of Stirling engine specifically suited for high-temperature solar heat input. The approach is to design an engine incorporting components whose maturity date is circa 1985. For the 1985 engine-generator, efficiency is estimated to be in excess of 40% at 1500^{o}F.

Both kinematic and free-piston Stirling are candidates for solar energy conversion systems. The kinematic Stirling engine transmits power through connecting rods of other linkages to a rotating alternator. In the free piston engine, the power piston is in the same cavity as the linear alternator. But the heat input components would be almost identical for both types of engines. The kinematic Stirling engine has a much longer and more extensive development history than the free piston engine whose conception is of recent origin. After thousands of hours of engine operating in laboratories in the U.S., Holland and Sweden, the kinematic Stirling has well defined problem areas: shaft seal life is limited; improvements in heat transfer and fluid flow are required for the achievement of the engine's efficiency potential; and more cost-effective materials and production methods must be identified.

The design of free piston engines is an art and engine development is in the early experimental stage. Components modeling techniques have not been extensively validated and laboratory engines larger than 3 kW have not yet been built. Linear alternators required for direct electrical output need considerable development to achieve the 90-95% efficiency projected.

However, free piston engine-alternator offers a potentially higher overall efficiency because of low friction and flow losses. The absence of dynamic seal offers potentially higher reliability, longer life, and lower maintenance requirements.

Required engine development areas are the gas bearings and gas springs, close clearance seals, and controls for stable engine alternator operation. Designs must be developed which minimize flow losses, assure reliable operation over an extended load range, and enable starting without significant wear of the bearing surface.

2. Programmatic Approach

The approach which has been pursued consists of two parallel activities: 1) identification and analysis of promising free piston and kinematic advanced engine designs, incorporating technology which can be expected to be mature in the 1985 time period, and 2) simultaneously assembling near term test bed systems to explore and solve system integration problems. The test bed engine should approach the advanced engine configuration design with currently available components technology. Based on the more advanced state-of-the-art of kinematic engine, and the ongoing support of their development for automotive propulsion, the free piston engine will require the greater development support for solar application. Since solar heater head technology is similar for both engine types, its basic development can be carried out on either engine.

In September 1978 work was begun by MTI under contract DEN 3-56 on the conceptual design and analysis of free piston engines. This work was completed in April 1979. Work on the advanced kinematic Stirling engine was begun in October 1978. Configuration definition and analysis was completed and conceptual design and analysis has been in progress. As discussed previously, in order to obtain system integration and operational experience at the earliest possible date procurements are being initiated for both the USS P-40 and the GE/NAP 1-98 engines.

3. Free Piston Engine

The 15 kWe engine conceptual design study is shown in Figure 3-6. The engine was designed specifically for integration with a sodium heat pipe receiver. Significant features include: a cast Inconel 1713 heater head on which sodium vapor will condense; an annular regenerator packed with knitted wire; a power piston which carries the permanent magnet alternator plunger; a starter within the alternator plunger, cantilevered from the end of the pressure vessel; and chrome oxide coated gas bearings utilizing engine working fluid pressure. To keep the piston mass low, samarium cobalt magnets are used in the alternator. Engine cooling water circulates through starter cooling coil.

The engine will produce a net output of 15 kWe with a heater head temperature of 1500°F, and a cooling water temperature of 110°F. Alternator output frequency is 60 Hz.

General discussions and operating parameters are given in Table 3-1.

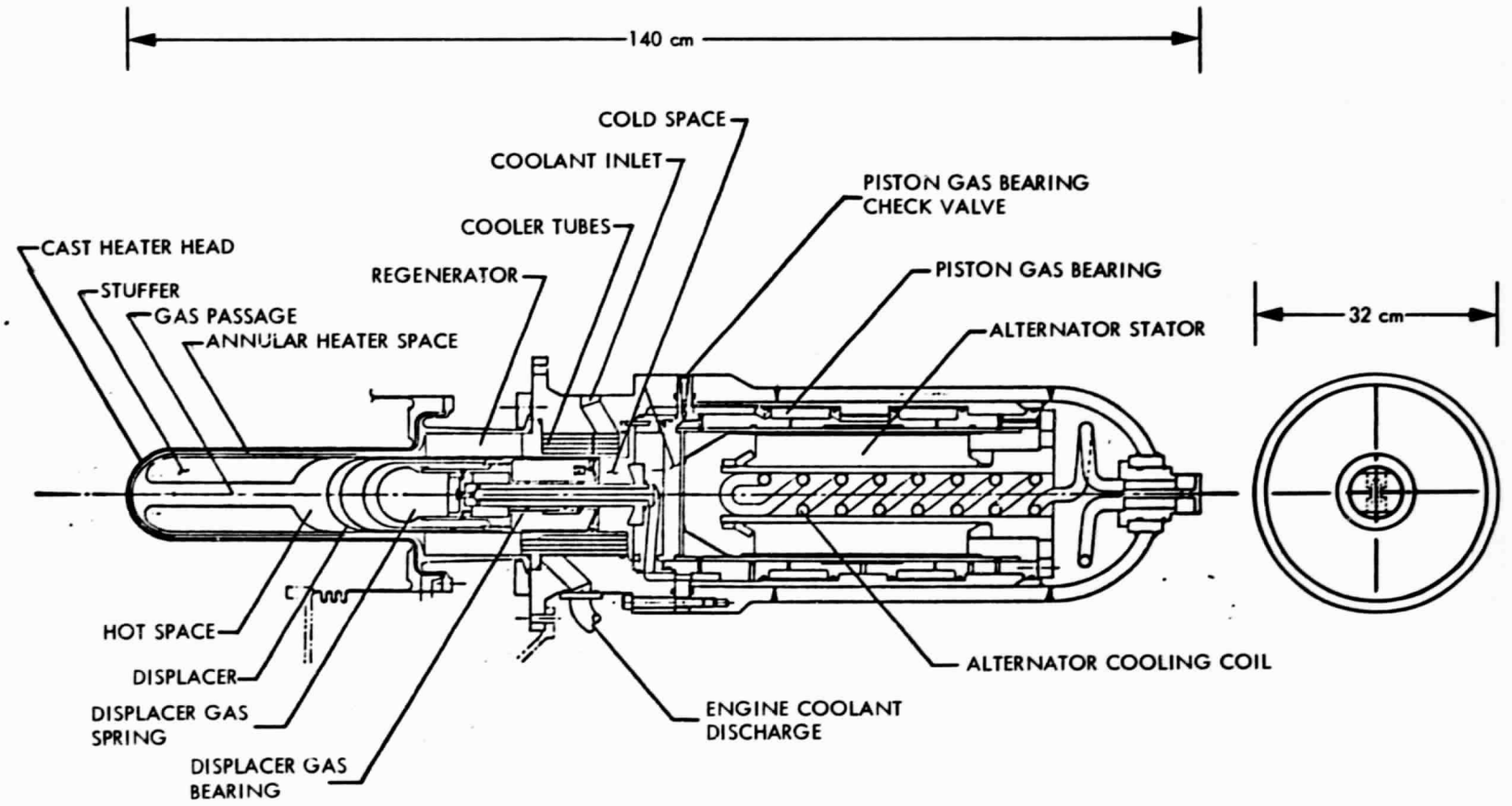

Figure 3-6 15kWe Free-Piston Engine-Alternator
Conceptual Design

Table 3-1

15 kWe Free Piston Engine Dimension and Operating Parameters

Net Output	15 kWe	
Overall Length	55 in.	140 cm
Max Dia.	12.6 in.	32 cm
Displacer Dia.	4 in.	10 cm
Displacer Amplitude	1.3 in.	3.3 cm
Displacer Weight	3.2 lb	1.45 kg
Piston Diameter	7 in.	17.8 cm
Piston Amplitude	0.67 in.	1.7cm
Piston-Alternator Mass	34 lb	15.5 kg
Heater Head Metal Temp.	1500°F	800°C
Cooling Water Temperature	110°F	29°C
Operating Frequency	60 Hz	
Output Voltage	240v single phase	
Engine Thermal Efficiency	41%	
Alternator Efficiency	90%	
Charge Pressure	58 bar	
Working fluid	Helium	

Here the engine design incorporates many state-of-the-art technology components to make it suitable for a test bed engine. The integration of these components will require development to assure dependable operation. A component state-of-the-art assessment is presented in Table 3-2.

A major task in this study was the assessment of the economic and technical issues involved in bringing the free piston engine to production.

Detail production studies of the major components were made to determine production process and direct material and labor costs as a function of production quantities. Some of the results are shown in Figure 3-7.

The growth potential of the conceptual design was studied using various approaches, for example: arrangement of six cylinders in hexagonal configuration was projected for a total output of 50 kWe. This growth engine would be completely balanced with respect to reciprocating and rocking forces.

The complete implementation assessment also included a failure mode analysis and durability assessments.

4. Kinematic Stirling Engine Configuration Design and Analysis

As a subcontractor to MTI, United Stirling (Sweden) conducted a survey of Stirling engine concepts applicable to solar heat input applications. Among the chief criteria to assess applicability were efficiency in excess of 40%, reliability, growth potential and cost. The configuration considered included the following engine types and components:

Engine Types:	Single acting with rhombic drive. Multiple cylinder double acting with a V or U crank shaft or swash plate drives.
Seals	Rollsock, sliding seal, and sliding seal-diaphragm combination.
Regenerators	Multiple cartridge and annular.
Heater Head	Direct insolation. Sodium vapor condensation

United Stirling concluded that the calculated performance of the different engine types are equal within the accuracy of the calculations. In addition, it is not possible at the present level of detail design to identify any significant differences in the technological risk involved in the different concepts.

The selection of engine concept therefore has to be based on other factors. For small power levels the single acting concept is the most suitable mainly because it minimizes the number of

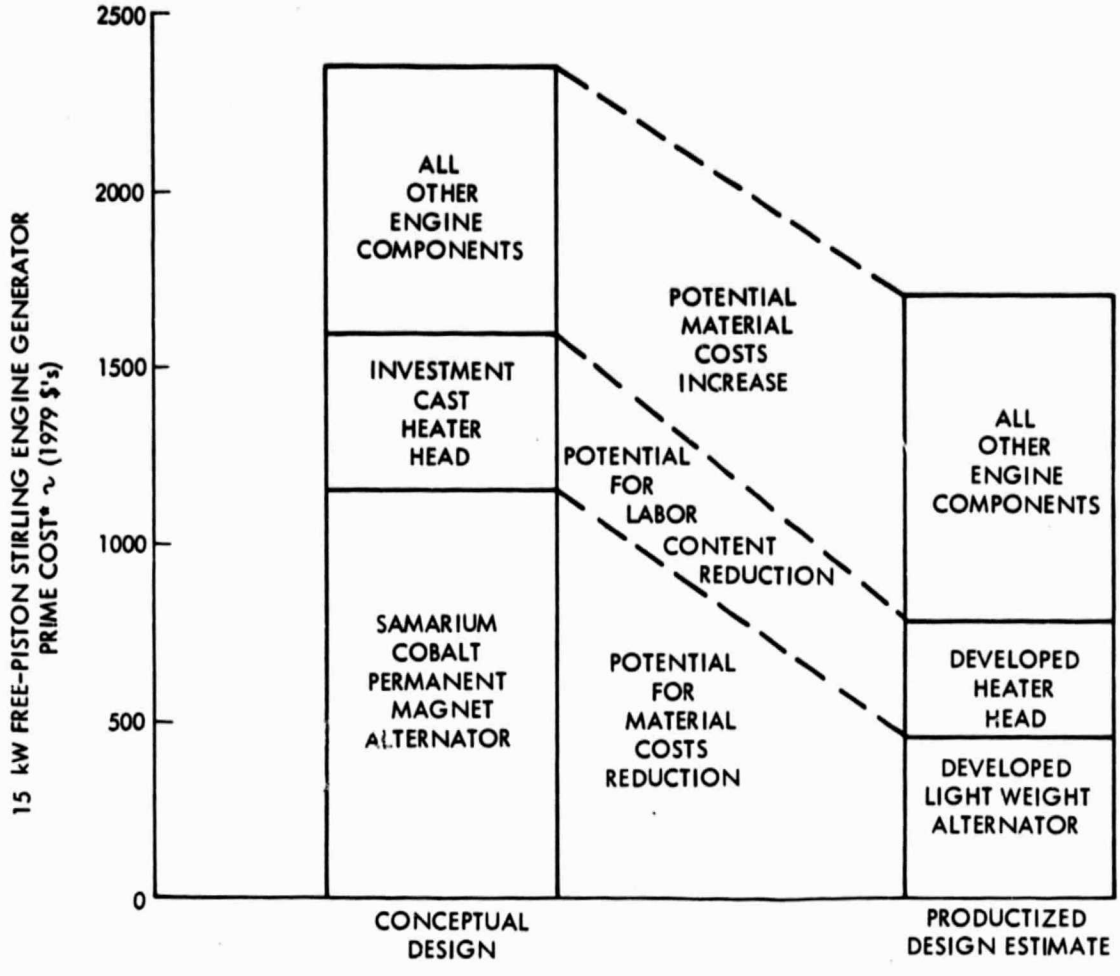

Figure 3-7. Unit Direct Labor and Materials Cost for 25,000 Units/Year

Table 3-2

Component State-of-the-Art Assessment

Critical Component	Key Technology	Technology Status
1) Heater Head	Condensing Liquid Metal Heat Transfer	Significant Improvement
	Cast Heater Head	Significant Improvement For High Heat Transfer
2) Regenerator	High-Volume Processing with Effective Material Utilization to Lower Cost	Adaptation of State-of-the-Art
3) Bearing System	Internally Supplied Bearing Gas	Adaptation of Current Technology
	Surface Coatings Techniques	State-of-the-Art
4) Seals	Close Tolerance Seal	Extension of State-of-the-Art for Life
5) Displacer Drive	Posted Displacer and Gas Spring	Improvement Required
6) Alternator		
- Plunger	Rare Earth Permanent Magnet Manufacturability	Adaptation of Current Technology, but Replacement of Cobalt Alloy without Significantly Affecting Engine Characteristics Requires Significant Improvement
- Stator	Manufacturing Technique (Microlamination, etc.)	Adaptation of Current Technology
7) Control	Engine/Alternator Stability Matching	Adaptation of Current Technology
	Displacer Gas Spring Volume Control	Adaptation of Current Technology
	Engine/Receiver Interface Control	Less than Required

components. For larger power levels this advantage becomes less pronounced which makes the double acting multiple cylinder concept more suitable. It seems that power level of 15 kW may be approximately the transition level from single to multicylinder type of engine.

Therefore the strongest influence on engine selections is the possible growth of power level. This criterion resulted in the selection of a four-cylinder, double acting engine with a U-type crank shaft. Another factor which promoted this selection is that recent development activities concerning single-acting engines have been minor, whereas a substantial effort has been made to develop double-acting engines which have given the double-acting engine a lead over the single-acting engine.

Figure 3-8 is a cross-section of the 4-cylinder, double-acting design configuration which was chosen for the conceptual design. The engine-alternator will have the following characteristics:

Alternator Output	20 kW
Alternator Efficiency	95%
Number of Cylinders	4
Number of Regenerators: type	4 annular type
Heater Input Temperature	1500°F
Coolant Temperature	110°F
Efficiency Target	40 - 45%

The selected engine design is similar to the P-40 standard United Stirling Laboratory engine, but incorporates improvements in seals and regenerators.

The seal system incorporates, in addition to the shaft seal, a hermetic diaphragm which will provide much greater assurance of keeping even minute quantities of oil out of the heat exchangers.

The heater head shown in Figure 3-8 is typical for attachment to a heat pipe heat receiver. Bellows provide the closure between the receiver vapor chamber and the engine heater head. Structural mounts are between the colder surfaces of the engine and the receiver. For engine component maintenance other than the heater head, the integrity of the vapor chamber should not be disturbed.

5. Cooling

About half of the solar heat collected by a dish-Stirling unit will be transferred to the engine coolant. The heat contained in the coolant can then be rejected to atmosphere by individual dry heat exchangers, individual wet cooling towers, or central cooling towers. The costs of heat rejection by each of these three methods was compared and optimum heat rejection temperatures selected.

Dish-Stirling constants assumed were 50 m^2 area, 1.0 kW/m^2 peak insolation, 40 kW peak input to the engine, 17 kW peak shaft power, 15 kW peak generator power, 23 kW peak heat rejection,

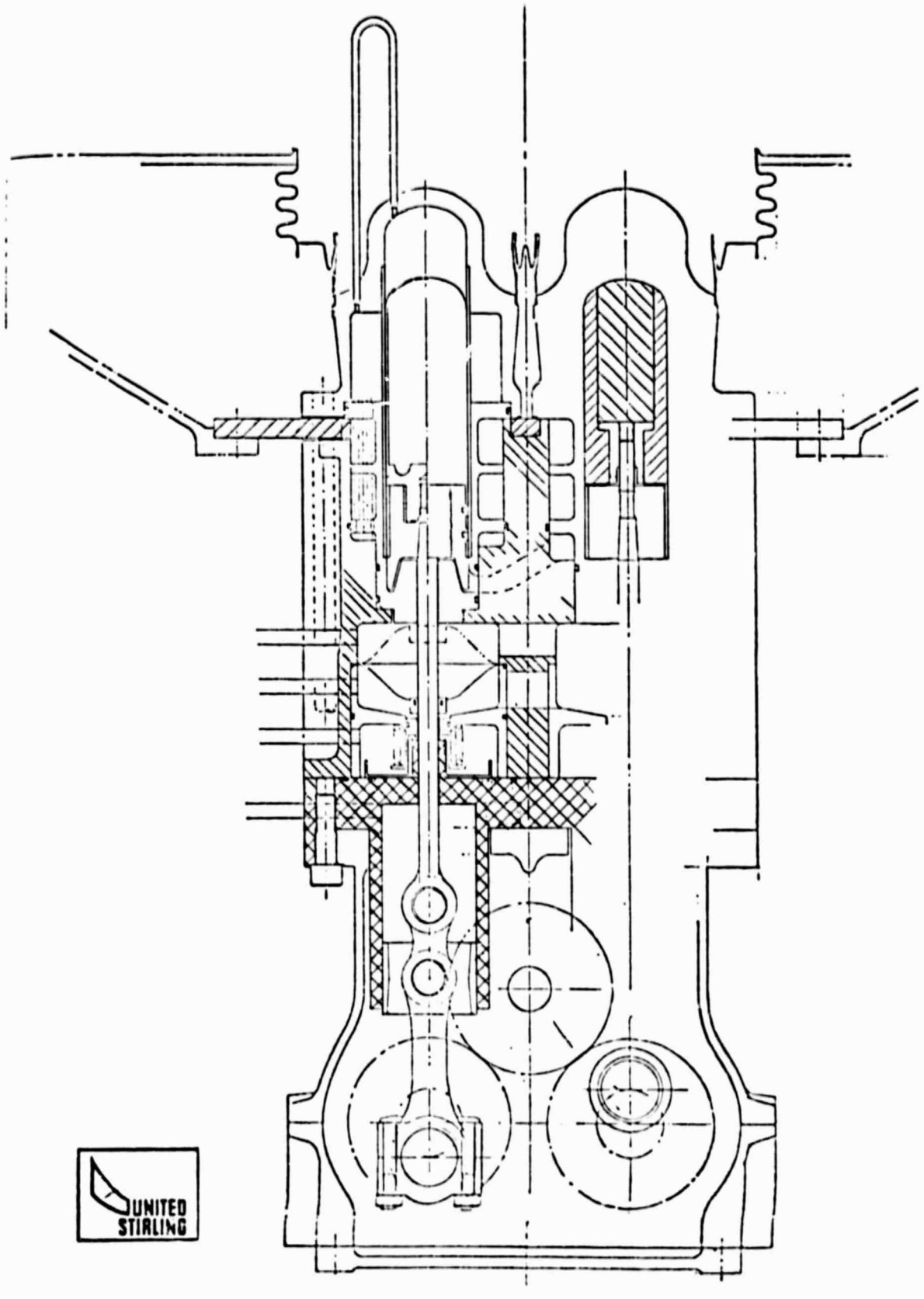

Figure 3-8. Kinematic Stirling Sodium Vapor Heaters

0.634 kW/m^2 average daylight hour insolation, and 4494 daylight hours per year. The value used for change in engine efficiency with rejection temperature was 0.11 percentage points per ^{o}C (the value for a P-40 Stirling engine).

The cost of individual dry heat exchangers was based on Aerofin Corporation Series 80 heat exchangers (16 mm diameter copper tubes with aluminum fins). The cost of individual wet cooling towers was based on a Marley Company unit of 23 kW nominal cooling capacity. The cost of central cooling towers was based on a Marley Company wooden tower of 10 MW nominal cooling capacity. The annual cost of the heat exchanger or cooling tower was taken as 10% of the capital cost.

In the calculations, the engine rejection temperature was reduced in small steps by increasing the size of the heat exchanger or cooling tower. The ratio of each increment in annual cooling cost to the increment in annual electric generation (after subtracting cooling fan power) was calculated as the marginal cost of energy production due to added cooling. The optimum rejection temperature was the one for which this marginal cost (assumed to be 5¢/kWh) equaled the cost of electric production for the plant as a whole.

Figure 3-9 shows the marginal cost as a function of engine rejection temperature for each of the three types of heat exchangers. To plot the dry heat exchanger on the same graph as the wet towers, the ambient temperature was assumed to be 10^{o}C above the wet-bulb temperature. This corresponds to an ambient temperature of 25^{o}C and a relative humidity of 35%.

Figure 3-9 also shows that the wet towers and dry heat exchangers have similar curves of marginal cost versus rejection temperature but each curve is centered at a different temperature level. For equal marginal costs of 5¢/kWh, the individual wet towers should be operated at a 3^{o}C higher temperature than central towers and the dry heat exchangers at another 13^{o}C higher.

From the data shown in this Figure 3-9, it was concluded that:

(1) For individual dry heat exchangers the optimum rejection temperature is about 15^{o}C above ambient temperature, which is approximately 25^{o}C above wet bulb.

(2) For central wet towers the optimum rejection temperature is about 9^{o}C above wet bulb, and for individual wet towers about 12^{o}C above wet bulb.

(3) The gain from using wet towers instead of dry heat exchangers is a reduction of 13 to 16^{o}C in rejection temperature, giving a gain of about 1.5 percentage points in engine efficiency.

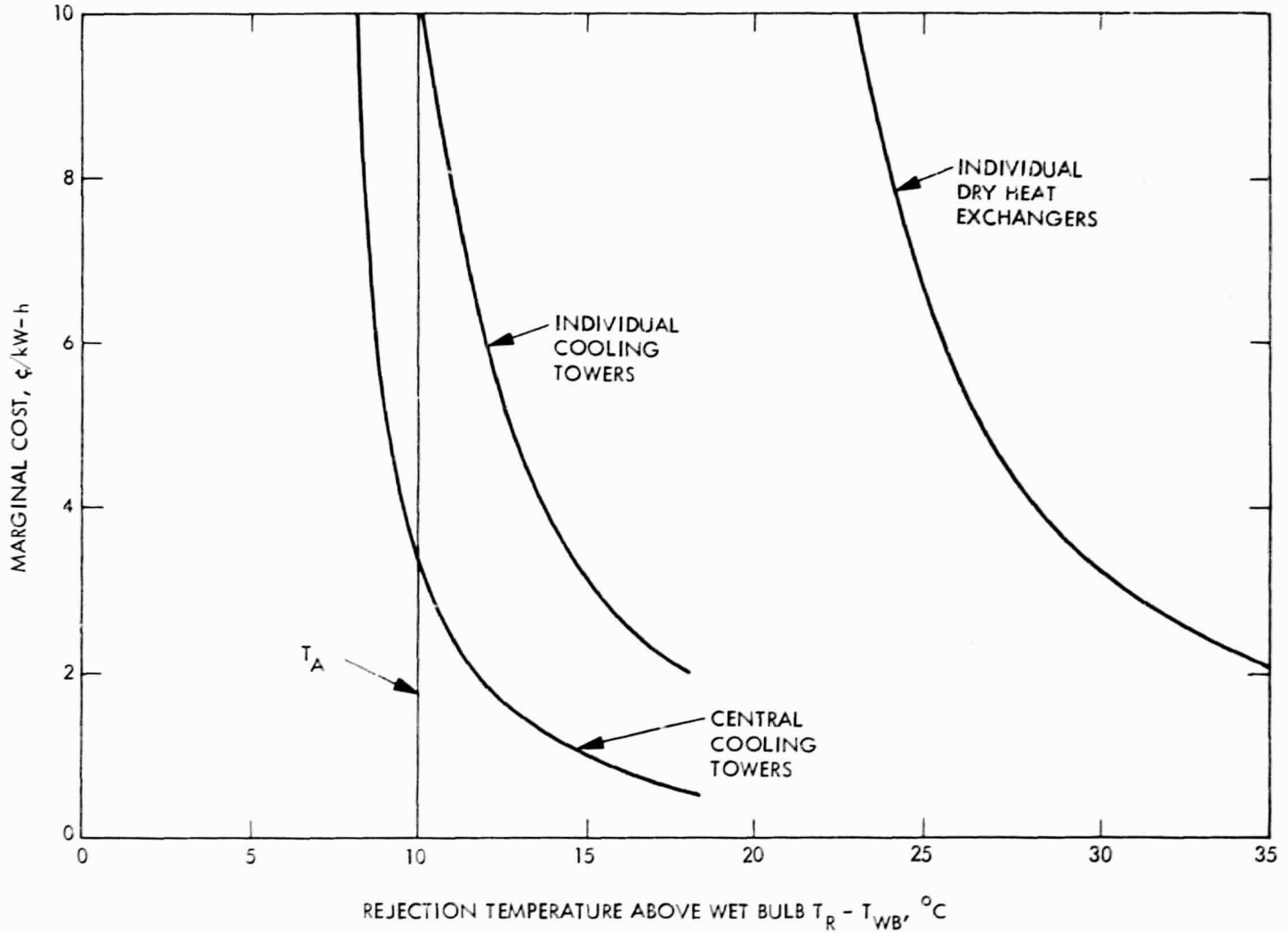

Figure 3-9. Marginal Cost of Electrical Output Due to Added Cooling

D. SOLAR CONCENTRATOR

1. Structural System

a. Introduction

Conceptual design study of a point-focusing, two-axis, tracking, paraboloidal solar concentrator has been continued during this reporting period. A configuration of this concentrator, as shown in Figure 3-10, was developed and shows promise of meeting the cost and performance goals of the Advanced Solar Thermal Technology Project.

A prototype concentrator design of this configuration is to be developed and key materials and sub-assemblies tested in order to provide empirical concentrator performance data and the integration of the concentrator with the receiver and power conversion subsystems.

An RFP (request for proposal) procurement package for the conceptual design and fabrication and testing of key components of a Prototype Advanced Solar Concentrator was prepared and released in December 1978. A decision was made in March 1979, after the proposal evaluation by JPL, to enter contract negotiation with Acurex Corporation of Mountain View, California, for this procurement. The term of the contract is approximately 20 months and key materials and components will be tested by JPL.

b. Baseline Prototype Description

The reflective surface of this design consists of two groups of optical quality reflective glass mirrored gores. They are installed in a cantilever fashion on both sides of a truss-type backup structural ring with a triangular cross-section to form a complete but physically discontinuous paraboloidal reflective surface. High reflectance and low mass of a reflective surface are of extreme importance. A relatively small reduction in reflecting efficiency together with higher reflector mass can translate into significant cost penalties. Due to these considerations, the effect of dust and contamination accumulation, stability of reflective metallization, environmental effects and cleaning effects, a representative design as shown in Figure 3-11 has been developed. It is of a high-quality back-silvered glass mirror, bonded continuously in the lightweight structural cellular glass substrate that is properly contoured before bonding. The reflector aperture diameter of this design is 10 m and has a focal ratio of f0.6.

A space frame serves as an intermediate structure between the reflector assembly and a stationary pedestal structure that provides the reflector with the azimuth and elevation movements for the tracking of the sun. This intermediate structure on which the reflector is attached is pivoted near its apex, about the azimuth axis at the top of the pedestal. Thrust loads are transmitted at that point to the pedestal through thrust bearings and through wheels at the lower corners of the structure. The reflector assembly is pivoted,

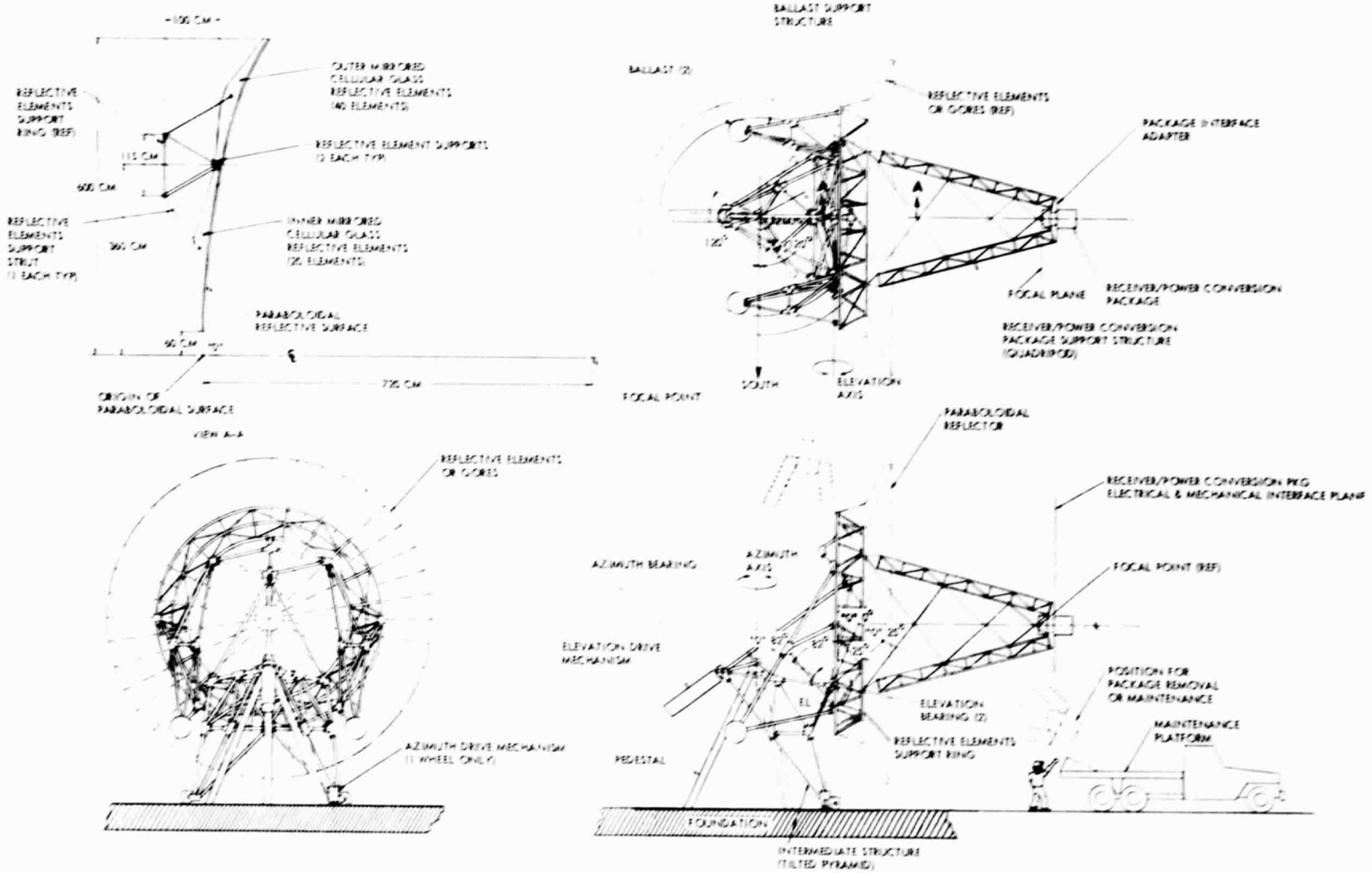

Figure 3-10. JPL Advanced Solar Concentrator Baseline Conceptual Design

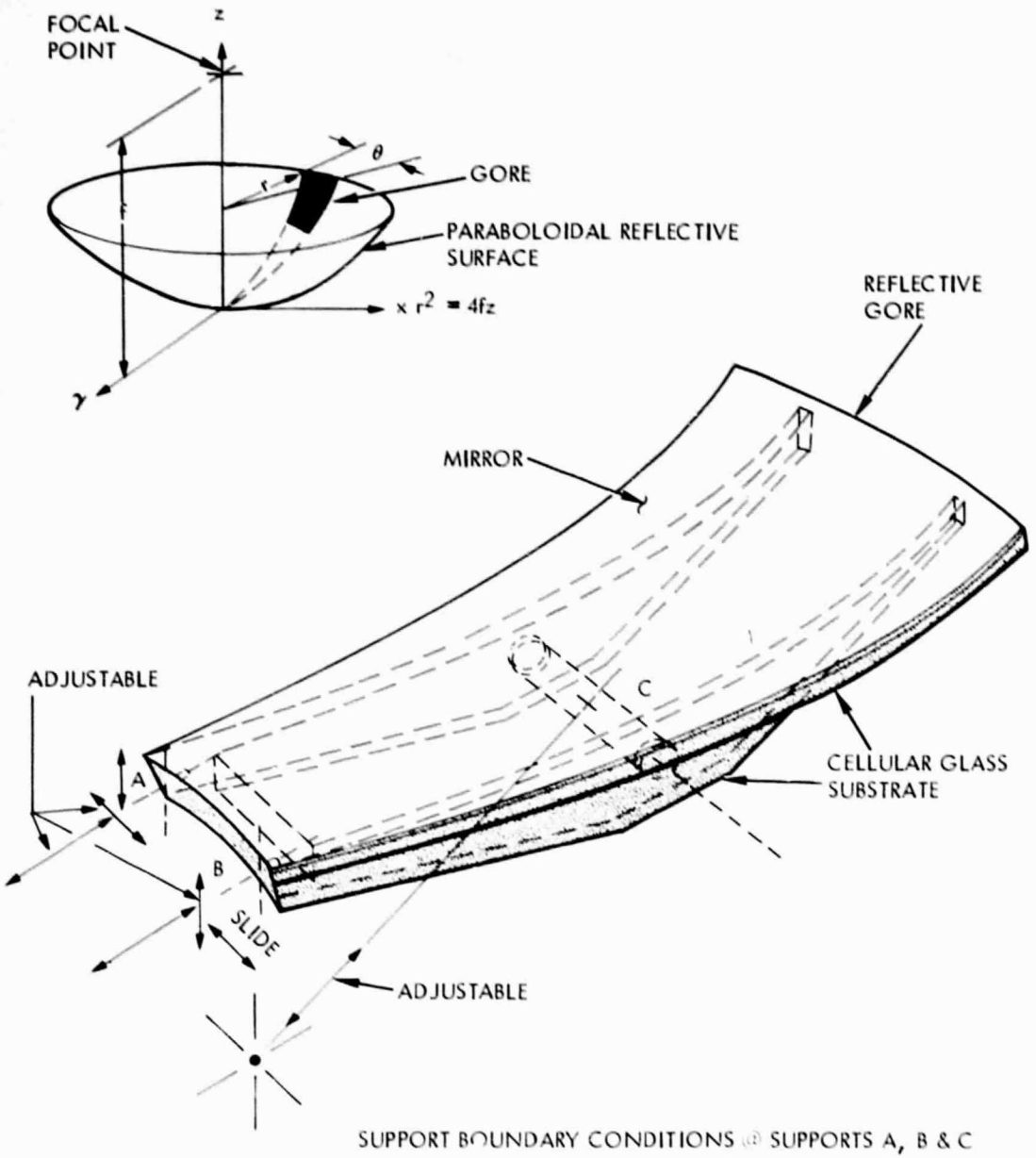

SUPPORT BOUNDARY CONDITIONS @ SUPPORTS A, B & C

- 6 DEGREES OF FREEDOM RESTRAINED (WITH 4 OF THESE DEGREES OF FREEDOM ADJUSTABLE)
- 1 SLIDING DEGREE OF FREEDOM SLIDING ALONG RING
- ALL ROTATIONS WILL BE UNRESTRAINED

Figure 3-11. Mirrored Cellular Glass Gore and the Support Boundary Conditions

in elevation, about the elevation axis, which passes through the two upper corners of the structure.

The solar radiation intercepted by this concentrator aperture normal to the solar flux is delivered to a 22-cm-diameter receiver aperture located at the focal plane with a minimum intercepted solar power of 56 kW under the following conditions:

(1) 845 W/m^2 as assumed average cloud-free insolation level

(2) Steady winds of 50 km/h at sea level density, measured 10 meters above ground level, with a 20% step-function gust factor from any direction

(3) Temperature range of -18°C to 50°C

(4) Clean reflector surface

(5) Receiver/power conversion package mass of 1350 kg with center of mass of 60 cm aft of the focal point of the receiver.

c. Structural Deformation Analysis

The Second Semiannual Progress Report showed the results of the ray intercepts at the displaced focal plane of the receiver for three separate loading conditions. While the mirrored glass gores and their associated support struts were treated as rigid bodies in those analyses, the effect of their distortion on the reflected rays were assumed to be small. This assumption was borne out by a recently performed elastic deformation analysis of a representative gore with its support strut rests on rigid bases. A range of values from 0.77 cm to 1.2 cm of diffusion or distortion of the reflected rays, which is a function of location on the reflective gore caused by the rotation of the gore surface under load, have been obtained from the analysis. They can be superimposed on the corresponding displacement of reflected rays as calculated before; e.g., the case of "horizontal look, G + 30 mph, 60° from normal wind" as shown in the last Progress report can be revised as shown in Figure 3-12. A reflected ray at the displaced focal point, shown as a discrete point, is now shown as a point randomly located within a circular boundary of radius r_{10}.

The diameter of the circular envelope of intercepts for the case considered has grown 25% from a diameter of 9.0 cm to 11.4 cm.

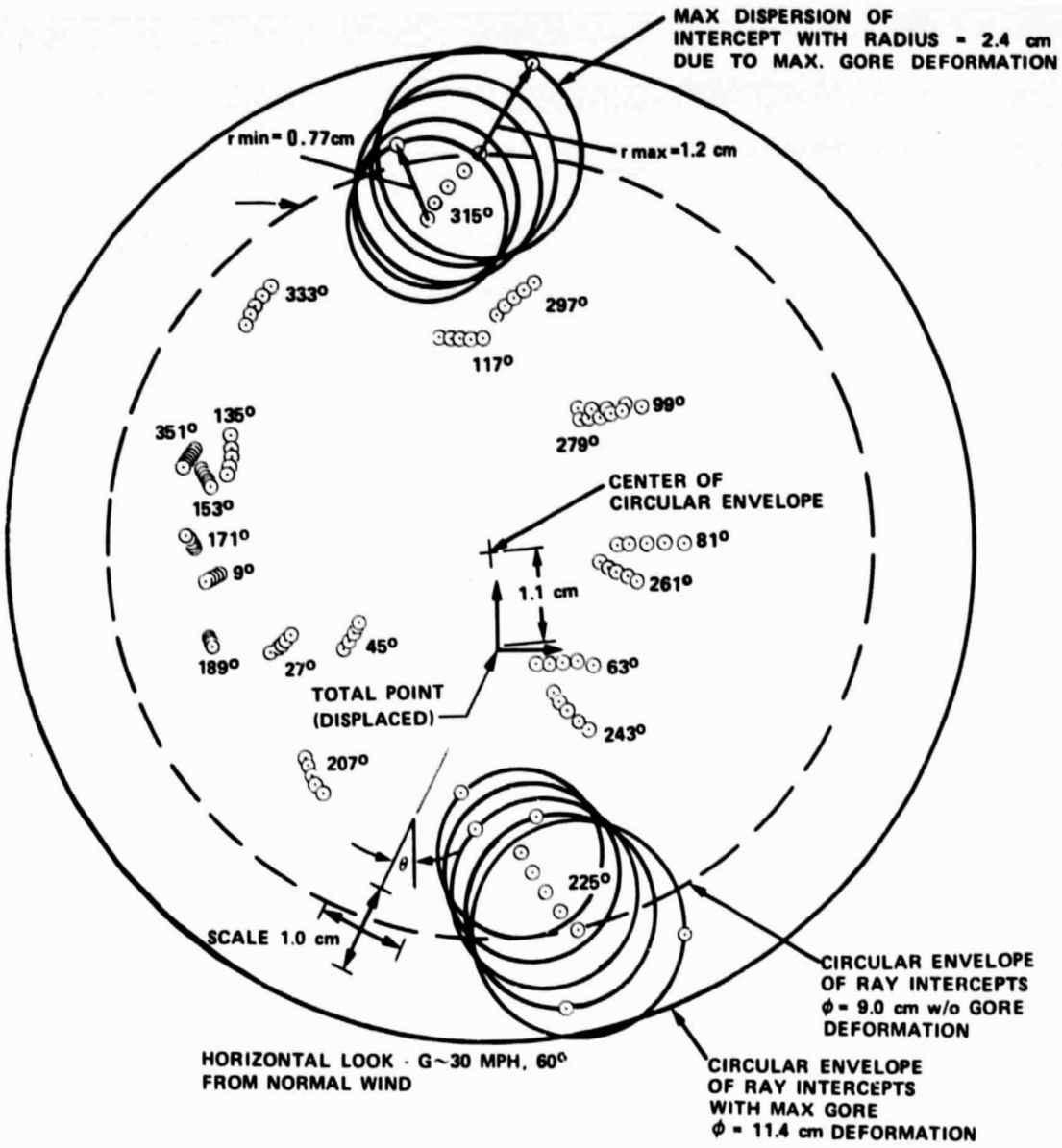

Figure 3-12. Ray Intercepts at Displaced Focal Point

d. Cellular Glass Material Characterization

The mechanical properties of Foamglas®, Foamsil®-70 and Solaramics soda lime cellular glass of varying densities were evaluated. Flexure, compression and slow crack growth tests were conducted on Foamglas® Analyses of the mechanical test data and physical properties supplied by the vendors were incorporated into the RFP for the Advanced Concentrator. Representative data for a typical cellular glass is presented in Tables 3-3, 3-4, 3-5.

Critical cellular glass structural properties (mechanical and environmental) were identified for concentrator applications. Among these are the materials' tensile strength, modulus and fracture toughness. Also included are the compressive and shear strengths and moduli and Poisson's ratio. These properties are required to design the concentrator component adequately to meet the specifications. Also of great importance and perhaps critical is the susceptibility of cellular glasses to the stress corrosion phenomenon of subcritical crack extension. This is a time-dependent phenomenon of the load, leading to premature failure of the component when subjected to a load at some fraction of its fast-fracture strength. This slow crack behavior severely reduces the allowable loads to which a material may be subjected during the component design lifetime. Therefore, it is critical for design purposes that the slow crack growth behavior of the cellular glasses be fully characterized. Parameters that may affect the material properties are the material's chemical composition, density and microstructure.

Table 3-3. Data for a Typical Cellular Glass

Density	240 kg/m^3
Flexural Strength	1.03/ x $10^6 N/m^2$
Young's Modulus	2.20 x 10^9 N/m^2
Shear Modulus	0.94 x 10^9 N/m^2
Poisson's Ratio	0.18

Cellular glass can have either an open or closed cell structure. Due to the porous surface topography of cellular glass, the closed cell material suffers serious degradation when subjected to continued freeze-thaw cycling in the presence of puddled water on its surface. Initial testing indicates that the expansion of the freezing water fractures the surface pore walls resulting in spalling of one or two cell layers per cycle. Open cell structures do not appear to suffer surface spalling because expansion from the freezing water can be accommodated in adjacent cells. In this case however, the weight gain due to absorbed water has been measured at as much as 100%.

This weight gain could not be tolerated in most structural applications. Table 3-4 presents the preliminary test results on uncoated cellular glasses.

Degradation due to freeze-thaw conditions may be prevented by the application of a low permeability conformal coating. A low-cost coating must be developed. The coating would prevent water collecting in the surface cells. In a preliminary test program FoamGlas® specimens were coated with Pittcote 404® and Chemglaz®, then subjected to environmental freeze-thaw cycling. The freeze-thaw cycle is illustrated in Figure 3-13. Table 3-5 presents the results of these tests. No degradation was apparent after 100 cycles but after 280 cycles some cracking and blistering occurred, resulting in structural degradation of test specimens.

Table 3-4. Results of Freeze Thaw Environmental Testing on Several Cellular Glass Materials

Material	Density (lbs/ft^3)	No. Tested	No. of Cycles	No. of Structural Failures	Remarks
Soda-Lime I	8.5	14	42	5	All Specimens: Structural and Chemical Degrad.
		13	101	0	
Soda-Lime II	16.5	2	42	0	Material Absorbs Water, No Material Spalling
		2	101	0	
Aluminoborosilicate	11.6	6	42	0	All Specimens: Structural Degrad.
		4	101	3	
	14.1	5	42	0	
		5	101	3	
	16.6	5	42	0	
		5	101	4	
	20.0	5	180	5	
	27.0	3	180	3	

Table 3-5. Results of Strength Measurements on Coated Soda-Lime Foamglas® After Environmental Freeze Thaw Testing

No. Tested	No. of Cycles	No. of Structural Failures During Testing	Average Tensile Strength of Intact Specimens After Environmental Cycling (psi)
12	143	0	86.8
13	280	4	83.8

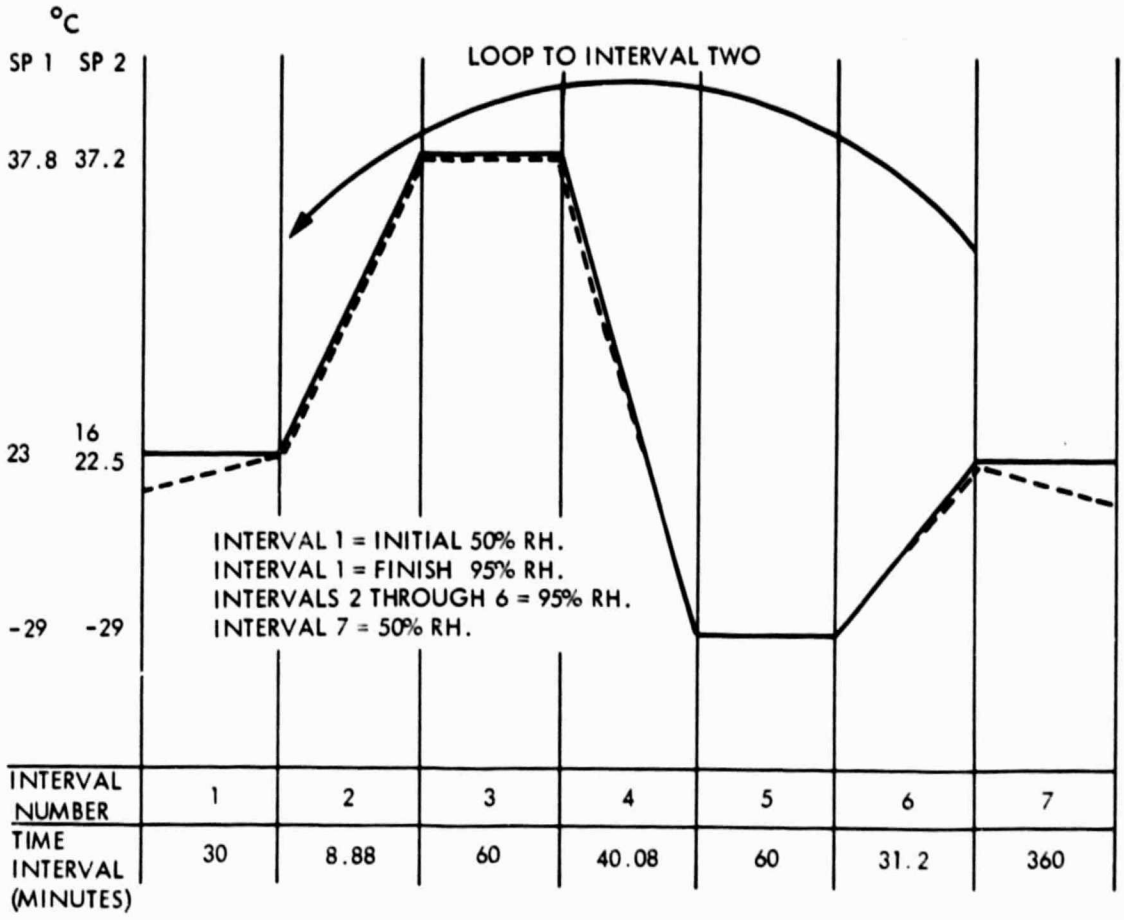

Figure 3-13. Profile Map of Foam Glass Substrate For Concentrator Mirrors

2. Optical System

The optical system consists of the paraboloidal reflector with a diameter of 10 m and the center of the receiver aperture situated at the focus. The rim angle is 45° and the f ratio is 0.603. Ideally, the surface of the solar concentrator should correspond exactly to that determined precisely by the geometric relationship and the optical axis of the paraboloid should be oriented along the direction of the sun. In practice, there are various errors that will degrade the optical performance from the ideal situation. These errors may be divided into three categories: pointing or tracking errors, surface-slope errors, and specular angular spreading.

a. Tracking Error

The tracking or pointing error is the angular offset of the direction to the sun from the optical axis of the reflector. It arises from sensor misalignments, solar tracker control offsets and hysteresis, and receiver-support deflection caused by gravity or wind load as the concentrator changes its orientation while tracking the sun. The net effect of tracking errors, provided that they are small, is to shift the flux distributions at the focal plane with very little distortion in their overall profile. The specification for the tracking mechanism and control design of the ADS-1 is that the tracking error will not exceed 1.7 mrad (0.1°) for normal operating conditions in steady winds of 50 km/h. The tracking error of 1.7 mrad causes a quantitative shift of the flux distribution at the focal plane of approximately 2 cm. The size of the receiver aperture must be enlarged to accommodate the shift. Furthermore, the control system transient response will be such that the tracking error will return to within 1.7 mrad in less than 20 seconds from the onset of a 20% gust condition.

b. Surface Slope Error

The surface slope error is the angular deviation of the actual surface normal of the fabricated concentrator from that of the ideal geometric surface and is most instrumental in spreading the flux distribution at the focus. It results from a number of sources; for example, macro-roughness due to manufacturing methods, subassembly manufacturing errors, installation misalignments and distortions, and structural deflections due to external forces. A statistical treatment is needed since such errors of the surface normals are usually random.

c. Specular Angular Spreading

Specular angular spreading is a measure of the angular spread of the reflected beam for a flat piece of the mirror and for a well-collimated incident beam at specified values of the angle of incidence and incident wavelength. The effect is quite small for

highly specular surfaces; i.e., a typical value for the standard deviation with respect to the specular spreading of Corning Code 0317 fusion glass is about 0.25 mrad.

d. Categorization of Optical Analysis Results

The optical analysis results are utilized both in the design of the advanced concentrator and the dish-Stirling Solar Receiver. For the following system configuration, a two-dimensional normal distribution for the surface normals is employed in our optical analysis based on Schrenk's solar simulation procedures (Reference 1).

(1) Diameter of paraboloidal concentrator = 10 m

(2) Rim angle of paraboloid = 45°

(3) Focal length = 6.034 m

(4) Radius of concentrator hole = 0.6 m (unless otherwise stated)

For design purposes it is important to perform computations for a matrix of parameters. The results may be categorized as follows:

(1) Flux distributions and intercept factor at the focal plane (Figures 3-14 through 3-21) for parameterized values of:

(a) Concentrator quality characterized by a single parameter ($\sigma_c = \sigma_r$) for the slope error where
σ_c = circumferential standard deviation and
σ_r = radial standard deviation

(b) Concentrator quality characterized by two parameters ($\sigma_c = \sigma_r$)

(c) Concentrator center hole radii

(2) Flux distributions along planes located at and behind focal planes (Figures 3-22 and 3-23)

(3) Flux distributions incident on the cavity walls of the Fairchild Receiver for two cases of slope errors (Figures 3-24 through 3-27)

These results were transmitted to Fairchild Stratos, and they were utilized in the design of dish-Stirling Solar Receivers. These results were also given to NASA Lewis Research Center to be used in their receiver-related tasks.

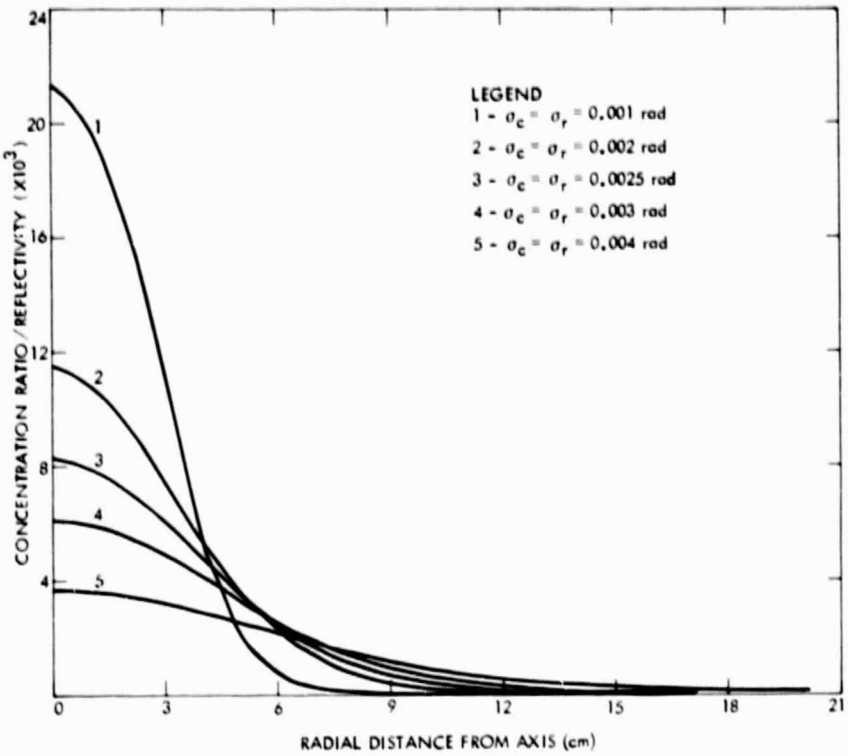

Figure 3-14. Distribution of Normalized Concentration Ratio along the Focal Plane using a Two-Dimensional Normal Distribution of Slope Errors ($\sigma_c = \sigma_r$)

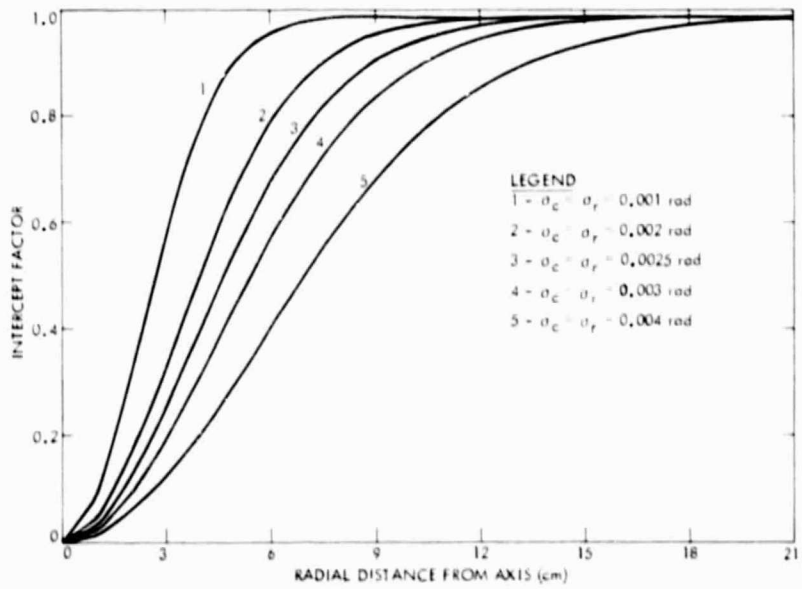

Figure 3-15. Intercept Factor as a Function of Radial Distance from Axis for a Two-Dimensional Normal Distribution of Slope Errors ($\sigma_c = \sigma_r$)

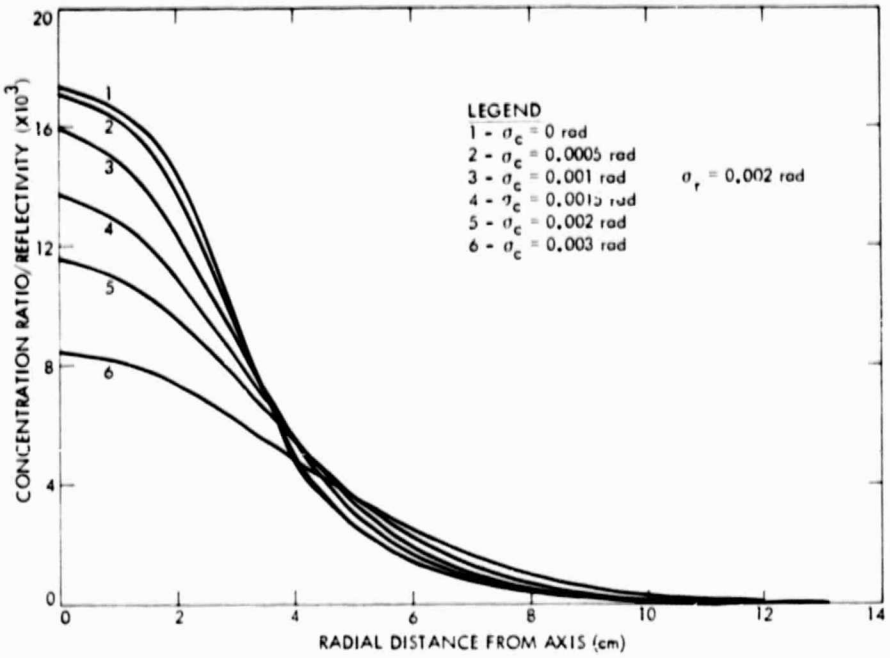

Figure 3-16. Distribution of Normalized Concentration Ratio along the Focal Plane for Various Slope Errors using Two-Dimensional Normal Distribution of Slope Errors (σ_r=0.002 rad)

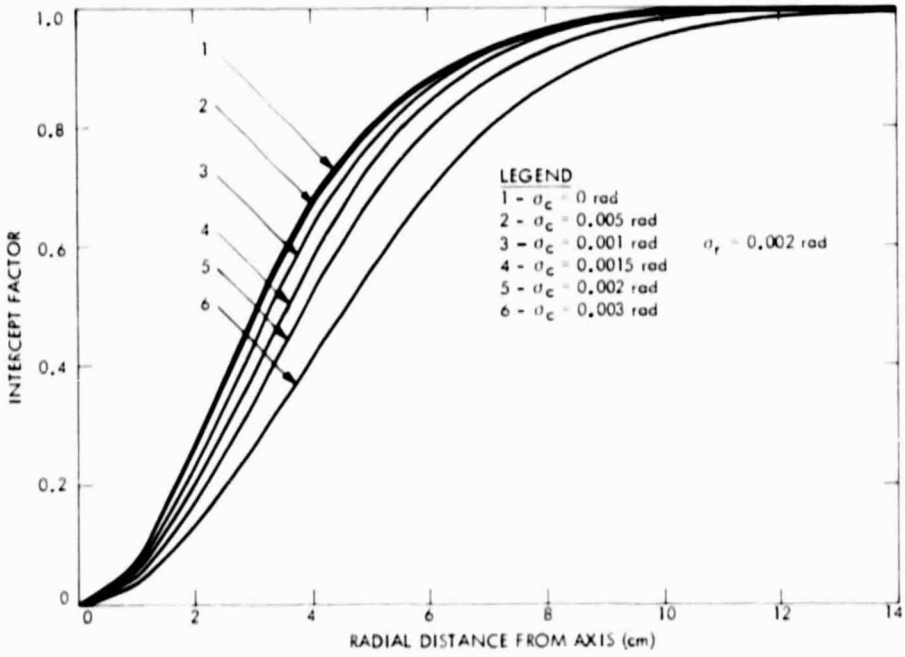

Figure 3-17. Intercept Factor as a Function of Radial Distance from Axis for Various Slope Errors using a Two-Dimensional Normal Distribution of Slope Errors (σ_r=0.002 rad)

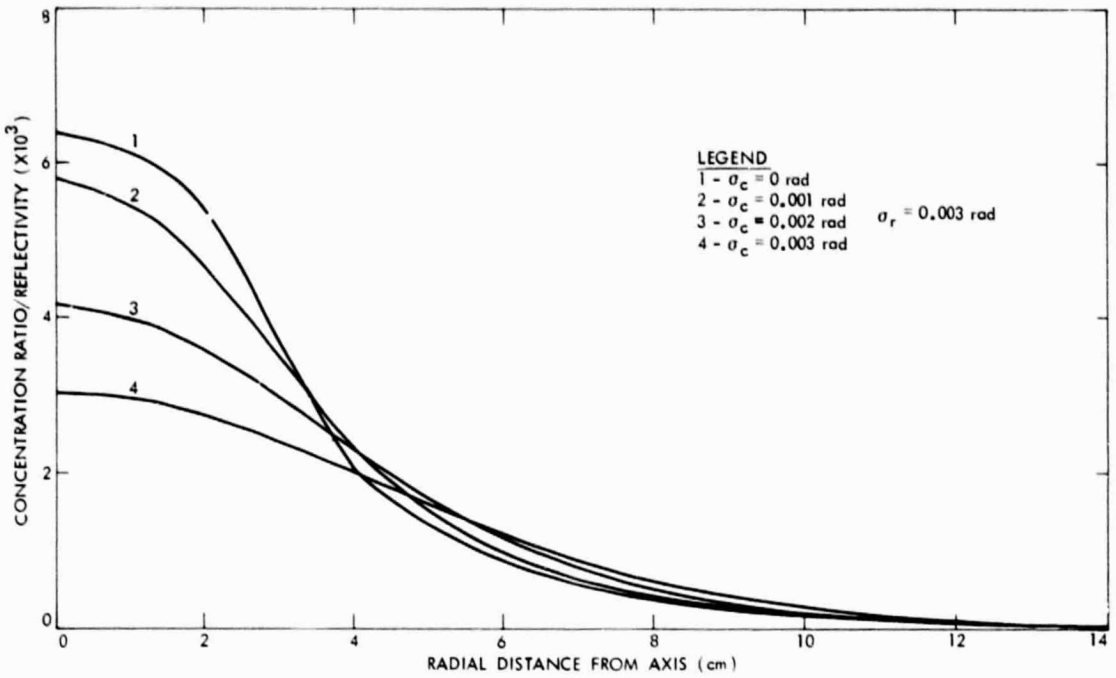

Figure 3-18. Distribution of Normalized Concentration Ratio along the Focal Plane using a Two-Dimensional Normal Distribution of Slope Error (σ_r=0.003 rad)

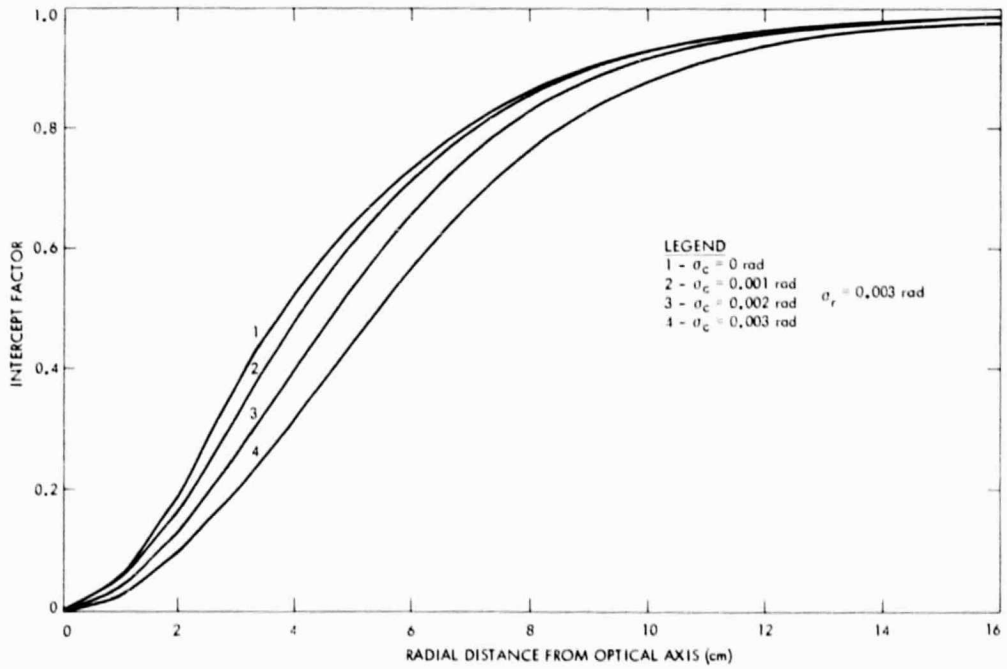

Figure 3-19. Intercept Factor as a Function of Radial Distance from the Optical Axis for Various Slope Error using a Two-Dimensional Normal Distribution of Slope Error (σ_r=0.003 rad)

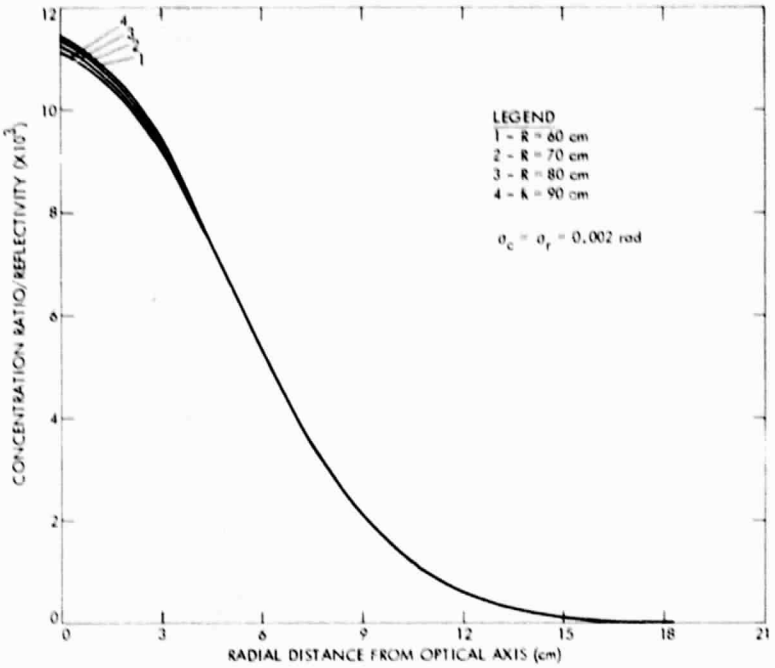

Figure 3-20. Distribution of Normalized Concentration Ratio along the Focal Plane for Several Cases of Concentrator Center Hole Radius (R)

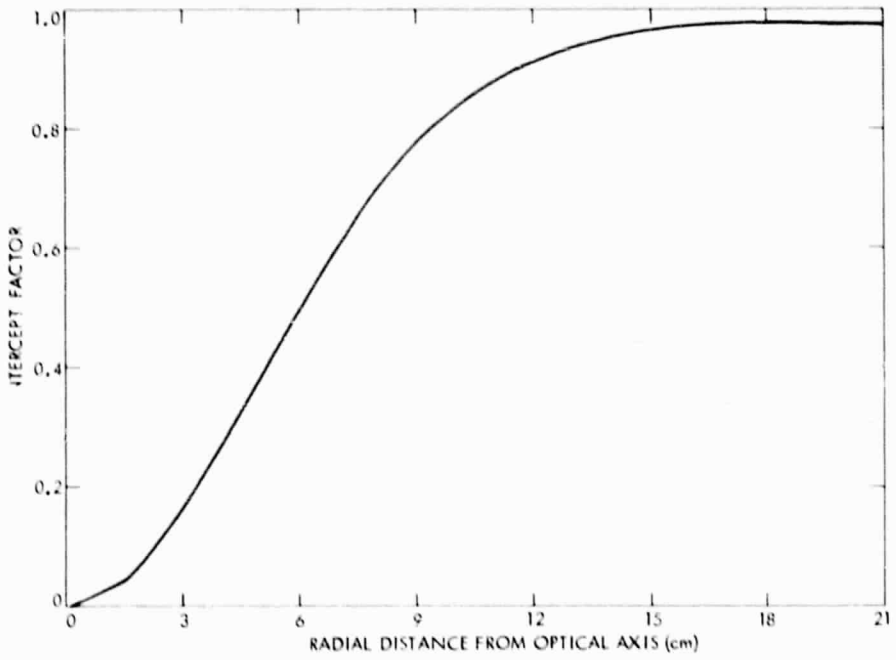

Figure 3-21. Intercept Factor as a Function of Radial Distance from Optical Axis for Several Cases of Concentrator Center Hole Radius

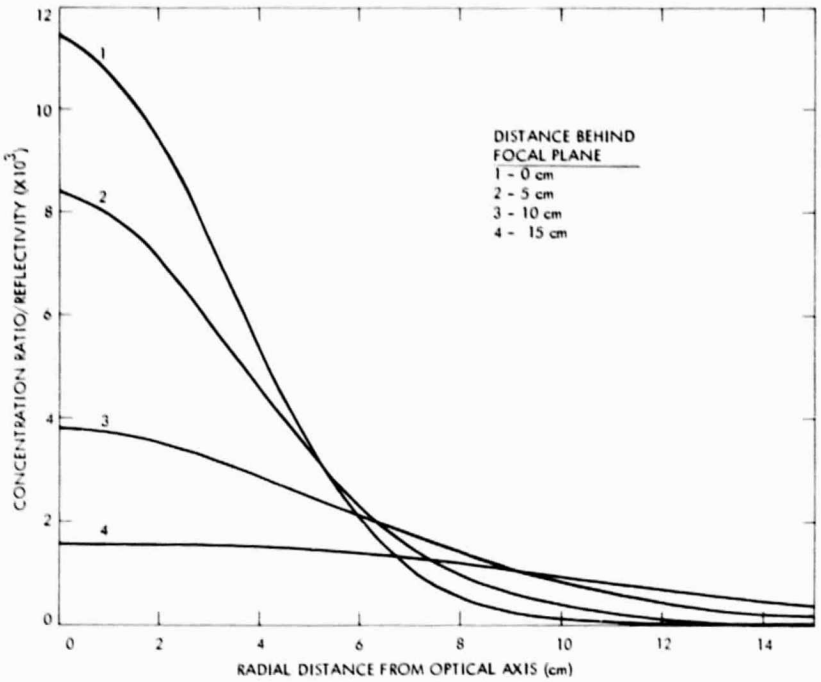

Figure 3-22. Distribution of Normalized Concentration Ratio along Various Planes Located Behind the Focal Plane as a Function of Radial Distance from Optical Axis ($\sigma_c = \sigma_r = 0.002$ rad)

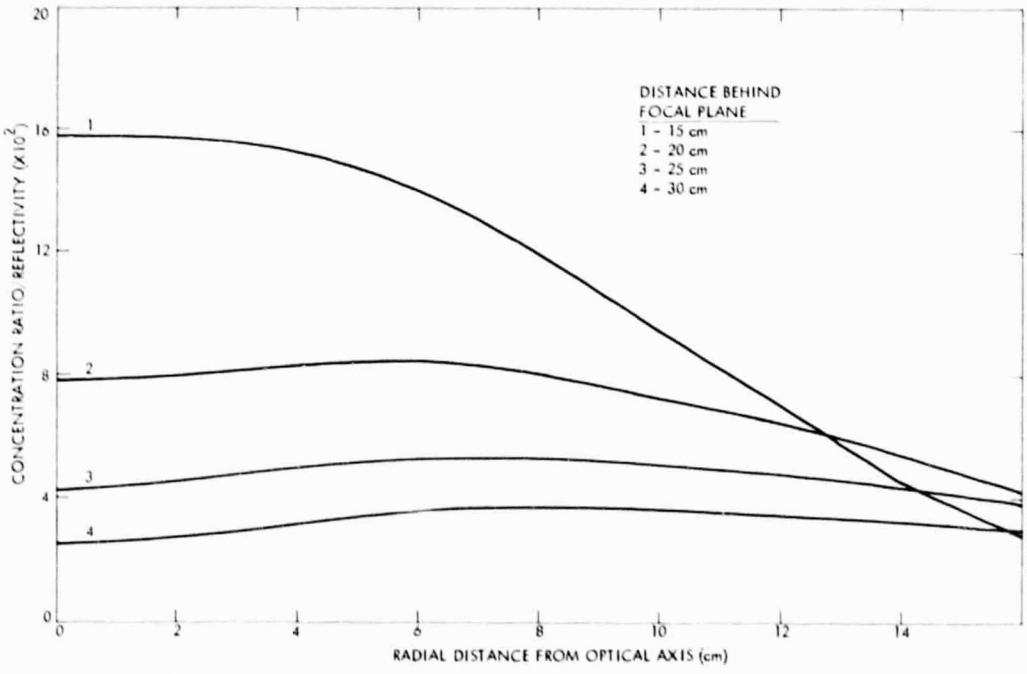

Figure 3-23. Distribution of Normalized Concentration Ratio along Various Planes Located Behind the Focal Plane as a Function of Radial Distance from Optical Axis ($\sigma_c = \sigma_r = 0.002$ rad)

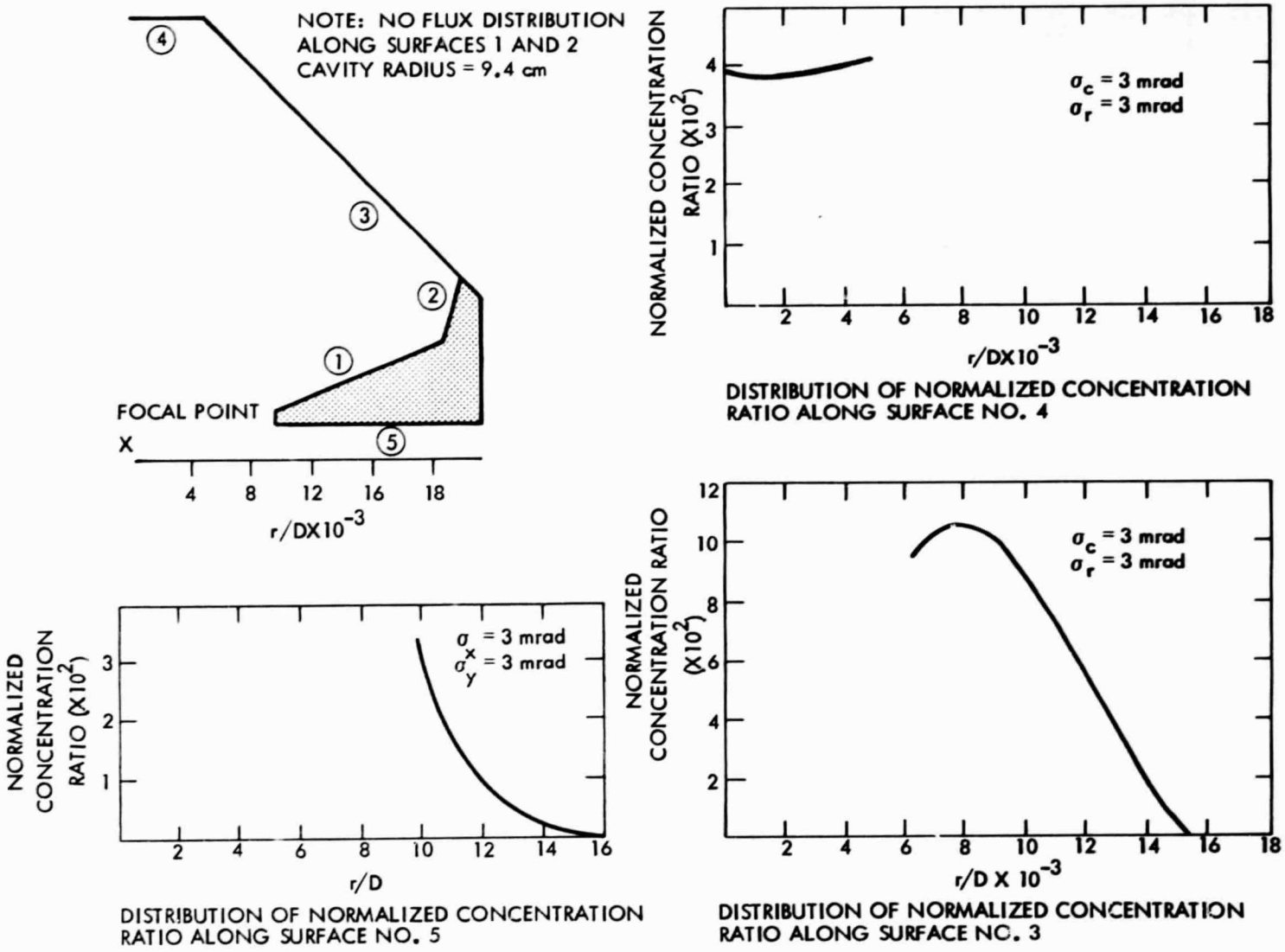

Figure 3-24. Distribution of Normalized Concentration Ratio along Cavity Walls of the Proposed Fairchild Receiver

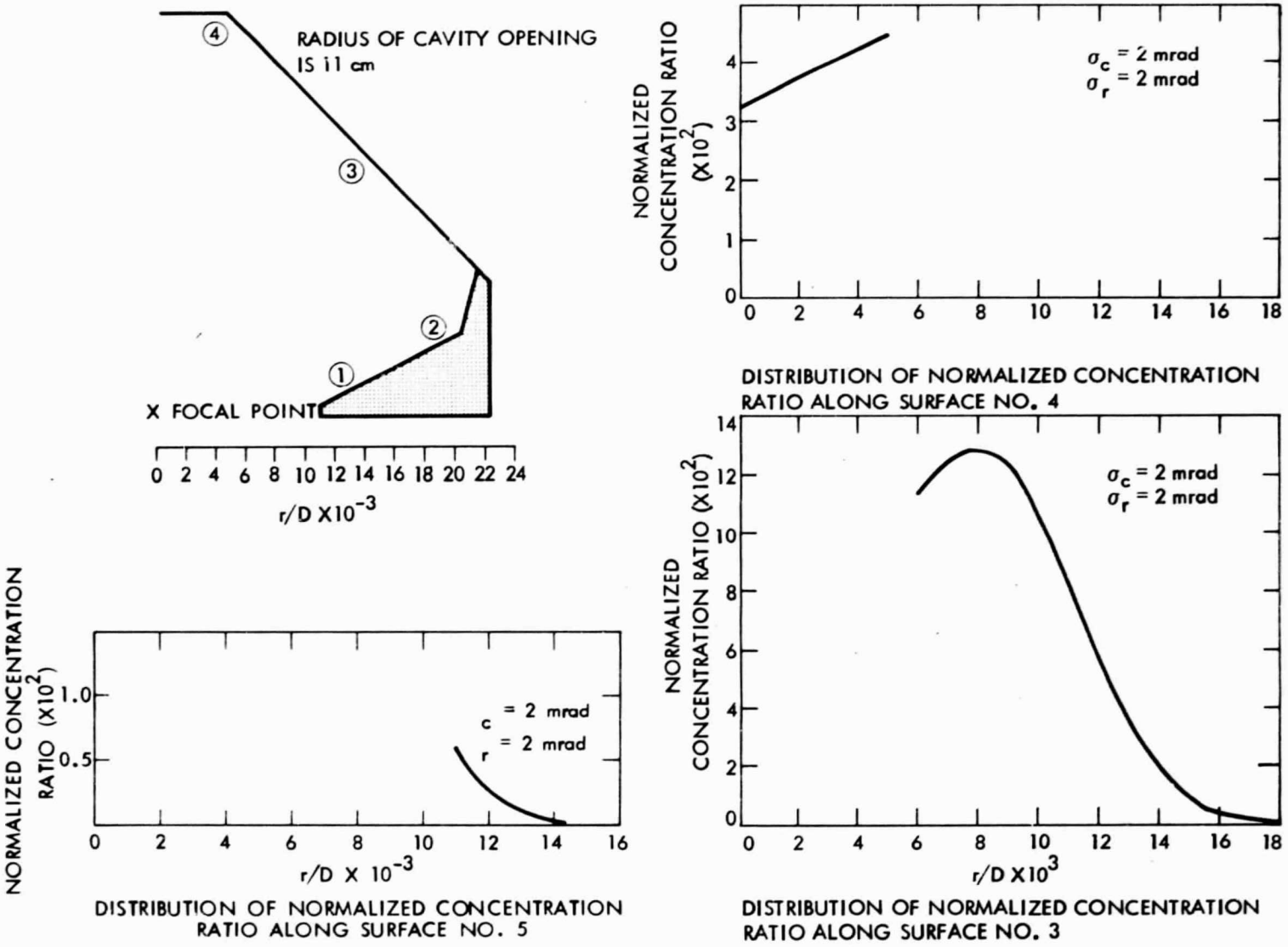

Figure 3-25. Distribution of Normalized Concentration Ratio along Cavity Walls of Proposed Fairchild Receiver

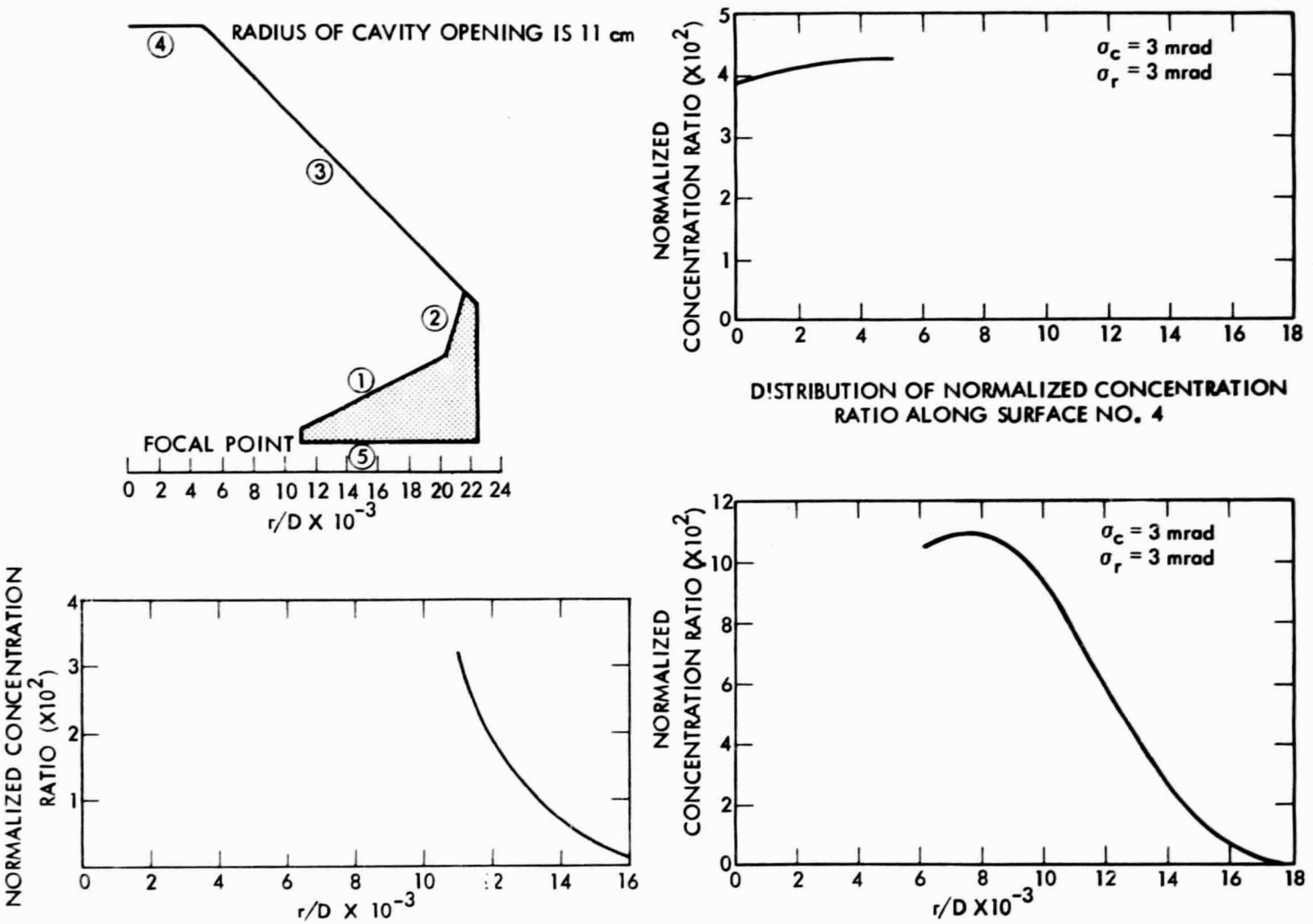

Figure 3-26. Distribution of Normalized Concentration Ratio along Cavity Walls of the Proposed Fairchild Receiver

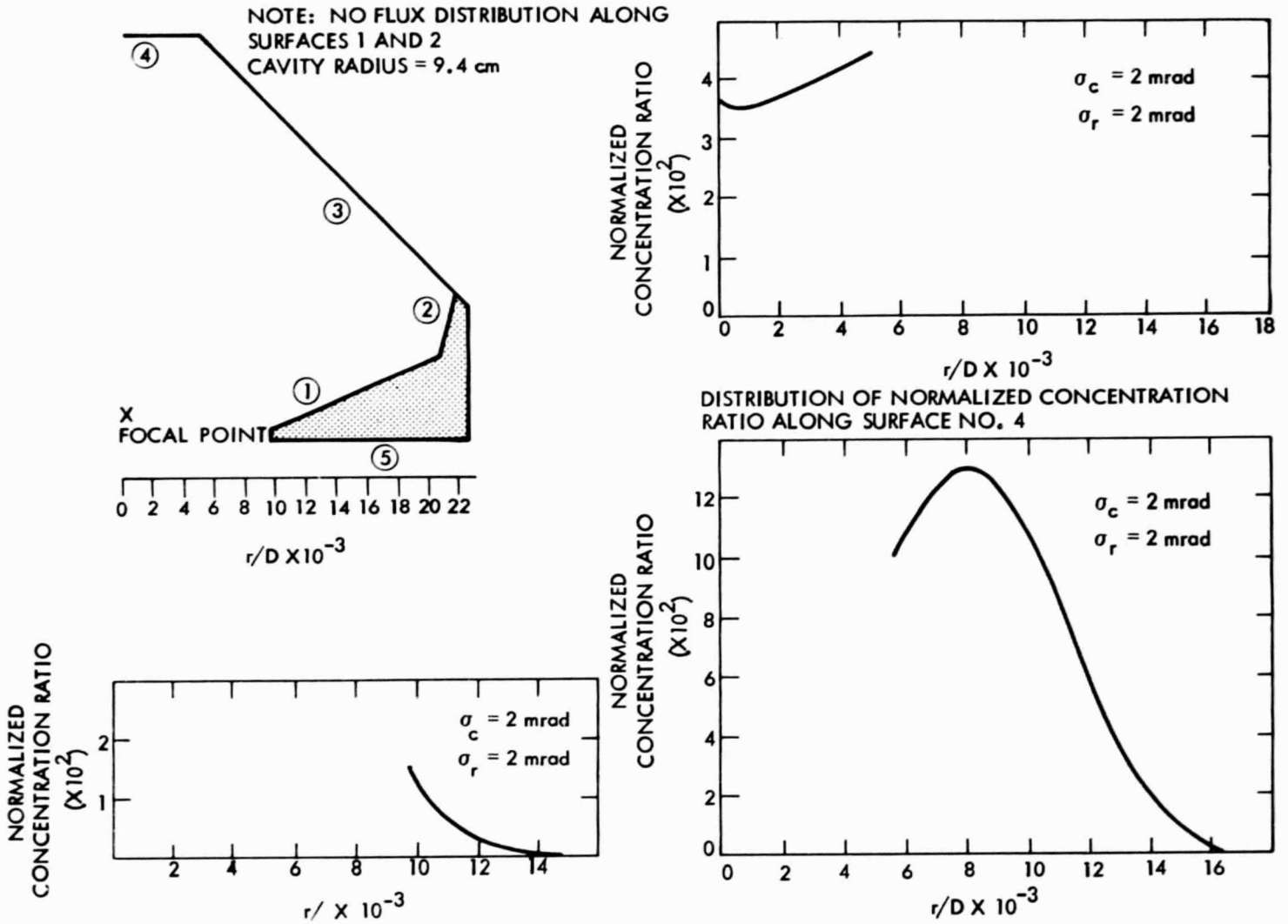

Figure 3-27. Distribution of Normalized Concentration Ratio along Cavity Walls of Proposed Fairchild Receiver

e. Optical Analysis Results and Discussions

Figure 3-14 shows a graph of normalized concentration ratios (defined as concentration ratio/reflectivity) along the focal plane for several cases of $\sigma_c = \sigma_r$. To obtain the flux distribution, multiply the normalized concentration ratio by reflectivity and the incident flux on the reflector. The simplest way to accomplish this is to relabel the ordinate on the graph. For example, if the incident flux is $0.8 kW/m^2$ and the reflectivity is 0.9, then a normalized concentration ratio of 10^4 corresponds to $0.8 \times 0.9 \times 10^4 = .72$ 10^4 kW/m^2. We shall use the terms "normalized concentration ratio" and "flux distribution" interchangeably. Figure 3-15 gives the intercept factor as a function of radial distance from the optical axis for the same cases of $\sigma_c = \sigma_r$. The intercept factor gives the fraction of the total energy reflected by the concentrator into the receiver for a given receiver aperture radius. It is an important quantity in determining the rate of collection of net thermal energy by the receiver.

Figures 3-16 and 3-17 give the normalized concentration ratio and the intercept factor for several cases of circumferential standard deviation, keeping the radial standard deviation constant. Figures 3-18 and 3-19 are graphs of the normalized concentration ratio and the intercept factor for several cases of radial standard deviation, keeping the circumferential standard deviation constant. In general, the circumferential standard deviation will be less than the radial standard deviation. However, the cases of $\sigma_c > \sigma_r$ are included for reference. It is clear that the slope error is instrumental in causing a spread of the total reflected flux.

The flux distributions along the receiver cavity walls are essential for establishing the receiver configuration and in determining the receiver performance. Figures 3-24 and 3-25 show the distribution of normalized concentration ratio along the walls of a receiver cavity as proposed by Fairchild Stratos for the case of $\sigma_c = \sigma_r = 2$ mrad and $\sigma_c = \sigma_r = 3$ mrad. The following assumptions are used to determine the graphs in Figures 3-24 to 3-27.

(1) The receiver aperture is located at the focal plane of the paraboloid.

(2) The concentrator center hole radius is taken to be 60 cm.

(3) The receiver aperture is assumed to have a radius of 9 cm (Figures 3-24 and 3-25) and 11 cm (Figures 3-26 and 3-27) respectively.

In Figures 3-24 and 3-25, a hot spot occurs along the conical surface between 6 and 12 cm from the optical axis. This is true for both cases of slope errors. Some of the energy reflected from the concentrator does not enter the receiver cavity. A fraction of the sunlight impinges along surface No. 5, constituting spillover losses. These losses may be reduced by increasing the cavity aperture radius. Figures 3-26 and 3-27 give the flux distributions along the receiver cavity walls for a larger aperture radius of 11 cm. Note that the hot

spot along the conical surface is still present. Changes in the inclination of this conical surface may result in a more uniform flux distribution.

f. Future Efforts

Future efforts in the Optical/Thermal Engineering area may be categorized thus:

Immediate Efforts

(1) Conduct an engineering analysis to determine the optimum receiver aperture size.

(2) Determine the receiver performance (efficiency, temperature distribution, etc.) using a thermal analysis program based on flux distributions presented earlier.

Continuing and Long-Term Efforts

(1) Provide technological inputs for various system components of ADS-1 (i.e., concentrator, receivers/engines).

(2) Provide technical management and guidance to subcontractors.

(3) Establish optical/thermal test requirements and advise on various test procedures.

(4) Provide an analysis and evaluation of optical/thermal test data.

(5) Provide technical assessment of advanced concentrator concepts and evaluate cost/performance competitive concepts from industries or in-house as possible candidates for future low-cost point-focusing systems.

3. Tracking and Control System

Work performed during this period considered different flux distributions as inputs for the dish-Stirling concept and generated efficiency reductions as a function of pointing error for optimized receiver apertures as outputs. The flux distributions were produced using numerical techniques and considered slope errors of 1, 2, 3, and 4 mrad.

An important parameter in the design of dish solar collectors is the nominal estimated value of the pointing error. If this value is large, then less energy is received through the aperture. If this value is small, then more energy will be received, but, the costs of the control system could be larger. Furthermore, the entire pointing error analysis is complicated by the need of receiver aperture size

optimization for the reduction of heat losses. References 1 and 2 give a theoretical basis for pointing-error analysis of dish collectors and Reference 3 gives a description of a zero error optimal control scheme.

A major item that affects the receiver aperture optimization and the control system analysis is the size and shape of the flux distribution produced by the concentrator's reflective surface. The major parameter affecting this flux distribution is the concentrator's slope error.

The intercept factor, Φ, is a measure of the percentage of concentrated energy that enters the receiver. The expected value of the intercept factor is a statistical expression that incorporates the expected long term pointing errors from the control algorithm. Analysis was made and the derived expression for this expected value is

$$E\{\Phi(R,A) = \int_0^{\sqrt{2A}} \Phi(R,\delta)\, f(\delta)\, d\delta \qquad (1)$$

where R is receiver aperture, A is deadband size, δ is the pointing error, and $f(\delta)$ is the error density function.*

The above analysis was done independently of the design of the receiver located at the focal plane. To obtain an energy loss function due to pointing errors, the receiver aperture has to be first optimized. To do this optimization on a rigorous basis requires a detailed thermodynamic description of the proposed receiver. Unfortunately, this is not currently available. However, using simple thermodynamic models, reasonable answers (at least on a relative scale) can be obtained.

As a simple model, assume the net power, Q, collected by the receiver is

$$Q = \rho I_o A G \Phi \alpha_{eff} - q_r \qquad (2)$$

where ρ is specular reflectance constant, I_o is the nominal direct insolation, A is the effective concentrator area, G is the shading factor, Φ is the expected value of the intercept factor, α_{eff} and q_r which describe the receiver are the most difficult to quantify. The following analysis uses values generated for a Brayton cycle with the exception that the temperatures are reduced to about 1500°F for the Stirling concept.

*R.O. Hughes, "Efficiency Degradation Due to Tracking Errors for Point Focusing Solar Collectors," 78-WA/SOL-4, ASME WA meeting, Dec. 1978.

Manipulation of equation 2 gives the following approximate expression for receiver aperture efficiency:

$$EFF = \frac{\alpha\phi(r) - 4\beta \quad (r/D)^2}{\alpha} \qquad (3)$$

where α is a concentrator parameter and β is a receiver parameter. Hence, it is desired to determine the aperture radius, r, which gives the maximum EFF for various control algorithm implementations. This results in an efficiency reduction as a function of control and is shown in Figure 3-28 for the four concentrator slope errors. These reductions are summarized in Table 3-6.

Two major observations can be made from the analysis performed herein:

(1) The reduction in efficiency for moderate pointing errors (say, 0 .1° or 0.2°) is modest. This indicates that a zero error system, if it is too expensive, would not be cost-effective.

(2) The graph/table within this study should <u>not</u> be used in an absolute fashion; i.e., efficiency numbers used in direct calculations of overall performance. Rather, because of uncertainties in the receiver model, they should be used in a relative way to compare various options.

Table 3-6. Reduction in Efficiency as a Function of Control Deadband

DEADBAND A ($\pm$deg.)	σ_s= 1 mrad	σ_s= 2 mrad	σ_s= 3 mrad	σ_s= 4 mrad	
0.0	96.48%	92.66%	87.60%	81.72%	← EFFICIENCY FOR ZERO ERROR
0.1	-0.24%	-0.19%	-0.16%	-0.08%	CHANGES IN EFFICIENCY
0.2	-0.83%	-0.68%	-0.60%	-0.46%	
0.3	-1.76%	-1.45%	-1.29%	-1.08%	
0.4		-2.45%	-2.22%	-1.93%	
0.5			-3.34%	-2.96%	

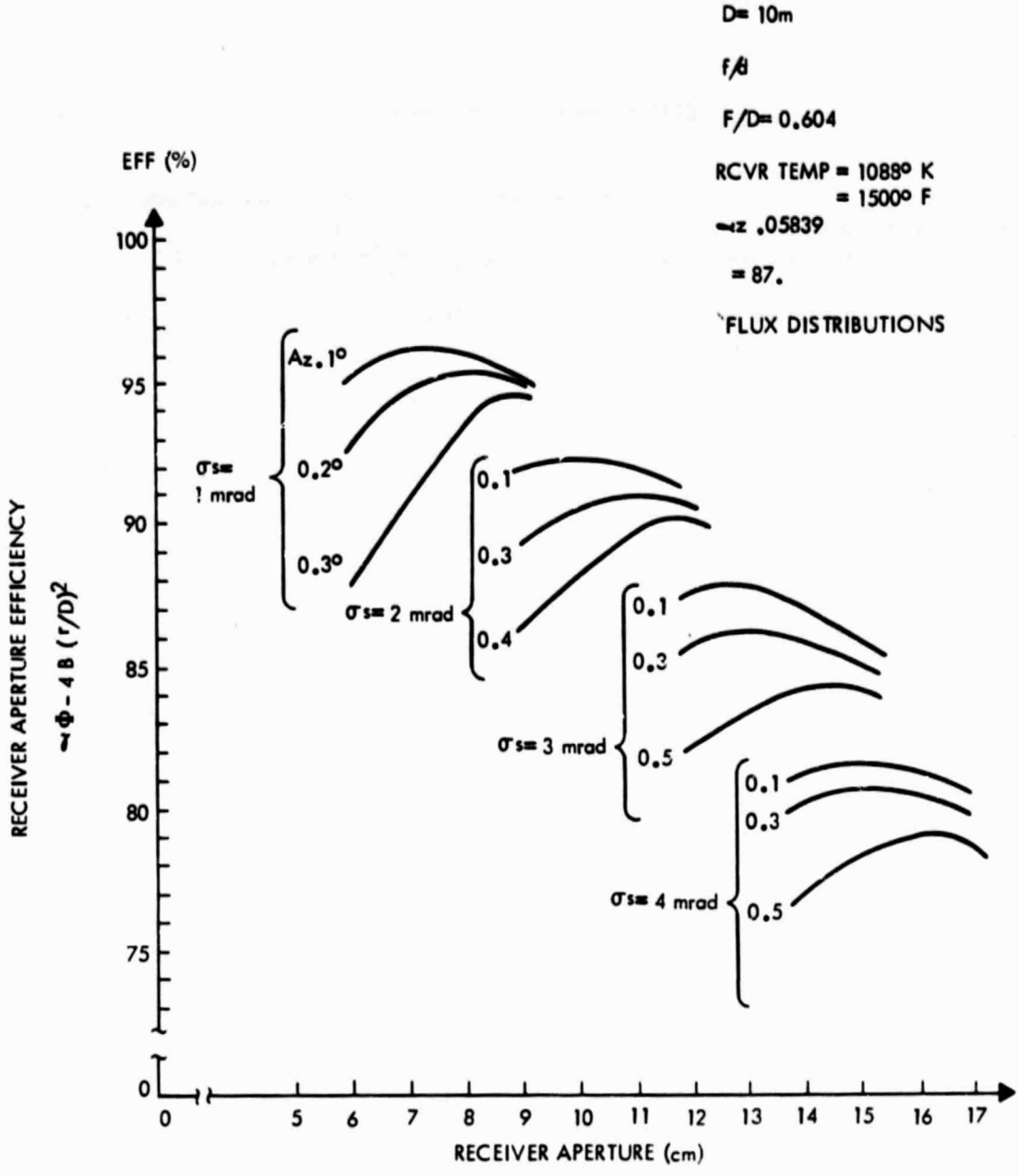

A : DEADBAND SIZE (± deg.)
Φ : EXPECTED VALVE OF INTERCEPT FACTOR
σs : STD. DEV. OF SLOPE ERROR (mrad)

Figure 3-28 Efficiency U.S. Receiver Aperture For Various Control Options

E. LIQUID-METAL TRANSPORT

1. Introduction

During an early stage of the conceptual design study on the use of liquid-metal heat-transfer technology in the distributed solar power systems, a number of benefit/cost analyses were conducted to evaluate various system alternatives. These analyses resulted in the selection of Heat-Pipe Solar Receiver (HPSR) as the baseline design, in which liquid metal heat pipes are used as a means of thermal energy transport. The conceptual design of HPSR with thermal-energy storage (TES) and its integration with Stirling engine/generator assembly was presented in the previous semi-annual progress report. The concept offered a relatively lightweight 15 kWe power conversion system with up to 2 hours of thermal energy storage.

Work for the current period has emphasized the technical and economic assessment of the more promising thermal transport and storage concepts. A single-collector pumped-loop concept was defined and its advantages, disadvantages and relative costs were compared with the focus-mounted heat-pipe heat receiver. As a result, liquid metal pumping by means of electromagnetic and gas lift pumps was considered.

In order to verify certain critical design concepts in the focus-mounted heat pipe heat receiver, experimental work was undertaken (1) to demonstrate the operation and capabilities of the primary heat pipes and (2) to measure, with easy fluids, the performance of the wicking intended for use in the secondary TES heat pipe and to predict the performance of those wicks in sodium at elevated temperatures.

Further assessments of the focus-mounted heat-pipe heat receiver were conducted with emphasis on (1) the optimization of thermal insulation configurations (a 2-in thick layer of vacuum multifoil insulation had been initially selected to minimize solar shadowing), (2) the cost effectiveness of various fused-salt storage materials and the effect of storage time on subsystem costs and, (3) operational assessments of the system for (a) failure modes and the consequences of failure, (b) function of the primary heat-pipe thermal diodes in the stored-overnight position and (c) the thermal effects of missed-aperture solar insolation.

2. Alternative System

During earlier work, alkali-metal pumped-loop thermal transport and storage systems were also considered for various single and multiple concentrator thermal transport and storage systems. The initial study indicated prohibitive heat losses for long runs of very high-temperature thermal transport fluids between collectors. Best possible potential advantages existed for simple collector pumped-loop

systems where larger thermal storage masses could be located behind the solar collector along with the power-conversion and liquid-metal pump components.

a. EM Pumped Loop

The physical arrangement of the single-concentrator pumped-loop concept is shown in Figure 3-29. The system was designed to meet the same design guidelines as the heat-pipe heat receiver for purposes of direct comparison. Only the liquid-metal-cooled heat receiver is mounted at the collector focal point. The much greater portion of the system weight, approximately 88%, is located behind the collector where the mass of the Stirling engine/generator, thermal energy storage, electromagnetic pump and liquid-metal valves can be used in place of some of the counterbalance weights currently placed behind the collector. This collector rear-face mounting position for the storage, pumping and power-conversion components also provides the opportunity for increased thermal storage mass and duration. Thermally insulated liquid-metal piping carries the heat from the heat receiver at the focal point along the collector struts and back to the power-conversion components. The heat receiver is a cavity-type receiver with liquid-metal-cooled walls. A flow diagram for the system is shown in Figure 3-30; it indicates the more complex nature of the positive, but flexible, control of heat to and from the various components and the need for a heat-control system to actuate the various control valves.

A cross section of the thermal storage and Stirling engine generator layout is shown in Figure 3-31. To minimize thermal losses the major components of the system including the liquid-metal TES heat

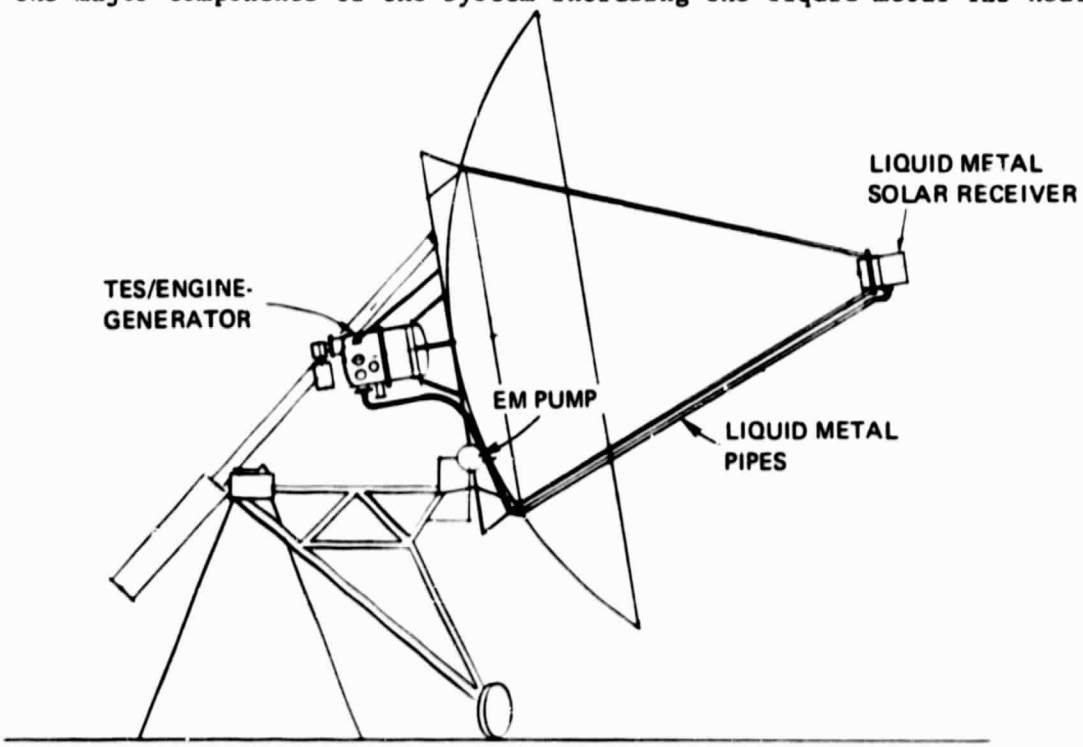

Figure 3-29. EM Pumped Loop

exchanger, the liquid-metal Stirling-engine heat exchanger and the various closely coupled control valves and piping are contained within a vacuum-insulated chamber containing fibrous insulation in the interior and having additional fibrous insulation surrounding the vacuum shell, which operates at a temperature approaching 1000°F (540°C). Table 3-7 provides a brief engineering definition of the critical characteristics of the system.

b. Gas Lift Pumps

As an alternative to the use of an electromagnetic pump, an inert-atmosphere gas-lift pump was considered. Such a pumping system involves the introduction of an inert dispersed gas in a vertically rising leg of a recirculating liquid-metal loop and the extraction of the gas from the sodium near the heat receiver. At a gas volume fraction of 0.6, a pressure head of 23.4 kPa (3.24 psi) can be achieved for the single-collector pumped-loop system. While the system appears simple in concept and free of the high-temperature problems in hot EM pump stators, much experimental work would be required to demonstrate the performance of such pumping devices at various angles of inclination and flow rates. A regenerator to cool the separated gases for cool-gas recirculation would be necessary to minimize losses in efficiency and special devices would be required to separate entrained sodium from these recirculating gases. An efficiency loss in the system from 3.4 to 9% could be expected, depending upon whether or not a recuperator were used and assuming that developmental effort could resolve expected operational problems without further losses in efficiency.

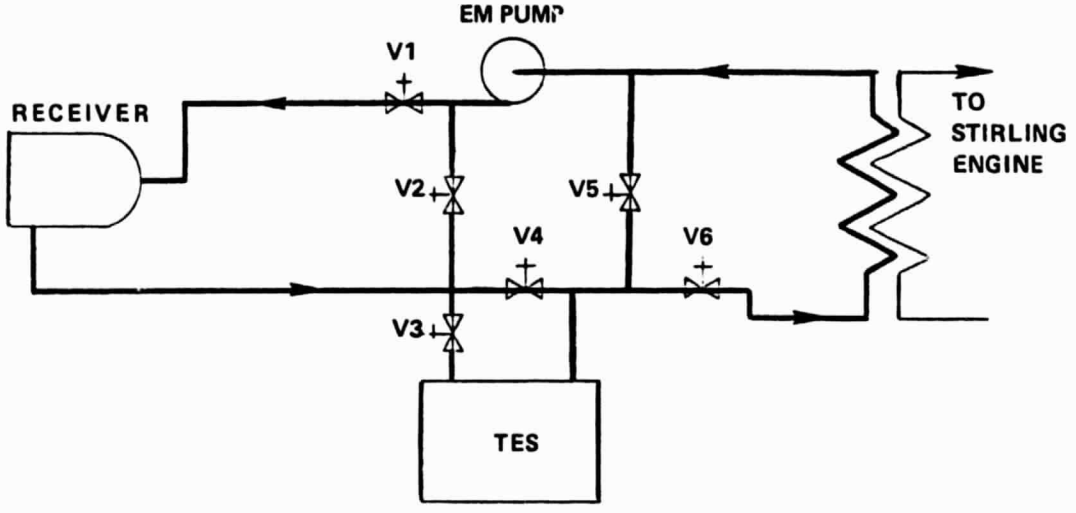

Figure 3-30. Flow Diagram of Heat Receiver

Table 3-7

Pumped Loop Engineering Definitions

Type of Salt	LiF
Weight of Salt	359 kg
Melting Temperature of the Salt	857°C (1575°F)
Number of Salt Containers	140
Diameter of Salt Containers	40 mm
Sodium Pipe Diameter	25 mm
Sodium Mass Flow (Nominal)	0.7 kg/s
Electromagnetic Pump*	
Weight	130 kg
Efficiency**	8%
Pressure Rise	27.6 kPa
Number of Valves	6
Sensible Heat Temperature Difference for Sodium to Deliver:	
52.5 kW_t	58°C (104°F)
62.1 kW_t	70°C (126°F)
LiF T for 52.5 kW_t at 95% Solidification	30°C (54°F)
LiF T Allowed for Superheat	8°C (14°F)
Maximum Sodium Temperature in Receiver:	
(857°C + 8°C + 73°C)	938°C (1720°F)
Maximum Sodium Temperature in Stirling HX:	
(857°C - 30°C - 58°C)	769°C (1384°F)
Normal Sodium Temperature in Stirling HX:	
(857°C - 58°C)	799°C (1470°F)
System Weight	3550/4530 kg***

* Engineering estimates only.
** Pump Power = 324 W plus possible extra power to cool the pump.
*** Electromagnetic Pump/Gas-Lift Pump.

On the other hand, the development of EM pumps to handle liquid sodium effectively at minimum system temperatures of approximately 1500°F (816°C) also represents a significant challenge. The technology has been demonstrated in Rankine-cycle development hardware for space-power applications to operate an EM pump with 1000°F stator temperatures in boiler feed pumps. An extension of this technology and the use of a greater degree of stator cooling would provide for the satisfactory development of EM pumps over a period of time.

c. Focus-Mounted vs Pumped-Loop Comparisons

A direct comparison of the focus-mounted heat-pipe heat receiver with the collector-mounted EM pumped-loop system can be made since both systems were conceptualized with LiF as the fused salt and both had identical thermal st ge periods. Earlier thermal-loss analysis indicated that a collecto ounted power-conversion system with its long liquid-metal thermal-transport piping would have more than double

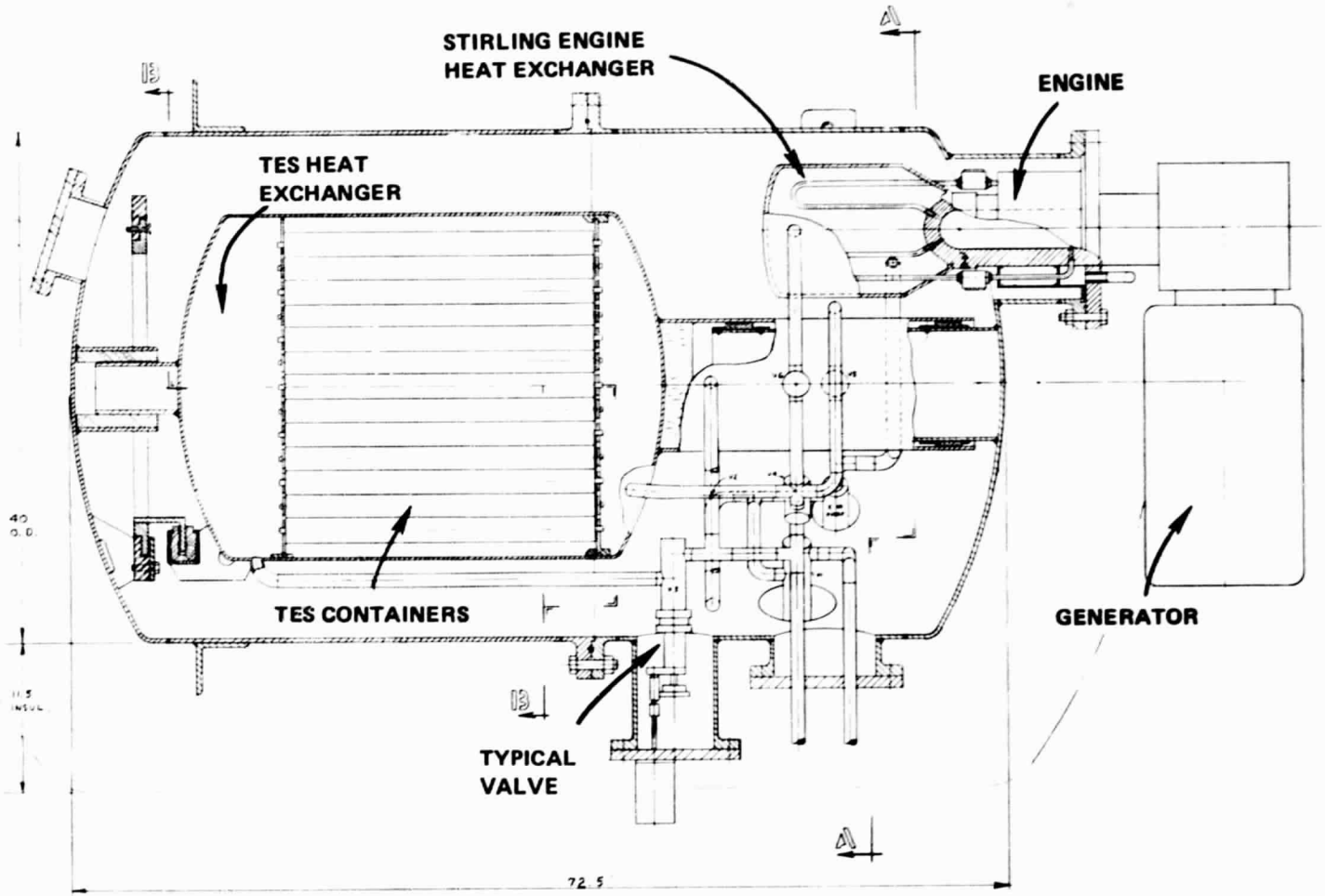

Figure 3-31. Cross Section of Thermal Storage and Stirling Engine Generator Layout.

the non-heat-receiver losses from the focal-mounted system. As indicated in Table 3-7, the loss in system operating temperature necessitated by sensible heat transfer in flowing liquid sodium at reasonable flow rates would impose a significant operating temperature span (approximately 344°F at the worst) between the heat receiver and the Stirling-engine heat exchanger; higher heat receiver temperatures, different fused-salt melting temperatures and significantly reduced Stirling operating temperatures with reduced system efficiencies would be entailed.

The pumped loop system does offer more positive and, at the same time, flexible control of the thermal energy to and from storage, as compared to the self-regulating thermal storage system in the heat-pipe heat receiver. But, it requires a control system and the incorporation of numerous high-temperature valves, for which significant development effort would be required.

The smaller and lighter receiver of the pumped-loop system should provide for more effective utilization of system weight in the concentrator and open the opportunity for the use of larger amounts of thermal energy storage material located at the rear of the collector, replacing some (if not all) of the concentrator counterweights.

From a design analysis it is expected that the pumped-loop system would weigh 3550 kg vs. 1488 kg for the heat-pipe heat receiver and would cost in mass production about 1.5 to 2.0 times the cost of the heat-pipe heat receiver.

Overall, the following advantages of the focus-mounted heat-pipe heat receiver appear to favor its use over pumped-loop systems.

(1) Self-regulating thermal control

(2) Near-constant Stirling-engine power capability

(3) No valves or pumps

(4) Negligible thermal pumping power required

(5) Minimized thermal losses

(6) More nearly isothermal system operating temperatures

(7) Economic mass production in complete power system modules

(8) No extensive on-site assembly required

(9) No major new component development required

(10) Lower system weight and cost

3. Heat-Pipe Transport System

a. System Assessments

The simplicity, compact modular design and thermally self-regulating aspects of the heat-pipe heat receiver encouraged its further exploitation. The major need in the assessment of the design, aside from the needs to prove a capability for long life operating reliability, lay in the following areas:

(1) Operation of primary heat-pipe thermal diodes in the heat receiver at various angles of inclination at a power of 2.3 kW_t and at temperatures near 1600°F (870°C)

(2) Pumping and flow capabilities of the metal wicks intended to supply sodium to the various heat sources within the secondary TES/Stirling-engine heat pipe

(3) Design improvements in thermal insulation to reduce the costs and weight of vacuum multifoil insulation with some minor increase in shadowing of the collector

(4) Consideration of alternate-thermal energy storage materials with greater economic potential

(5) Assessment of heat-pipe heat receiver operating procedures including startup, shutdown, control of primary heat-pipe losses overnight and the effects of missed-aperture insolation

(6) Assessment of potential failure modes

b. Heat-Pipe Tests

Five primary heat pipes, with various types of internal wicking, including 60-mesh wire screens and internally threaded or machined surfaces, are currently in the process of being prepared and tested.

Figure 3-32 shows a typical primary heat-pipe, one of 27 in the heat pipe heat receiver and the modular heat pipe test facility used to test these heat pipes at various angles of inclination. In testing thus far, the heat pipes have performed as expected without startup problems or wicking limitations. Continued testing should disclose the most economical wicking arrangement that meets the operational requirements.

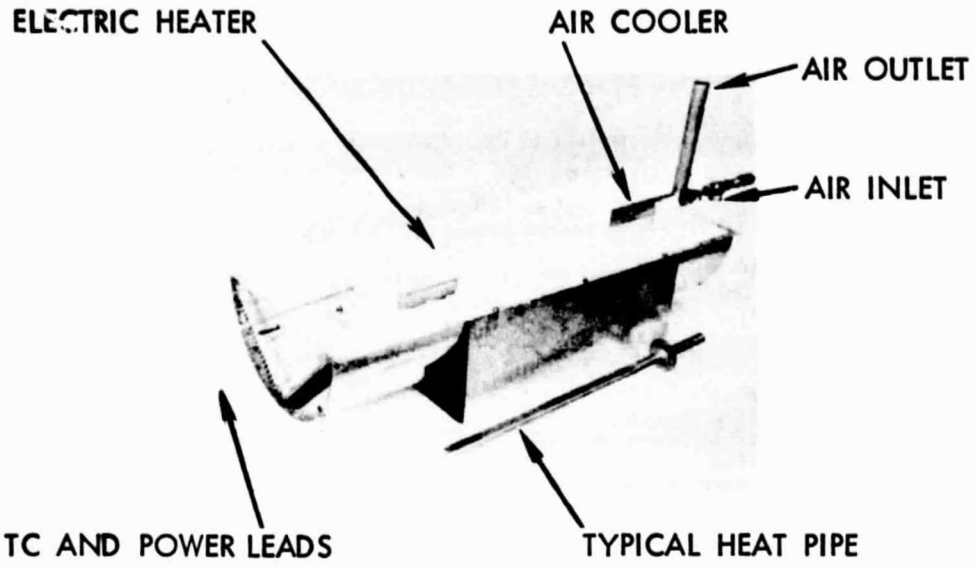

Figure 3-32. Instrumented Heat Pipes in Test Facility

c. Wicking Tests

While various unique pumping and flow requirements exist in the secondary heat pipe, wicks within that heat pipe must be capable of pumping sodium to heights up to 18 inches at a flow rate up to 0.04 lb/sec. Flow occurs through many wicking avenues and must occur across right-angle and butt joints between fiber-metal wicks and 60-mesh wire wicks. Easy-fluid cold-wicking tests have been conducted on various wicks and joints and across joints between wicks. Data in the form of flow rate vs. capillary pumping height, maximum capillary pumping height and flow across points are currently being evaluated to predict the capillary pumping pressure and flow rate vs. static head for the wicking configurations in the secondary heat pipe. The initial testing at various inclinations indicate the feasibility of wicked pumping over the interior of the secondary heat pipe. It remains to be determined, in subsequent modular tests and full-scale hardware testing, the extent to which wicking can be minimized for cost reduction purposes.

d. Thermal Insulation

Because of the great weight of multifoil insulation and the necessity of maintaining a vacuum between two relatively heavy metal shell structures, the use of more economical, but bulkier, multilayer fibrous insulation systems was studied. Figures 3-33 and 3-34 represent two of several methods for comparing the effectiveness of fibrous and multifoil insulations. Figure 3-33 indicates the cost reductions possible in utilizing either premium fiber insulation materials or more economical fibrous insulation materials. Figure 3-34 indicates the weight saving over the weight of vacuum

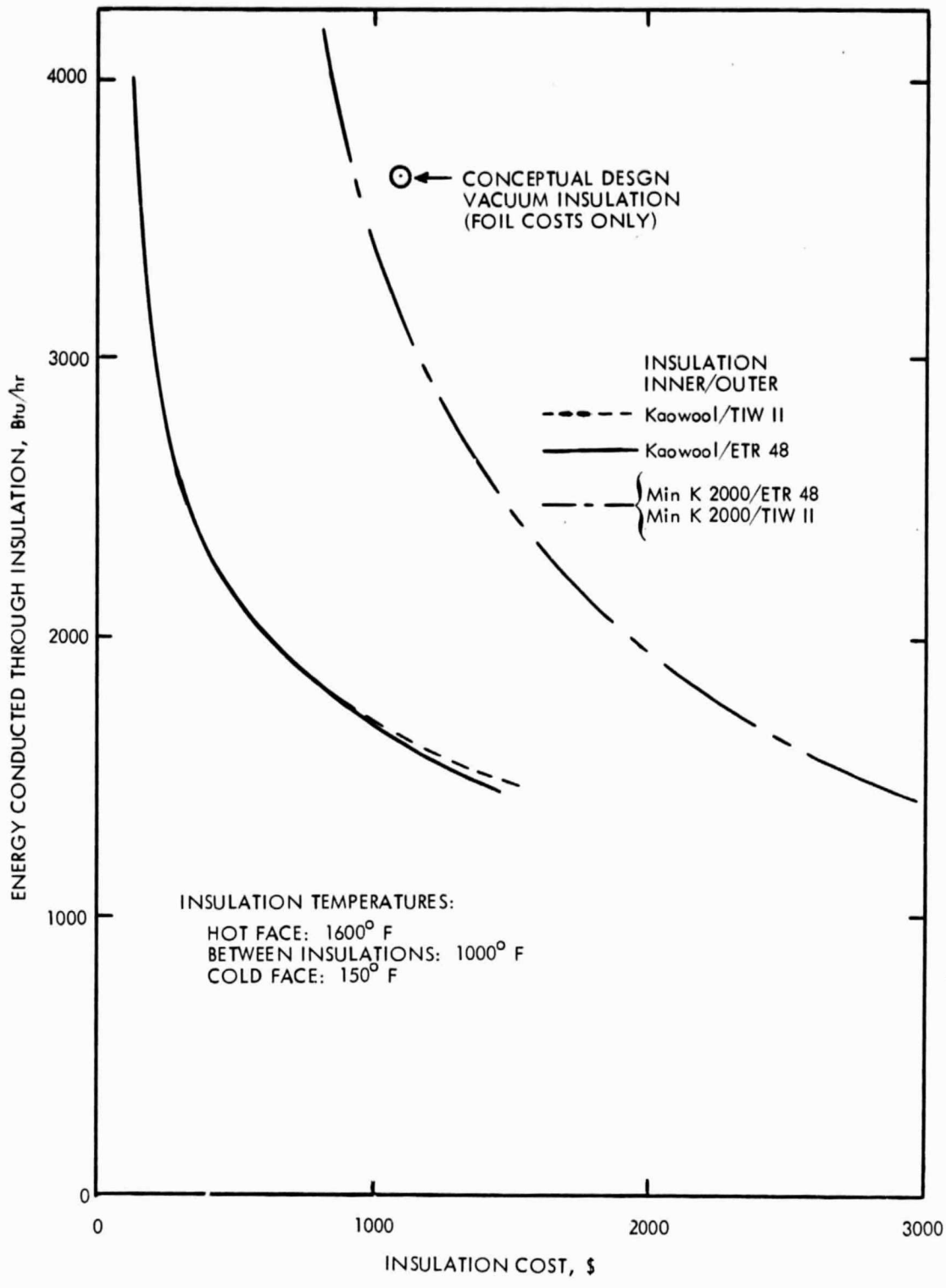

Figure 3-33. Insulation Cost Versus Energy Lost

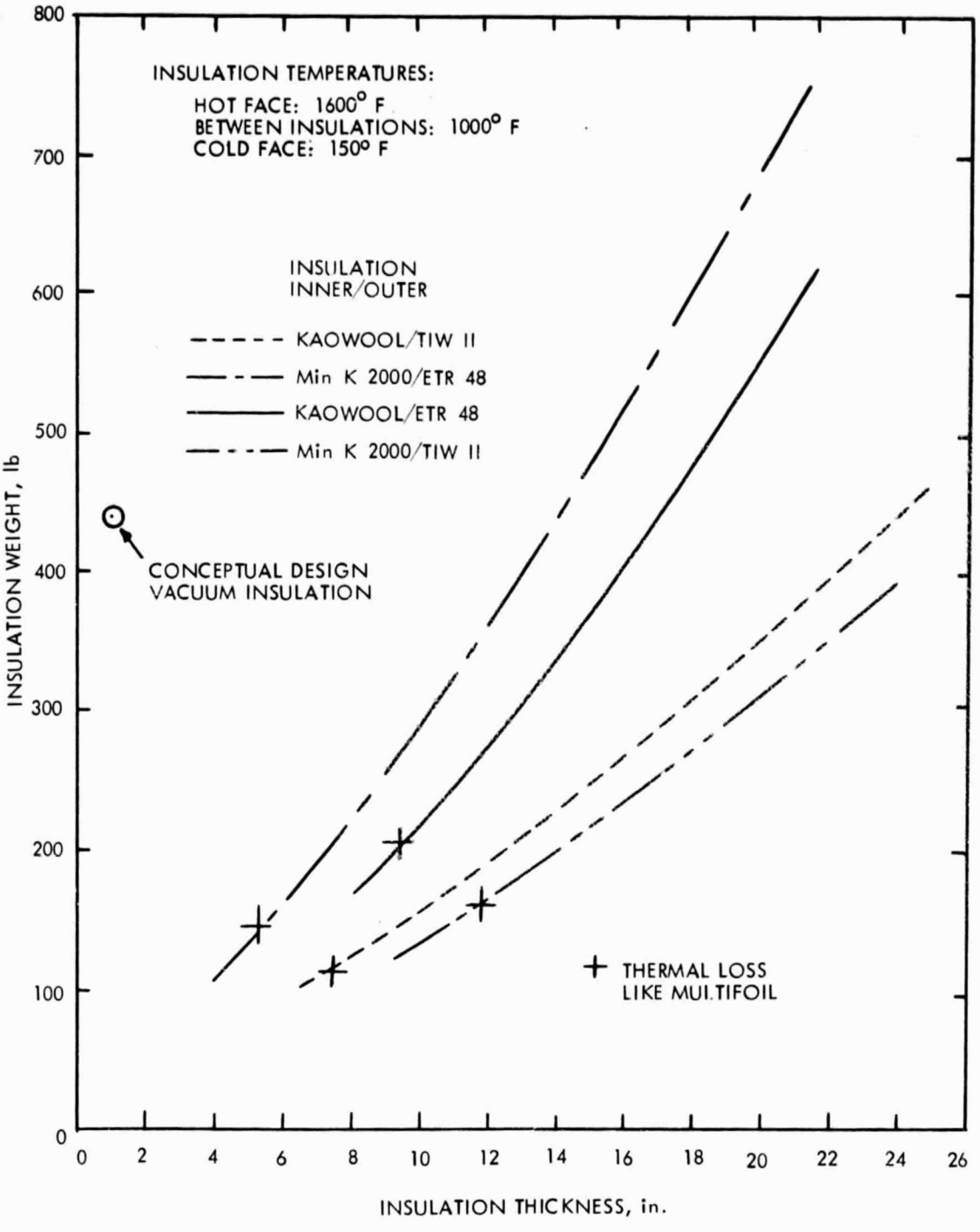

Figure 3-34. Insulation Weight Versus Thickness

multi-foil alone which can be achieved at some reasonable increase in insulation thickness. Not indicated is the additional weight saving that might occur by replacing the outer cylindrical vacuum shell and flexible bellows in the original concept with a potentially lighter-weight trussed structure.

e. Thermal Energy Storage Materials

Alternative thermal-storage materials to LiF have been considered. These include 33% NaF-66% MgF_2 and Na_2CO_3. A comparison of the relative costs of these materials in the conceptual design is shown in Table 3-8 for the basic TES materials cost involving salt, containment can, containment can wicking, support structure and support-structure wicking. Although sodium carbonate is extremely inexpensive, compared to either of the other two salts, its heat of fusion and density do not compare as well with the NaF-MgF_2 eutectic. When placed in the large container required, the cost of the can and wicking required to provide a unit of thermal storage is overriding and the advantages of salt economy, alone, are lost.

In order to assess the effect of change in storage time as it affects the complete design, a 15-min storage subsystem capable of supplying 52.5 kWt and including the heat receiver, insulation, structure, etc., was defined as in Table 3-9; its component weights and the materials costs were determined. A comparison of these heat-receiver/TES subsystem materials costs at 15 minutes and at 1.27h of storage for the NaF-MgF_2 TES material indicated a materials cost of \$4170/h of storage at 52.5 kW or \$79.50/kWh. (See Figure 3-35). Since receiver and structure costs are more significant as the storage is reduced, it is expected that the true materials cost of thermal storage in these systems lies well below \$79.50/kWh and perhaps slightly above \$40.00/kWh (as evidenced by Table 3-8).

Further design improvements can be expected to further reduce the wicking, containment and other structural costs associated with changes in the amount of energy storage in the system.

f. Operational Analysis

An initial failure mode receiver analysis has been completed for the heat pipe, heat receiver with TES. Each principal component has been reviewed with respect to potential failure modes, relative probability of occurrence, consequences of failure, methods of avoiding or detecting failure, repair methods, relative repair costs and safety aspects.

Thermal fatigue, oxidation creep-rupture and heat pipe performance reliability are principal areas where adequate design, good production quality control and long-term system test experience will be required to assure long operating life. The primary heat pipe design in the heat receiver, where cyclic thermal loading will be more severe, is

one in which failure of one or more heat pipes will not significantly affect system performance. Because of the single heat-pipe construction in the secondary TES/Stirling-engine heat pipe, the consequences of a gross failure would require system shutdown. However, the large thermal inertia and stable operating temperature within this large heat pipe, the compartmentalization of the TES material and the redundancy in wicking for liquid-metal pumping makes this system potentially less susceptible to significant failures. A simple temperature sensor in this TES heat pipe is required for thermal control during operating and as a warning device for potential or actual failure.

Because the heat pipe heat receiver with TES can be mass-produced at the factory under well-controlled conditions, quality control, product reliability and component reproducibility should be excellent. As a single model, service beyond simple maintenance operations can be achieved by removing the module and correcting deficiencies either in an on-site shop or by return to the factory. Field service at the site could be held to a minimum.

Since each heat pipe in the receiver contains a negligible amount of sodium, the failure of any primary heat pipe has no significant safety hazard. The hazard from loss of sodium from the secondary heat pipe is similarly limited because of the relatively small quantity of sodium it contains and the dispersed nature of the solar-concentrator power-collection system.

The startup of the primary heat pipes does not appear to offer any significant systems limitations. The secondary heat pipe will be capable of transferring heat provided that the sodium in this large heat pipe is molten. Accordingly, thermal input to the secondary heat pipe may be limited, during initial operation, until all the parts of the TES heat pipe reach a temperature above 210°F(98.9°C). Electrical trace-heating elements may be added to precondition the secondary heat pipe thermally for immediate solar operation at more substantial power levels. Since it is expected that the system will be maintained overnight with the TES at an elevated temperature above 1500°F(816°C), no routine startup problems are expected.

Table 3-8. Relative Thermal Energy Storage Materials Costs

TES Material	LiF	33%NaF-66%MgF	Na_2CO_3
Melting Point	857°C (1575°F)	832°C (1530°F)	851°C (1564°F)
H_f	400 Btu/Lb	265 Btu/Lb	120 Btu/Lb
TES Material Cost	$3.15/Lb	$0.45/Lb	$0.03/Lb
Density	144.9 Lb/Ft^3	108.8 Lb/Ft^3	156.5 Lb/Ft^3
Costs: ($/$kWh_t$)			
Salt	$26.89	$ 5.80	$ 0.84
Can & Can Wicking	$ 8.32	$10.78	$16.54
Sub Total	$35.21	$16.58	$17.38
Support Structure, etc.*	$21.18	$21.18	$21.18
Grand Total	$56.39	$37.76	$38.56

*Includes latent and sensible heats and cost for fore and aft capsule support and fore and aft capsule support wicking.

Table 3-9. Comparison of Two Thermal Energy Storage Systems

	1/4 Hour (Nominal) TES System	1.27 Hour TES System
Capsule Size	318 x 32 mm	622 x 58.4 mm
Weight of Salt (33%NaF-66%MgF_2)	81 Kg	330 Kg
Weight of Overall System (without engine or generator)	680 Kg	1124 Kg
Number of Capsules	151	97
Discharged Capsule Temperature Gradient	31°C (56°F)	40°C (72°F)
Center of Gravity of Heat Receiver/TES (distance from the primary heat pipe bulkhead)	20 mm	279 mm
Material Cost	$6400	$10,400
Storage Time*	0.30 hr.	1.27 hr.

*Includes latent heat plus 100°F sensible heat for structure and 1/4 of salt.

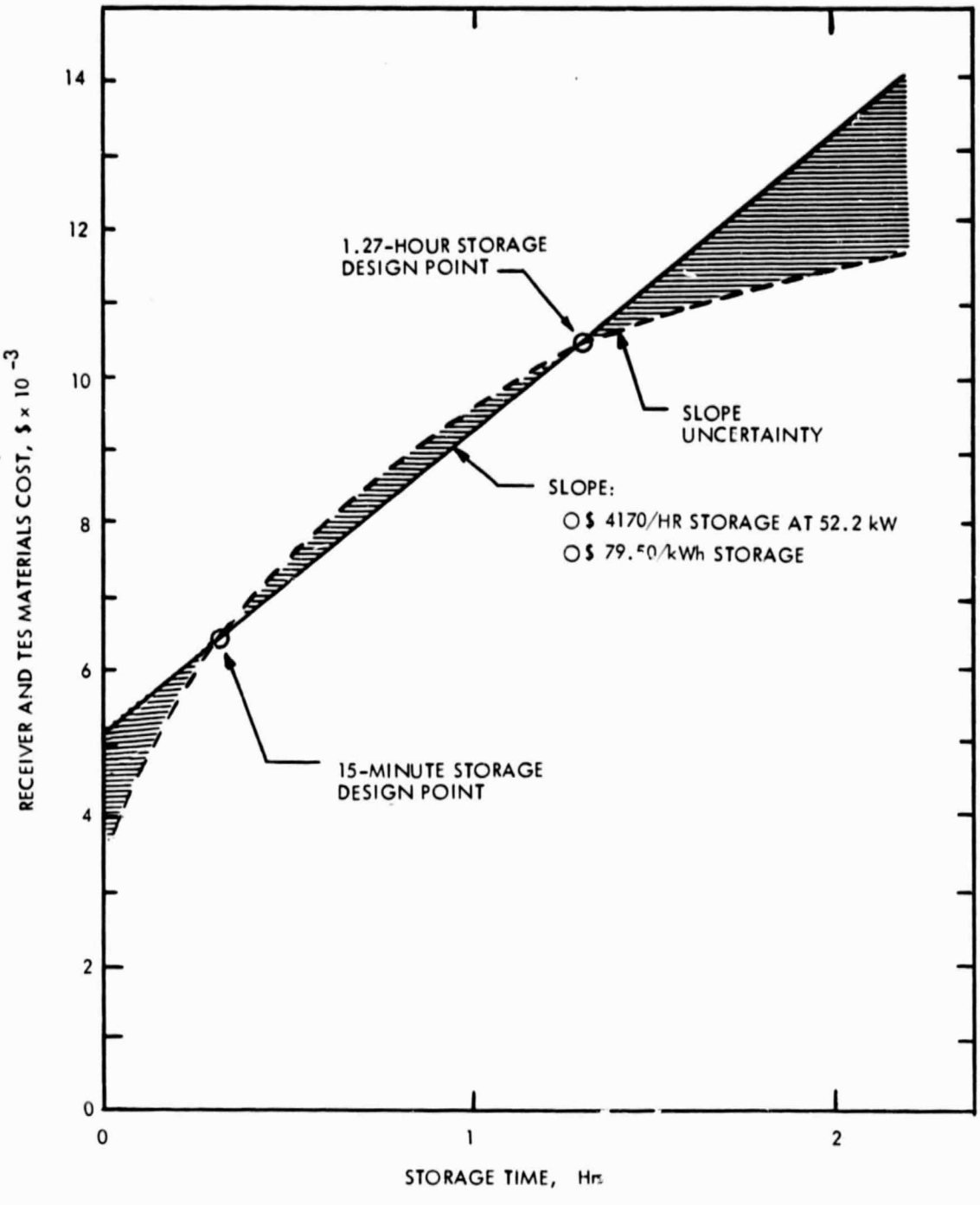

Figure 3-35. Receiver/TES Subsystem Materials Costs Vs. Storage Time at 52.5 kW Using $NaF-MgF_2$ Salt

During storage overnight in the nose down position, heat could flow in the reverse direction from the TES to the heat receiver and be lost through radiation. One way to avoid this is to allow the receiver to cool so that this sodium for the primary heat pipes solidifies near the aperture and cannot flow to the TES end of the primary heat pipe when the concentrator is moved to the nose down position. To determine if solidifacation of the sodium will occur, as indicated in Figure 3-36, thermal analysis has been performed assuming infinite thermal conductivity in the heat-pipe evaporator section or thermal conductivity of the metal wall only. While it appears that the lower thermal transport of the heat pipe at low temperatures will restrict the heat flow to the aperture end of the heat pipe and permit the sodium to solidify, more elaborate thermal analysis that includes model performance of the heat pipe or simple experimental verification will be necessary.

Thermal analysis studies are also being performed to determine the effect of the solar focal point missing the aperture or traversing the enclosed end face of the heat receiver as the focal point is repositioned in the heat receiver. Initial analysis indicates exceedingly high equilibrium temperatures would be achieved approaching the melting point of the ceramic shield; however, brief tracking of the focal point across the low-expansion corderite ceramic is not expected to be of significant effect.

4. Future Plans

The heat-pipe test data and the wicking capillary pumping and flow test data will be reduced and assessed. The final operating analysis, failure mode analysis and economic assessments of the heat-pipe heat receiver will be completed for incorporation in a later program report.

Under a separate contract, work is starting on the design, fabrication and ultimate testing of a heat-pipe heat receiver with more than 1h of thermal-energy storage. This heat-pipe receiver will be integrated with a 20 kWe Stirling engine/generator system for test on the 11-meter collector. A fossil-fuel burner is to be added to surround the primary solar receiver heat pipes and to permit both mixed-mode operation and operation on either solar or fossil fuel energy sources alone.

F. POWER PROCESSING, POWER MANAGEMENT AND UTILITY INTERFACE

This section discusses hybrid solar generating system configuration dynamics and controls associated with the combustion system and the Stirling engine and considers power processing requirements of a 10 MWe plant with AC and DC link generation schemes. It also presents a plant layout with utility interface.

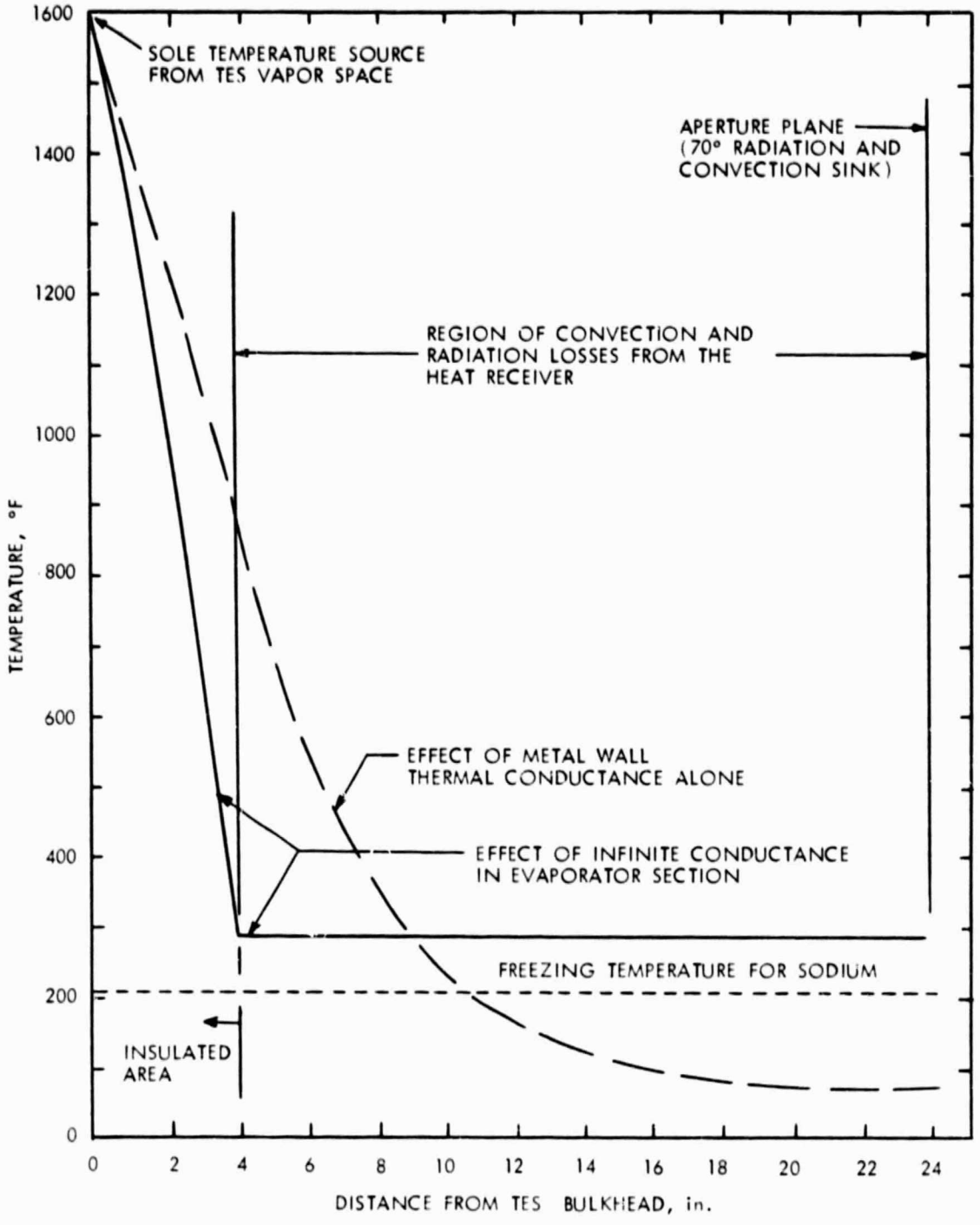

Figure 3-36 Nightime Steady State Temperature Distribution for a Primary Heat Pipe in the Solar Receiver

1. Generators

Induction generators are cheaper, lighter and more efficient than synchronous generators in the power range of 20-30 kW. Induction machines may be used to start the Stirling engine. However, induction generators present some problems that do not arise if synchronous generators are used. Because the induction machine rotor carries no exciting current, as does a synchronous machine, it is essential that the exciting field be produced by the stator winding. This requirement has to be met by a synchronous machine connected to the line. In addition, the power factor of the induction generator output is always leading, independent of the external circuit. Therefore any lagging component of current required by a load must be supplied by other synchronous apparatus such as a synchronous condenser. In AC-link operation, induction generators can be used without any difficulties if the solar generating unit feeds a grid. If the unit is required to feed an isolated load and there is no synchronous machine available, an induction machine cannot be used as a generator.

In DC-link operation with variable power output, the engine speed is not controlled. An AC generator is used and the generator output is first rectified and then inverted before introducing into the grid. In this operation, the heat input to the engine does not have to be constant. There is an apparent loss of efficiency in DC-link operation. An induction generator may be used if the load is a utility grid. The control requirement is simpler but the cost is increased due to conversion devices.

2. Combustion Control Systems

A simple closed-loop fuel-to-air ratio control system is shown in Figure 3-37. A block schematic diagram showing combustion and speed controls is shown in Figure 3-38. The combustion control system is activated only when the value of solar flux is smaller than that required to generate rated electrical power output. An error signal initiates the fuel control system and air control system simultaneously. This simultaneous control action is necessary because even a small delay in matching required fuel-to-air ratio for additional combustion heat output will seriously upset the combustion condition in the combustor. The reference signal is set at the peak value of the solar insolation for which the hybrid system is designed. Values of K_1 and K_2 are set according to the error signal. As the error signal increases both K_1 and K_2 will assume higher values, since the combustor will need more fuel and air to produce more heat input to the engine. Fuel flow and air flow for proper fuel-to-air ratio are matched because the values of K_1 and K_2 are calibrated in the field combustion tests. If the engine speed deviates from the rated value, the actuating signal, e, is adjusted continuously until the heat input to the engine restores the engine speed.

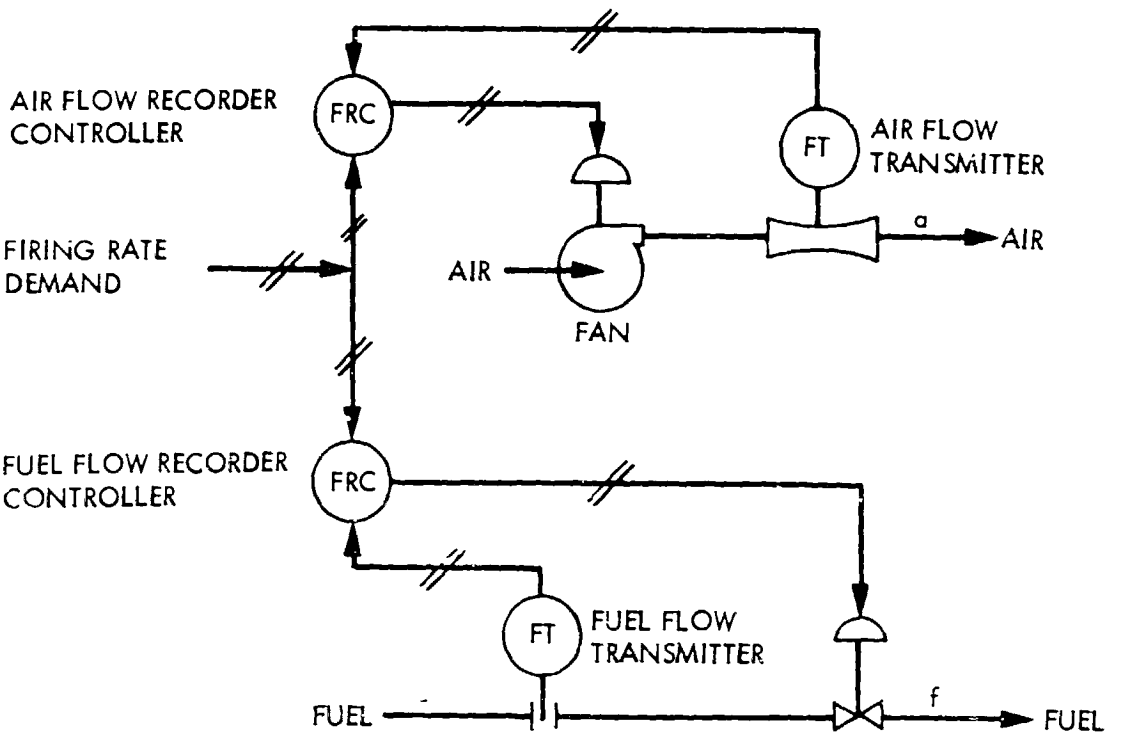

Figure 3-37. A Closed-Loop Fuel/Air Ratio Control in a Combustion System

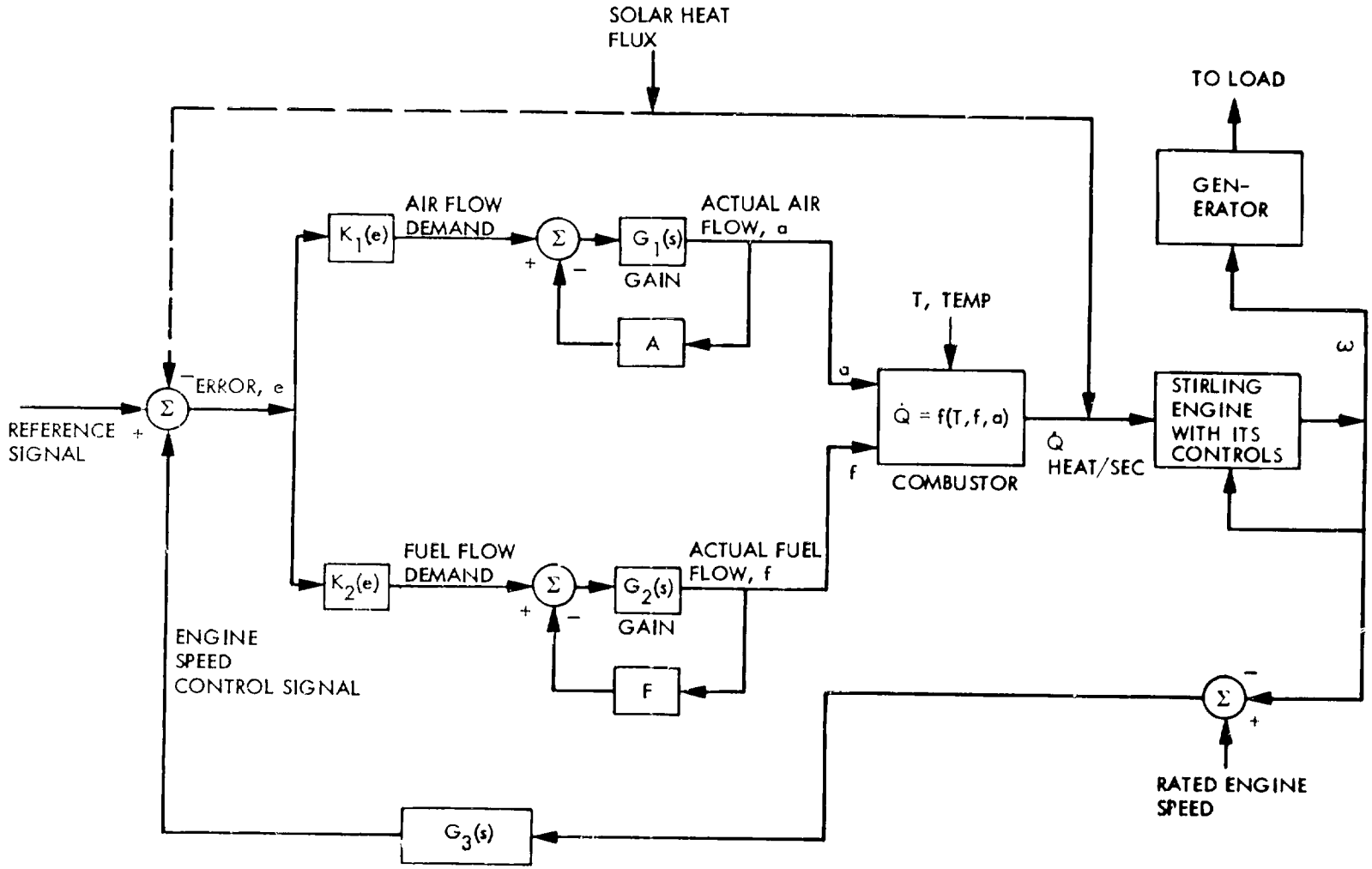

Figure 3-38. A Block Schematic Diagram for Combustion and Speed Control Systems

3. Engine Controls

a. Kinematic Stirling Engine

Figure 3-39 shows a typical performance map of a kinematic Stirling engine. For a given working fluid mean pressure the engine torque increases at first and then, after reaching a peak value, it begins to decrease as the engine speed is increased. For the same speed the torque is higher for higher mean pressure. The engine efficiency is higher for higher mean pressure. For constant-power operation, the engine torque decreases with increasing speed. The engine will normally run at the design speed and will idle at lower speed.

Consider a Stirling engine with constant power input. In order to increase the output power of the engine, the control valve allows additional working fluid from the cylinder into the working volume. In order to decrease the output power the working fluid is pumped back into the cylinder. The control valve is speed-sensitive and allows the flow of additional working fluid when the speed goes down as a result of increased load demand. When the load demand is decreased the speed tends to increase and the valve allows working fluid to return to the cylinder.

If the insolation is increased, the engine output power, P_o, is increased. Since $P_o = T$ and the speed cannot change instantaneously, the torque tends to go up. As the torque increases, the speed begins to increase. In response to increasing speed the control valve allows mean pressure to control the torque and restore the speed. Finally, in equilibrium, the torque has a higher value and the speed is essentially at the previous value. A similar sequence of operation characterizes the dynamics when insolation is decreased. In this case the final value of the torque is lower and that of the speed is essentially restored.

b. Free-Piston Stirling Engine

A free-piston Stirling engine is a thermally driven mechanical oscillator that operates on a Stirling engine cycle. The engine has three basic components: a cylinder, a displacer and a power piston. The expansion space is between the cylinder and the displacer, the compression space is between the displacer and the power piston, and the bounce volume is between the power piston and the cylinder. There are three types of forces that determine the engine dynamics: the force on components due to displacement of components the force on components due to velocity of components and the force on masses due to acceleration. Forces due to displacement and velocity may be determined from the thermodynamic properties of the cycle and the engine geometry. If the working fluid is assumed to obey the perfect gas law for adiabatic expansions and compressions, the force due to displacement will be proportional to the relative displacement and is analogous to a force in a linear spring. The spring action is due to the interaction between the pressurized fluid and the engine piston.

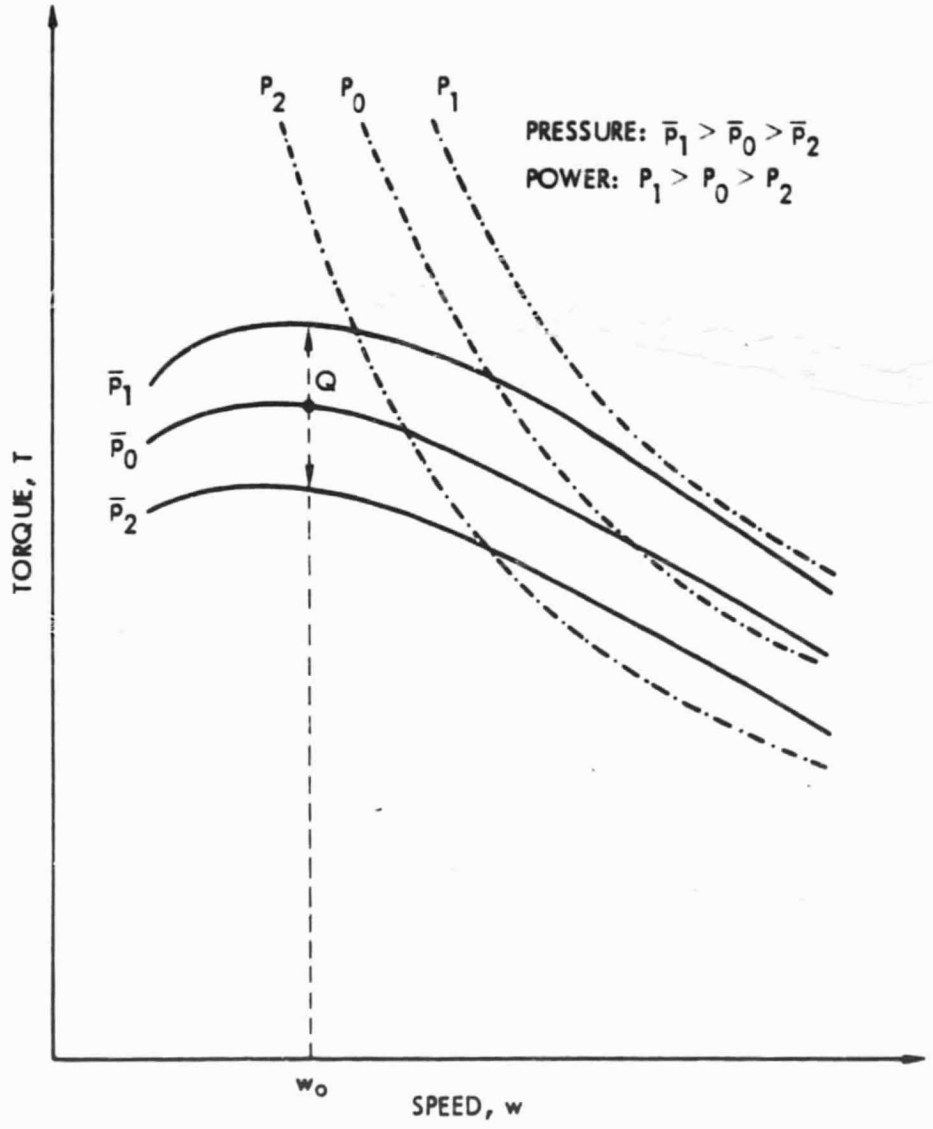

Figure 3-39. Typical Performance Map of a Kinematic Stirling Engine and its Constant Speed Operation by Mean Pressure Control

The force due to the velocity is dissipative in nature and is proportional to the relative velocity. It is analogous to a force in linear damping. The force due to acceleration of mass is proportional to the acceleration of the mass. Mechanical and electric analogs representing the dynamics of a free-piston Stirling engine are shown in Figures 3-40 and 3-41. Electrical analog parameter values may be obtained by the knowledge of engine parameters.

There are two approaches to generating 15 kWe using a free-piston Stirling engine and alternator combination: three 15-kWe combinations and one 15-kWe combination. In each case the electrical output will be single-phase AC. In order to obtain a balanced three-phase output, the alternator output(s) may be rectified and inverted and filtered. In the case of a kinematic Stirling engine a single 15-kWe three-phase AC output is possible with a single engine and a single three-phase AC generator.

4. Plant Power Processing

In a solar electric plant of 1-10 MWe size, a large number of solar generating units will be operating in parallel. From the viewpoints of plant efficiency, layout, reliability, available equipment size, cost and ease of maintenance, these generating units will be grouped into four groups.

Assuming a single 13.8 kV/480 kV output transformer of efficiency 0.99, each group with AC link operation will consist of nearly 121 SGUs with each unit generating 20.8 kWe. Each group with AC link operation is shown in Figure 3-42.

Similarly, assuming a single 13.8 kW/480 kV output transformer of efficiency 0.99 and a single inverter of efficiency 0.93, each group with DC link operating will consist of nearly 132 SGUs with each unit generating 20.8 kWe. Each group with DC link operating is shown in Figure 3-43. Plants with AC link groups and DC link groups are shown in Figures 3-44 and 3-45, respectively.

5. Utility Interface

A schematic layout of a concentrator field and a power collection network is shown in Figure 3-46. One group is located in each of the four quadrants. Power may be collected at generation voltage level, 480 V or at 13.8 kV. The Figure 3-46 shows power collection at 480 V for AC link generation approach. The cable cost, the total transformer cost and the power loss in transport network will determine the transport network layout. The concentrator field will also include a control building.

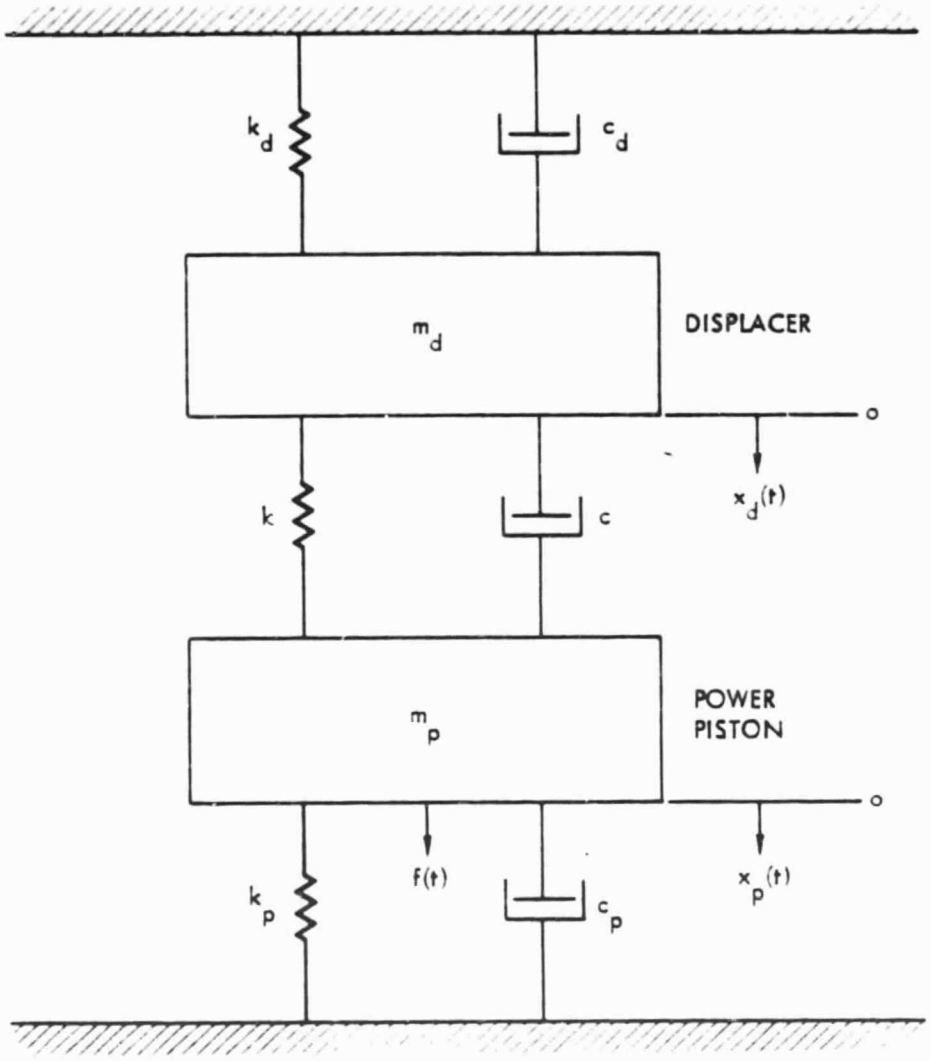

Figure 3-40. A Mechanical Analog of a Free Piston Stirling Engine

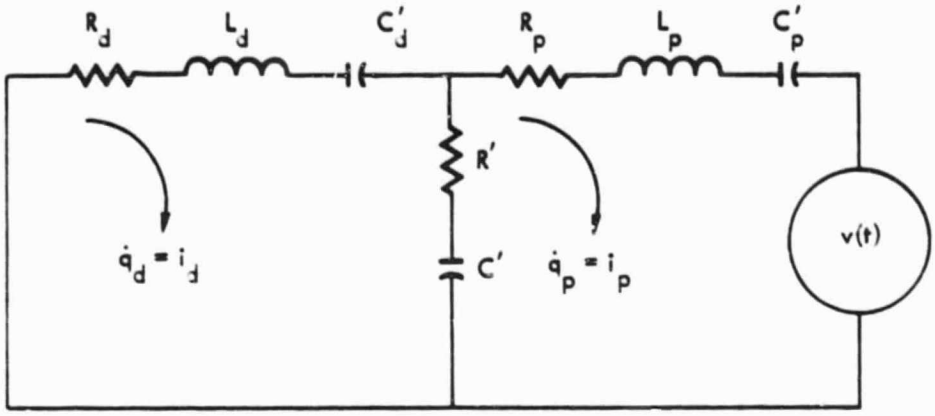

Figure 3-41. An Electrical Circuit Analog of a Free-Piston Stirling Engine (q x, v f, i, q)

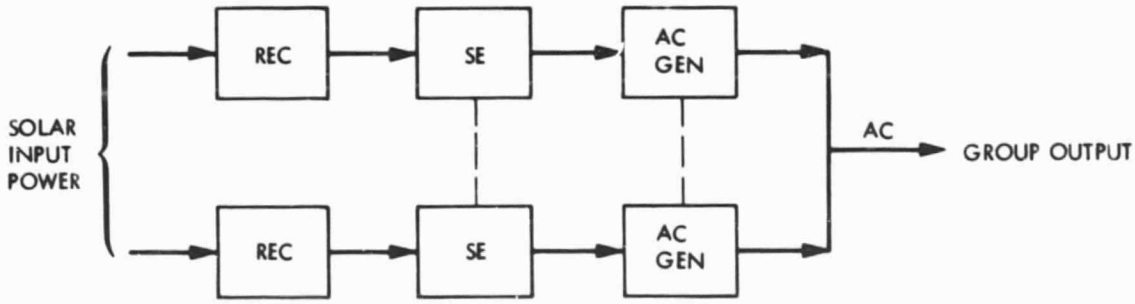

Figure 3-42. A Group of SGUs with AC-Link Operation

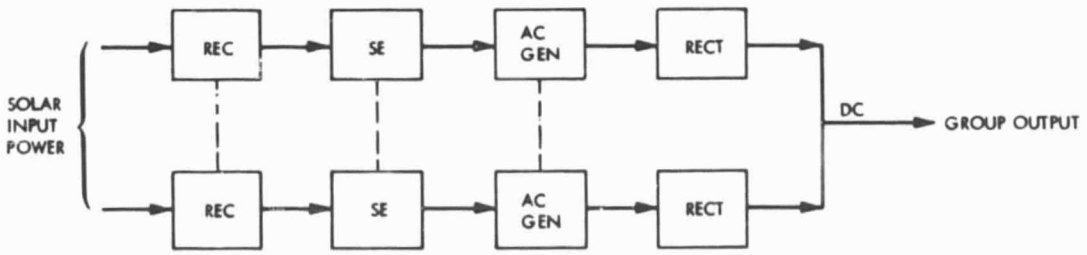

Figure 3-43. A Group of SGUs with DC-Link Operation

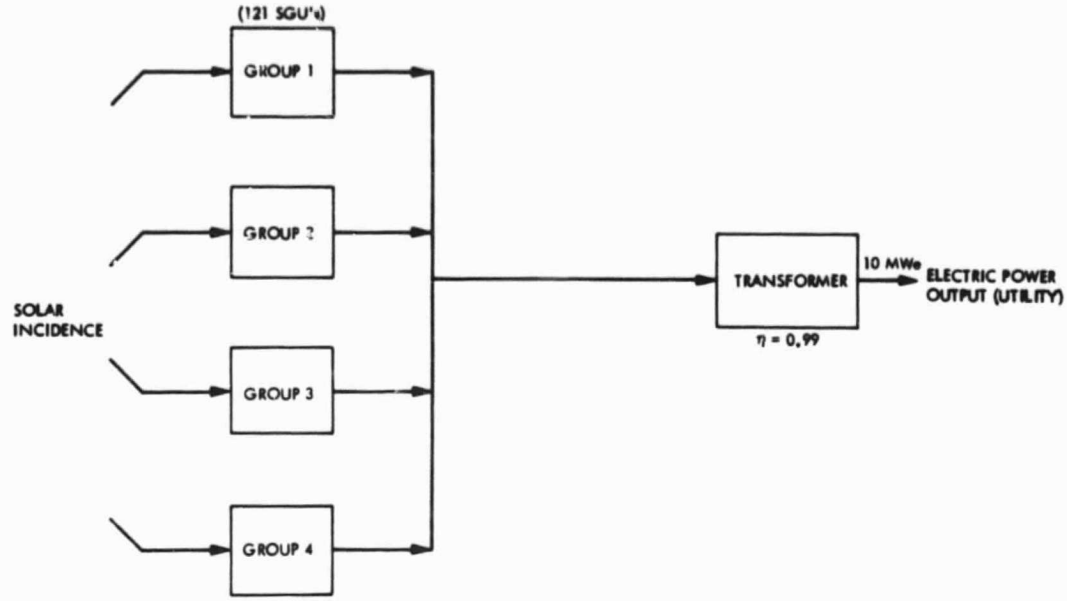

Figure 3-44. A 10 MWe Ac-Link Hybrid Solar Plant with Four Groups. Each Group with 121 SGUs

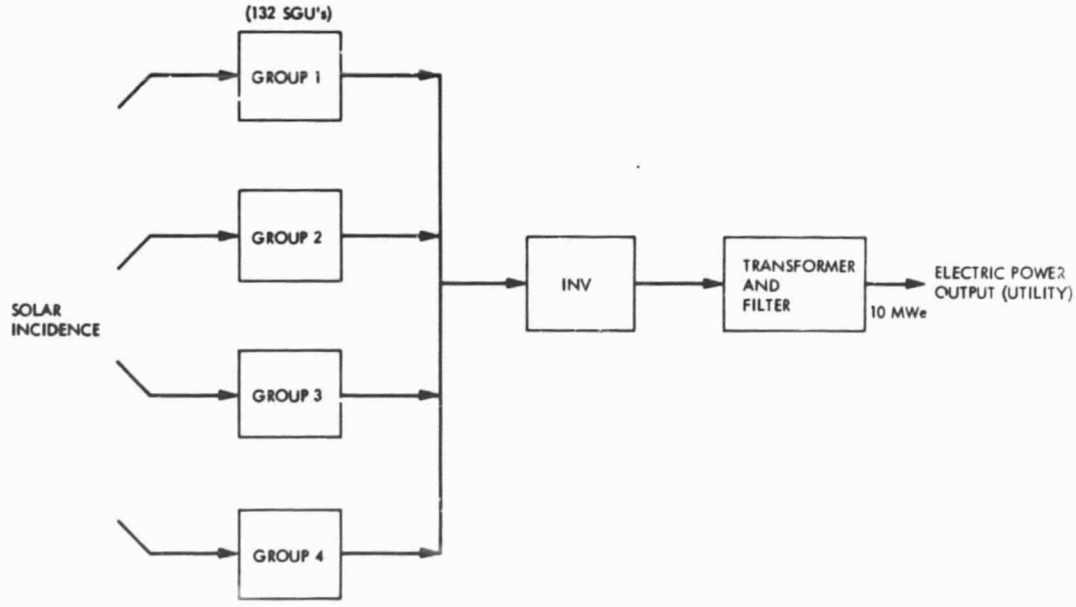

Figure 3-45. A 10 MWe DC-Liner Hybrid Solar Plant with Four Groups. Each Group with 132 SGUs

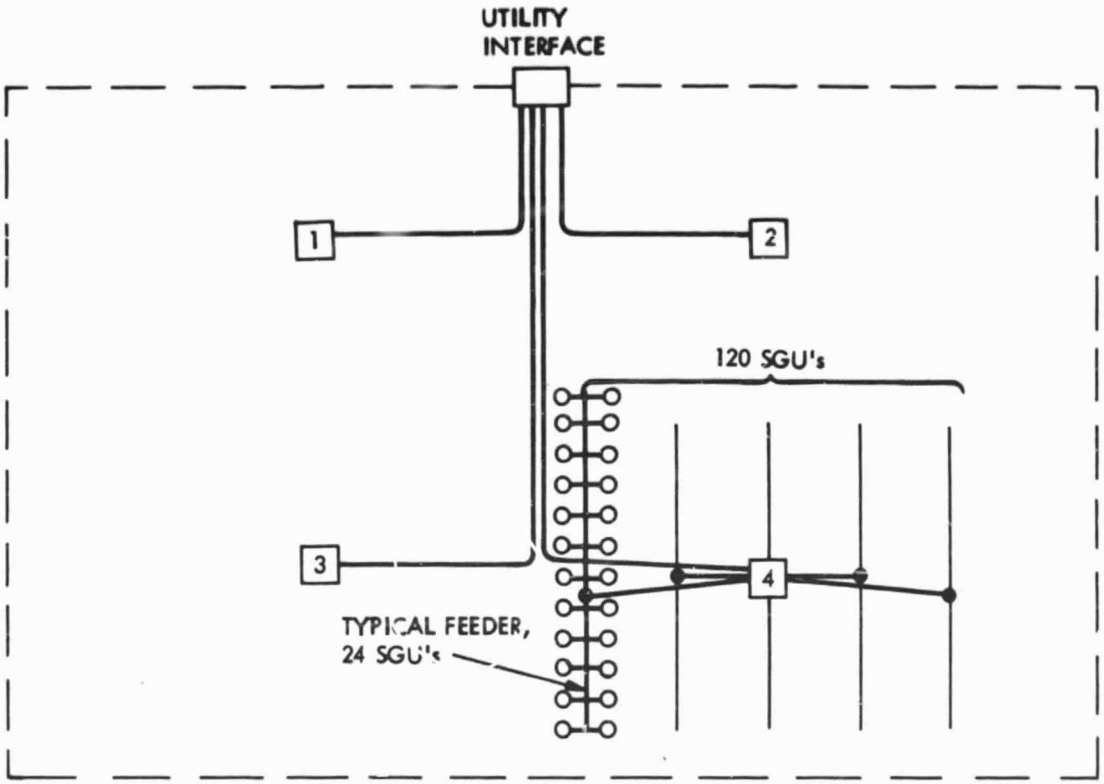

Figure 3-46. A Schematic Layout of a Concentrator Field and a Power Collection Network

6. Conclusion

Both free-piston and kinematic Stirling engines for solar thermal application are presently in experimental stages though the kinematic Stirling engine has a much longer and more extensive development history than the free-piston engine. There are several ways to design a combustion-control system. What is presented here is one method to control combustion and engine speed. A more detailed study is needed in this area. A processing power plant and collector field layout are presented. However, an optimization study of the power collection network cost, including equipment cost and the transport network cost, together with the overall plant performance, will be necessary before the plant layout is completed.

Stability concerns are greater with free-piston engines than with kinematic Stirling engines. A kinematic engine is inherently stable in its normal operational mode. A free-piston Stirling engine has two thermodynamically coupled masses in mechanical oscillation. During the design a detailed parametric sensitivity analysis for reasonable stability margin will be necessary.

A detailed stability analysis of an SGU is very important because a large number of these SGUs will operate in parallel in a solar electric plant. Interaction among these units in both stand-alone and grid-connected systems may lead to system instability and needs to be analyzed.

Control problems associated with obtaining a three-phase balanced-power output are of higher difficulty in free-piston engines than in kinematic engines. This is because only one single-phase linear alternator is used in a free-piston engine assembly. Maintaining an equality of voltage, frequency and phase difference of 120^{o} among voltage output of three solar generating units with free-piston engines will require monitoring and control equipment. This will not be needed with a single kinematic engine and conventional AC generator combination of the same power output.